AD-A112 489 CALIFORNIA UNIV LOS ANGELES INTEGRATED ELECTROMAGNET--ETC F/G 9/5
PRINTED CIRCUIT DIPOLE CHARACTERISTICS FOR MICROWAVE, MILLIMETE--ETC(U)
DEC 81 P L KATEHI, N G ALEXOPOULOS DAAG29-79-C-0050

UNCLASSIFIED UCLA-ENG-81-28 ARO-15965.9-EL NL

1 OF 2
AD
A112489

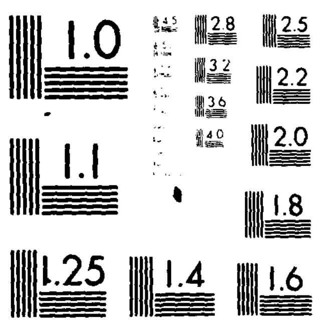

MICROCOPY RESOLUTION TEST CHART

NATIONAL BUREAU OF STANDARDS 1963-A

ARO 15965.9-EL

(12)

AD A112439

Integrated Electromagnetics Laboratory Report No. 1
UCLA Report No. ENG 81-28

DTIC
ELECTE
MAR 26 1982

S

"PRINTED CIRCUIT DIPOLE CHARACTERISTICS FOR MICROWAVE, MILLIMETER AND SUBMILLIMETER WAVE APPLICATIONS."

by

P.L. Katehi and
N.G. Alexopoulos

Sponsored by:

U.S. Army Contract DAAG 29-79-C-0050
U.S. Navy Contract N00014-79-C-0856

DTIC FILE COPY

82 03 24 029

UCLA • SCHOOL OF ENGINEERING AND APPLIED SCIENCE

SECURITY CLASSIFICATION OF THIS PAGE (When Data Entered)

REPORT DOCUMENTATION PAGE		READ INSTRUCTIONS BEFORE COMPLETING FORM
1. REPORT NUMBER	2. GOVT ACCESSION NO. AD-A11	3. RECIPIENT'S CATALOG NUMBER
4. TITLE (and Subtitle) Printed Circuit Dipole Characteristics for Microwave, Millimeter and Submillimeter Wave Applications.		5. TYPE OF REPORT & PERIOD COVERED Technical Laboratory Report
		6. PERFORMING ORG. REPORT NUMBER
7. AUTHOR(s) P. L. Katehi and N. G. Alexopoulos		8. CONTRACT OR GRANT NUMBER(s) DAAG 29-79-C-0050 N00014-79-C-0856
9. PERFORMING ORGANIZATION NAME AND ADDRESS Electrical Engineering Department UCLA Los Angeles, CA 90024		10. PROGRAM ELEMENT, PROJECT, TASK AREA & WORK UNIT NUMBERS
11. CONTROLLING OFFICE NAME AND ADDRESS Dr. James Mink ARO - P 4800-C-81		12. REPORT DATE December 1981
		13. NUMBER OF PAGES 100
14. MONITORING AGENCY NAME & ADDRESS (if different from Controlling Office) Army Research Office Research Triangle Park North Carolina		15. SECURITY CLASS. (of this report) Unclassified
		15a. DECLASSIFICATION DOWNGRADING SCHEDULE

16. DISTRIBUTION STATEMENT (of this Report)

17. DISTRIBUTION STATEMENT (of the abstract entered in Block 20, if different from Report)

18. SUPPLEMENTARY NOTES

THE VIEW, OPINIONS, AND/OR FINDINGS CONTAINED IN THIS REPORT ARE THOSE OF THE AUTHOR(S) AND SHOULD NOT BE CONSTRUED AS AN OFFICIAL DEPARTMENT OF THE ARMY POSITION, POLICY, OR DECISION, UNLESS SO DESIGNATED BY OTHER DOCUMENTATION.

19. KEY WORDS (Continue on reverse side if necessary and identify by block number)

Microwave Printed Circuit Dipole
Millimeter Submillimeter

20. ABSTRACT (Continue on reverse side if necessary and identify by block number)

This report deals with the theory and design of antennas printed on or embedded in a grounded substrate. A theoretical approach is implemented which accounts accurately for the physical effects involved including surface waves. The Green's function has been obtained synthesizing the fields of Hertzian dipoles which are oriented in arbitrary directions and which are printed on or embedded in the substrate. By considering Pocklington's integral equation with proper choice of expansion and testing functions, solution for current distribution and input impedance is obtained by matrix inversion.

DD FORM 1 JAN 73 1473 EDITION OF 1 NOV 65 IS OBSOLETE
S/N 0102 LF 014 6601

SECURITY CLASSIFICATION OF THIS PAGE (When Data Entered)

Classification 20. (Continued)

As an example, thin-type printed and embedded circuit antennas with symmetric or asymmetric excitation are considered. Antenna currents input impedance, bandwidth and resonant resistance are obtained for a variety of antenna arrangements. A serious amount of effort is also being placed in evaluating the importance of higher order surface wave modes which are determined by the relative dielectric constant and the thickness of the substrate.

Integrated Electromagnetics Laboratory Report No. 1

UCLA Report No. ENG 81-28

"PRINTED CIRCUIT DIPOLE CHARACTERISTICS FOR MICROWAVE, MILLIMETER AND SUBMILLIMETER WAVE APPLICATIONS."

by

P.L. Katehi

and N.G. Alexopoulos

Sponsored by

U.S. Army Contract DAAG 29-79-C-0050
U.S. Navy Contract N00014-79-C-0856

TABLE OF CONTENTS

LIST OF FIGURES

ABSTRACT

This report deals with the theory and design of antennas printed on or embedded in a grounded substrate. A theoretical approach is implemented which accounts accurately for the physical effects involved including surface waves. The Green's function has been obtained by synthesizing the fields of Hertzian dipoles which are oriented in arbitrary directions and which are printed on or embedded in the substrate. By considering Pocklington's integral equation with proper choice of expansion and testing functions, solution for current distribution and input impedance is obtained by matrix inversion.

As an example, thin-type printed and embedded circuit antennas with symmetric or asymmetric excitation are considered. Antenna currents, input impedance, bandwidth and resonant resistance are obtained for a variety of antenna arrangements. A serious amount of effort is also being placed in evaluating the importance of higher order surface wave modes which are determined by the relative dielectric constant and the thickness of the substrate.

CHAPTER 1

INTRODUCTION

Monolithic or hybrid integrated circuits are finding increased use in the microwave, millimeter and far infrared frequency ranges. Therefore the development of antennas which are amenable to integration with other printed circuit elements is of significant technological importance.

Printed circuit (microstrip) antennas were apparently introduced first in the early 1950's [1], [2]. However, their inherent advantages (conformality to a given surface, light weight, negligible volume, inexpensiveness), were not put to widespread practice until the 1970's [3] - [20]. The need to integrate microwave components, including antennas, necessitated the development of substrate materials with the appropriate thermal, mechanical and electrical properties in the desired frequency ranges [21] - [23]. The environmental and technological constraints having been resolved, the task remained to develop analytical methods which would provide accurate design criteria. Extensive efforts have been expended to provide models which predict correctly the electrical characteristics of microstrip antennas. These methods rely either on a transmission line model of the printed circuit antenna [3] - [7] or an open resonator model [8] - [20]. The former approach gives a heuristic explanation of the radiation properties of the antenna while the latter provides a more accurate prediction of the antenna characteristics. Both models apply mainly to the dominant resonator mode and their accuracy is questionable for higher order

modes, especially because they do not account for the excitation of surface waves.

Surface waves are important contributors to the printed circuit antenna current distribution as well as input impedance characteristics [24]. In addition, since surface modes decay as the inverse square root of distance from their source they can be significant to mutual impedance computation [25], a calculation of importance in phased array design. It has been established that regardless of how thin the substrate is, the dominant surface wave mode is always excited. The efficiency of launching of this mode depends on the thickness of the substrate and its dielectric constant. As more energy is trapped in the substrate the microstrip antenna becomes less efficient. In many applications, such as in the millimeter or far infrared region [28]- [30], today's technology provides substrates which are several wavelengths thick. This permits many surface modes (TE and TM) to exist in the substrate, further complicating the design. These modes, too, can cause impairment of efficiency.

It becomes evident from this discussion that a theoretical approach must be implemented which accounts accurately for the physical effects involved, including surface waves. Such an approach excludes either of the previously mentioned techniques and relies on treating the microstrip element as an antenna rather than as a transmission line section or as a resonator. This requires that the antenna current distribution be obtained first by solving a two-dimensional Pocklington integral equation. The Green's function in this case can be obtained by synthesizing the fields of Hertzian dipoles which are oriented in arbitrary directions and which are printed on the substrate, thus

accounting properly for all the boundary conditions pertinent to the problem.

An analytical solution of the two dimensional Pocklington's integral equation is precluded due to the immense complexity of the problem. One must resort to numerical techniques, with the integral equation discretized and the current distribution obtained by matrix inversion. A numerical method which has found widespread and successful use for the solution of Pocklington type integral equations is the method of moments [24] - [27]. It has the disadvantage, like other numerical techniques, of requiring extensive computing time in some applications, e.g., in the computation of electromagnetic scattering from objects large compared to wavelength. For the present application, the Green's function pertinent to the problem is given by Sommerfeld-type integrals which require special integration techniques when field and source points are both on the substrate [24], [25], [31]. At present, evaluation of these integrals is numerically time-consuming, thus making the applicability of the method of moments to arbitrarily shaped planar printed circuit antennas difficult.

In the present work, thin wire-type printed circuit antennas with symmetric or asymmetric excitation are considered. The excitation is assumed to be caused by a unit voltage generator and the printed wires are taken to be thin compared to wavelength. The azimuthal asymmetry of the current distribution is assumed to be a second order effect. The antenna currents, input impedance, bandwidth and resonant resistance are obtained for a variety of antenna arrangements. A serious amount of effort is also being placed in determining the importance of higher-

order surface wave modes so that a correct trade-off analysis of bandwidth with substrate thickness can be implemented.

CHAPTER 2

GREEN'S FUNCTION FOR PRINTED/EMBEDDED DIPOLES AND POCKLINGTON'S INTEGRAL EQUATION

2-1. DERIVATION OF GREEN'S FUNCTION

This chapter presents the development of the Green's Function pertinent to the problem of linear antennas printed on or embedded in a grounded dielectric substrate of thickness b and relative dielectric constant ε_r.

In order to formulate the Green's function, an elementary horizontal electric dipole (HED) is considered to be at (x', y', -h) as shown in Figure 2.1. The assumed time dependence is $e^{j\omega t}$ and it is suppressed throughout the report. Maxwell's equations take now the following form in region II (z < o)

$$\vec{\nabla} \times \vec{H}^d = \vec{J}^d + j\omega\varepsilon_r\varepsilon_o \vec{E}^d \tag{2.1}$$

$$\vec{\nabla} \times \vec{E}^d = -j\omega\mu_o \vec{H}^d \tag{2.2}$$

$$\vec{\nabla} \cdot \vec{B} = 0 \tag{2.3}$$

$$\vec{\nabla} \cdot \vec{E}^d = \frac{\rho^d}{\varepsilon_r\varepsilon_o} \tag{2.4}$$

where the superscript d indicates field and source quantities in the dielectric substrate. The following potential function is now introduced,

$$\vec{B}^d = \mu_o \vec{H}^d = -\frac{k^2}{j\omega} \vec{\nabla} \times \vec{G}^d \tag{2.5}$$

where $\vec{G}^d$ will turn out to be the Green's function in region II. Since $\vec{\nabla} \cdot (\vec{\nabla} \times \vec{G}^d) = 0$, equation (2.5) indicates that (2.3) is satisfied. A substitution of (2.5) into the curl equation for $\vec{E}^d$ gives the following

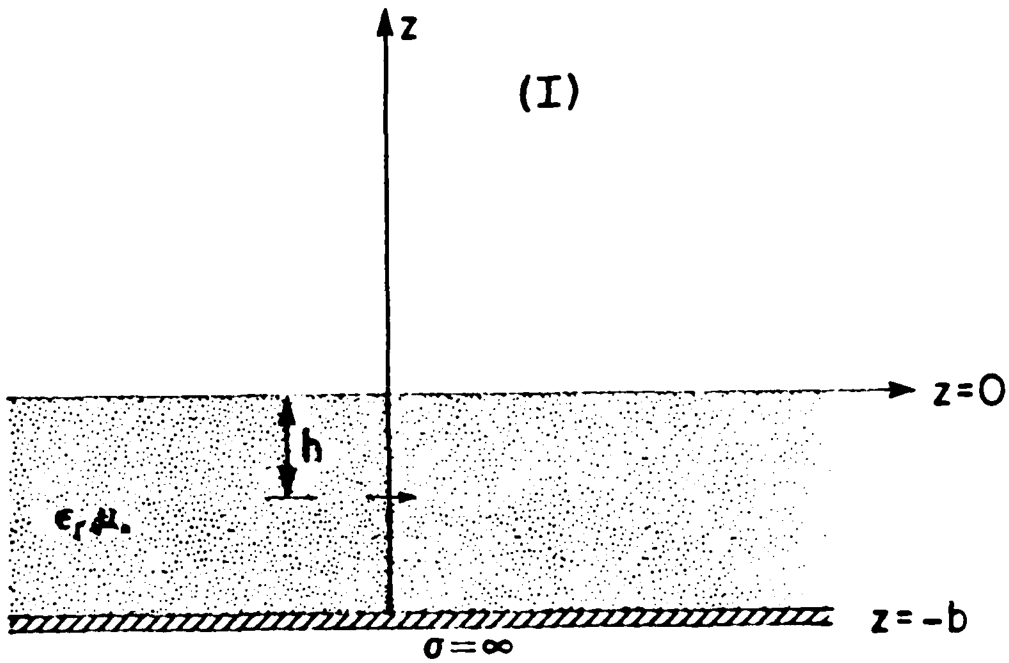

Figure 2.1: HED Embedded in a Grounded Dielectric Slab

result

$$\vec{\nabla} \times (\vec{E}^{d} - k^{2}\vec{G}^{d}) = 0 \tag{2.6}$$

where $k^2 = \omega^2 \mu_o \epsilon_r \epsilon_o$. Since $\vec{\nabla} \times (\vec{\nabla}\phi^d) = 0$ it follows that

$$\vec{E}^{d} = k^{2}\vec{G}^{d} - \nabla\phi^{d} \tag{2.7}$$

with ϕ^d the scalar potential function for region II. The relationship between ϕ^d and $\vec{G}^d$ can be obtained by a substitution of (2.5) and (2.7) into (2.1), i.e.

$$\vec{\nabla} \times \vec{\nabla} \times \vec{G}^{d} = \vec{\nabla}(\vec{\nabla} \cdot \vec{G}^{d}) - \vec{\nabla}^{2}\vec{G}^{d} = -\frac{j\omega\mu_o}{k^2}\vec{J}^{d} + k^{2}\vec{G}^{d} - \nabla\phi^{d} \tag{2.8}$$

Since the curl of $\vec{G}^d$ has been defined and, in addition, since $\vec{G}^d$ is arbitrary, one can choose its divergence to be

$$\vec{\nabla} \cdot \vec{G}^{d} = -\phi^{d} \tag{2.9}$$

which is the Lorentz condition. The wave equation for $\vec{G}^d$ can now be obtained from (2.8) and (2.9) in the form

$$(\nabla^{2} + k^{2})\vec{G}^{d} = \frac{j\omega\mu_o}{k^2}\vec{J}^{d} \tag{2.10}$$

The Lorentz condition enables one to write in region II for $\vec{E}^d$ and $\vec{H}^d$ the result

$$\vec{E}^{d} = \vec{\nabla}(\vec{\nabla} \cdot \vec{G}^{d}) + k^{2}\vec{G}^{d} \tag{2.11}$$

and

$$\vec{H}^{d} = -\frac{k^2}{j\omega\mu_o}\vec{\nabla} \times \vec{G}^{d} \tag{2.12}$$

In a similar manner the electromagnetic field in region I is given by

$$\vec{E} = \vec{\nabla}(\vec{\nabla} \cdot \vec{G}) + k_o^{2}\vec{G} \tag{2.13}$$

and

$$\vec{H} = -\frac{k_o^2}{j\omega\mu_o}\nabla \times \vec{G} \tag{2.14}$$

where k_o is the free space wavenumber, i.e. $k_o^2 = \omega^2\mu_o\epsilon_o$. $\vec{G}$ is the

Green's function for region I and it satisfies the wave equation

$$(\nabla^2 + k_o^2)\,\vec{G} = \frac{j\omega\mu_o}{k_o^2}\,\vec{J} \tag{2.15}$$

for a given current source $\vec{J}$.

The solution which satisfies the wave equation and the appropriate boundary conditions, in each region of interest, consists of two parts; the secondary solution which is the solution to the corresponding homogeneous equation, and the primary solution which is the particular solution to the wave equation. The complete solution is therefore

$$\vec{G} = \vec{G}p + \vec{G}s \qquad \text{(region I)} \tag{2.16}$$

and

$$\vec{G}^d = \vec{G}p^d + \vec{G}s^d \qquad \text{(region II)} \tag{2.17}$$

The existence of the primary solution is strictly related to the presence of current sources in the region of interest.

For the cases considered here the primary solution has an x-component only [32]-[34] given by (see Appendix A)

$$Gp_x^d = -\frac{j\omega\mu_o}{4\pi k^2}\int_0^\infty J_o(\lambda\rho)\, e^{-u|z+h|}\,\frac{\lambda d\lambda}{u} \tag{2.18}$$

where

$$u_o = [\lambda^2 - k_o^2]^{\frac{1}{2}}, \quad u = [\lambda^2 - k^2]^{\frac{1}{2}}$$

$$\rho = [(x - x')^2 + (y - y')^2]^{\frac{1}{2}}$$

and

$$\cos\phi = \frac{x-x'}{\rho}$$

Due to the absence of sources in region I the secondary components are [32] - [34];

$$G_{sx} = -\frac{j\omega\mu_o}{4\pi k_o^2}\int_o^\infty F(\lambda)\ J_o(\lambda\rho)\ e^{-u_o z} d\lambda \tag{2.19}$$

$$G_{sz} = -\frac{j\omega\mu_o}{4\pi k_o^2}\cos\phi\int_o^\infty \phi(\lambda)\ J_1(\lambda\rho)\ e^{-u_o z} d\lambda \tag{2.20}$$

and

$$G_{sx}^d = -\frac{j\omega\mu_o}{4\pi k^2}\int_o^\infty J_o(\lambda\rho)\,[F^d(\lambda)e^{uz} + R^d(\lambda)e^{-uz}]\ d\lambda \tag{2.21}$$

$$G_{sz}^d = -\frac{j\omega\mu_o}{4\pi k^2}\cos\phi\int_o^\infty J_1(\lambda\rho)\,[\phi^d(\lambda)e^{uz} + \psi^d(\lambda)e^{-uz}]\,d\lambda \tag{2.22}$$

In the equations above $F(\lambda)$, $\phi(\lambda)$, $F^d(\lambda)$, $R^d(\lambda)$, $\phi^d(\lambda)$ and $\psi^d(\lambda)$ are determined by the boundary conditions at $z = 0, -b$ given by:

$$E_y = E_y^d,\ E_x = E_x^d,\ H_y = H_y^d,\ H_x = H_x^d\ (z = 0) \tag{2.23}$$

and

$$E_y^d = 0 \quad E_x^d = 0 \quad (z = -b) \tag{2.24}$$

Application of these boundary conditions yields

$$\phi^d(\lambda) = \frac{(1-\varepsilon_r)\lambda^2\ e^{ub}\ \sinh[u(b-h)]}{f_1(\lambda,b)\cdot f_2(\lambda,b)} \tag{2.25}$$

$$\psi^d(\lambda) = \phi^d(\lambda)\ e^{-2ub} \tag{2.26}$$

$$F^d(\lambda) = \frac{\lambda}{u}\ \frac{(u-u_o)\ \sinh[u(b-h)]}{f_1(\lambda,b)} \tag{2.27}$$

$$R^d(\lambda) = -[\frac{\lambda}{u}\ e^{-uh} + F^d(\lambda)]\ e^{-2ub} \tag{2.28}$$

$$F(\lambda) = \frac{2\varepsilon_r\lambda\sinh[u(b-h)]}{f_1(\lambda,b)} \tag{2.29}$$

$$\phi(\lambda) = \frac{2\varepsilon_r(1-\varepsilon_r)\lambda^2\sinh[u(b-h)]\cosh(ub)}{f_1(\lambda,b)\ \ f_2(\lambda,b)} \tag{2.30}$$

in which

$$f_1(\lambda,b) = u_o \sinh(ub) + u\cosh(ub) \tag{2.31}$$

$$f_2(\lambda,b) = \varepsilon_r\, u_o \cosh(ub) + u\sinh(ub) \tag{2.32}$$

With the above expressions substituted in equations (2.18) - (2.22) the final form of the Green's function is

$$G_x = -\frac{j\omega\mu_o}{2\pi k_o^2}\int_o^\infty J_o(\lambda\rho)e^{-u_o z}\,\frac{\sinh[u(b-h)]}{f_1(\lambda,b)}\,\lambda d\lambda \tag{2.33}$$

$$G_z = -\frac{j\omega\mu_o}{2\pi k_o^2}(1-\varepsilon_r)\cos\phi\int_o^\infty J_1(\lambda\rho)e^{-u_o z}\,\frac{\sinh[u(b-h)\cosh(ub)}{f_1(\lambda,b)\cdot f_2(\lambda,b)}\,\lambda^2 d\lambda \tag{2.34}$$

$$G_x^d = -\frac{j\omega\mu_o}{2\pi k^2}\int_o^\infty J_o(\lambda\rho)\,\frac{\sinh[u(z+b)]\cdot[u\cosh(uh)+u_o\sinh(uh)]}{f_1(\lambda,b)}\,\frac{\lambda}{u}\,d\lambda,\ -b\leq z\leq -h \tag{2.35}$$

$$G_x^d = -\frac{j\omega\mu_o}{2\pi k^2}\int_o^\infty J_o(\lambda\rho)\,\frac{\sinh[u(b-h)]\ [u\cosh(uz)-u_o\sinh(uz)]}{f_1(\lambda,b)}\,\frac{\lambda}{u}\,d\lambda,\ -h\leq z\leq 0 \tag{2.36}$$

$$G_z^d = -\frac{j\omega\mu_o}{2\pi k^2}(1-\varepsilon_r)\cos\phi\int_o^\infty J_1(\lambda\rho)\,\frac{\sinh[u(b-h)]\cosh[u(z+b)]}{f_1(\lambda,b)\cdot f_2(\lambda,b)}\,\lambda^2 d\lambda \tag{2.37}$$

For the case of the HED on the dielectric interface the Green's function is given by equations (2.33),(2.34) for region (I), and by (2.35), (2.37) for region (II) with h = 0.

2-2. POCKLINGTON'S INTEGRAL EQUATION.

It is assumed that the dipole shown in Figure 2.2 is very thin so that its radius a is much smaller than the wavelength λ_g in the dielectric, i.e.

$$a \ll \lambda_g,\ \lambda_g = \lambda_o/\sqrt{\varepsilon_r} \tag{2.38}$$

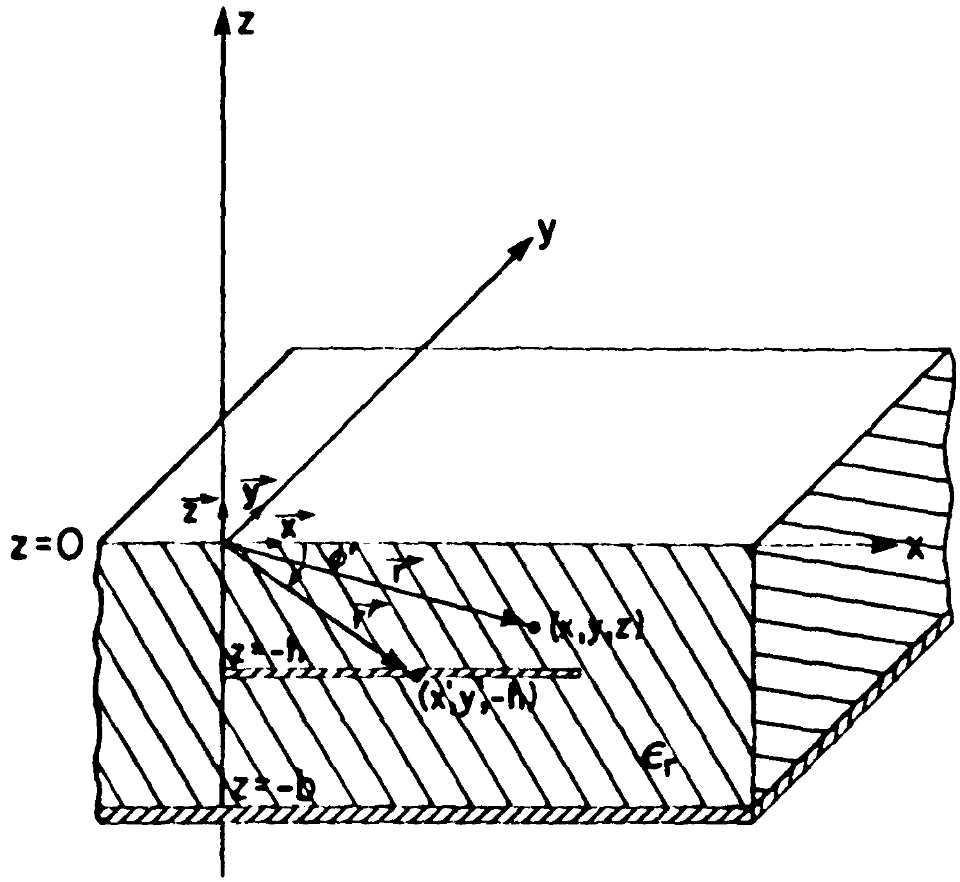

$$\vec{r}_x = \frac{\vec{r}'\cos\phi'}{|\vec{r}'\cos\phi'|}$$

Figure 2.2: Wire Dipole Embedded in a Grounded Dielectric Slab

If it is assumed that the current density on the dipole is given by

$$\vec{J}^{\,d} = J_x^d(\vec{r})\ \vec{r}_x \tag{2.39}$$

the integral equation for this problem is

$$\vec{E}^{\,d}(x,y,z) = \int_0^L [k^2 \bar{\bar{I}} + \nabla\nabla]\cdot\bar{\bar{G}}^d(\vec{r}/\vec{r}\,')\cdot\vec{J}^{\,d}(\vec{r}\,')\,dr_x \tag{2.40}$$

where $\bar{\bar{G}}^d(\vec{r}/\vec{r}\,')$ is the dyadic Green's Function and is given by

$$\bar{\bar{G}}^d(\vec{r}/\vec{r}\,') = G_x^d(\vec{r}/\vec{r}\,')\,\vec{x}\,\vec{x} + G_z^d(\vec{r}/\vec{r}\,')\,\vec{z}\,\vec{x} \tag{2.41}$$

and L the length of the dipole.

In addition $\bar{\bar{I}}$ denotes the idemfactor (unit dyadic) and it has the form

$$\bar{\bar{I}} = \vec{x}\,\vec{x} + \vec{y}\,\vec{y} + \vec{z}\,\vec{z} \tag{2.42}$$

while

$$\nabla = \vec{x}\frac{\partial}{\partial x} + \vec{y}\frac{\partial}{\partial y} + \vec{z}\frac{\partial}{\partial z} \tag{2.43}$$

Equation (2.40) can be rewritten as

$$\begin{aligned}\vec{E}^{\,d}(\vec{r}) = \int_0^L \Bigg[&\left\{ \left(k^2 G_x^d + \frac{\partial^2 G_x^d}{\partial x^2} + \frac{\partial^2 G_z^d}{\partial x \partial z}\right\} J_x^d\,\vec{x} \right. + \\ &+ \left(k^2 G_z^d + \frac{\partial^2 G_x^d}{\partial y \partial x} + \frac{\partial^2 G_z^d}{\partial y \partial z}\right) J_x^d\,\vec{y} + \\ &+ \left(\frac{\partial^2 G_x^d}{\partial z \partial x} + \frac{\partial^2 G_z^d}{\partial z^2}\right) J_x^d\,\vec{z}\Bigg] dr_x'\end{aligned} \tag{2.44}$$

From relation (2.44) it is observed that the electric field consists of three components E_x^d, E_y^d and E_z^d. However, only the E_x^d component enters the integral equation for the current distribution. From equation (2.44) the E_x^d component is given by

$$E_x^d(\vec{r}) = \int_o^L \left(k^2 G_x^d + \frac{\partial^2 G_x^d}{\partial x^2} + \frac{\partial^2 G_z^d}{\partial x \partial z} \right) J_x^d \, dr_x' \tag{2.45}$$

It is easily determined now that the x-component of the electric field for the case $h = 0$ is as follows:

$$E_x(\vec{r}) = \int_o^L \left(k_o^2 G_x + \frac{\partial^2 G_x}{\partial x^2} + \frac{\partial^2 G_z}{\partial x \partial z} \right) J_x \, dr_x' \tag{2.46}$$

with G_x, G_x^d, G_z, G_z^d defined previously.

A consideration of the following relationships

$$\frac{\partial G_z^d}{\partial z} = - \frac{\partial G^d}{\partial x} \tag{2.47}$$

and

$$\frac{\partial G_z}{\partial x} = - \frac{\partial G}{\partial x} \tag{2.48}$$

leads to

$$E_x^d(\vec{r}) = \int_o^L \left[k^2 G_x^d + \frac{\partial^2}{\partial x^2} \left(G_x^d - G^d \right) \right] J_x^d \, dr_x' \tag{2.49}$$

$$E_x(\vec{r}) = \int_o^L \left[k_o^2 G_x + \frac{\partial 2}{\partial x^2} \left(G_x - G \right) \right] J_x \, dr_x' \tag{2.50}$$

with G^d, G given by (see Appendix B)

$$G^d = - \frac{j\omega\mu_o}{2\pi k^2} (1-\epsilon_r) \int_o^\infty J_o(\lambda\rho) \frac{\sinh[u(b-h)]}{f_1(\lambda,b)} u \cdot \frac{\sinh[u(z+b)]}{f_2(\lambda,b)} \lambda d\lambda \tag{2.51}$$

$$G = - \frac{j\omega\mu_o}{2\pi k_o^2} (\epsilon_r - 1) \int_o^\infty J_o(\lambda p) \, \epsilon^{-u_o z} u_o \frac{\sinh(ub)}{f_1(\lambda,b)} \cdot \frac{\cosh(ub)}{f_2(\lambda,b)} d\lambda \tag{2.52}$$

CHAPTER 3

FORMULATION OF THE PROBLEM FOR NUMERICAL ANALYSIS

3-1. METHOD OF MOMENTS

The purpose of this chapter is to present the basic principles of the Method of Moments [35],[37] as well as its application to the specific problem of the dipole embedded in a grounded dielectric substrate.

Throughout this chapter, the radius of the dipole is assumed to be much smaller than the wavelength in the dielectric, so that the current may be assumed to be distributed uniformly around the cylinder. If one observes the current distribution from an observation point on the cylinder axis then the distance between the source and the observation point reduces to

$$R = [(x - x')^2 + a^2]^{\frac{1}{2}}$$

It is to be emphasized that the dipole or wire cylinder is not assumed to be infinitesimally thin and therefore the singularity which arises in the computation of reactance is overcome when the wire radius goes to zero.

The unifying concept of the numerical treatment of input impedance and radiation problems is the method of moments. This general approach to this kind of problems is essentially a reduction of the associated integral equation to a system of linear algebraic equations in N unknowns. The N unknowns are usually coefficients in some appropriate expansion of the current distribution.

The general method of solution will be discussed in the notation of linear spaces and operators and hence the specific problem studied here will be put into this notation. The integral equations derived in Chapter 2 (2.52 and 2.53) can be put into the form of an operator equation using the concept of linear vector spaces as follows:

$$L_{op}\ (\vec{J}) = (E_x \vec{x}) \tag{3.1}$$

with L_{op} given by

$$L_{op} = \int_c^L \left[k_o^2 G_x + \frac{\partial^2}{\partial x^2} (G_x - G) \right] (\vec{x} \cdot d\vec{r}_x{}') \tag{3.2}$$

in air and

$$L_{op} = \int_o^L \left[k^2 G_x^d + \frac{\partial^2}{\partial x^2} (G_x^d - G^d) \right] (\vec{x} \cdot d\vec{r}_x{}') \tag{3.3}$$

in the dielectric substrate.

In equation (3.1) $(E_x \vec{x})$ is a known excitation function or source and $\vec{J}$ is the unknown current distribution. In addition to the above it is necessary to identify the inner product $< \vec{J}, (E_x \vec{x}) >$, which is defined to satisfy in Hilbert space the following relations:

$$< \vec{J}, (E_x \vec{x}) > = < (E_x \vec{x}), \vec{J} > \tag{3.4}$$

$$< \alpha \vec{J} + \beta (E_x \vec{x}), h > = \alpha < \vec{J}, \vec{h} > + \beta < (E_x \vec{x}), \vec{h} > \tag{3.5}$$

$$\begin{aligned} < \vec{J}^*, \vec{J} > \quad &> 0 \text{ if } \vec{J} \neq 0 \\ &= 0 \text{ if } \vec{J} = 0 \end{aligned} \tag{3.6}$$

where α, β are scalars; $\vec{J} \times \vec{h} = 0$ and * denotes a complex conjugate.

The inner product may be in the form

$$< \vec{J}, (E_x \vec{x}) > = \int_o^L \vec{J} \cdot (E_x \vec{x})\ dr \tag{3.7}$$

and since

$$\bar{\bar{G}}\ (\vec{r}/\vec{r}\,') = \bar{\bar{G}}\ (\vec{r}\,'/\vec{r}) \tag{3.8}$$

and

$$\frac{\partial^2}{\partial x^2} = \frac{\partial^2}{\partial x'^2} \tag{3.9}$$

then it can be shown easily from equations (3.2) and (3.3) that

$$< L_{op} (\vec{J}), (E_x\vec{x}) > = < \vec{J}, L_{op} (E_x\vec{x}) > \tag{3.10}$$

which means that the integral operator L_{op} is self-adjoint. Based on this fact and on the physics of the problem it is concluded (see Appendix C) that there exists a unique solution to functional equation (3.1) and therefore the existence of the inverse operator results as a consequence, i.e.

$$\vec{J} = L_{op}^{-1} (E_x\vec{x}) \tag{3.11}$$

The procedure for obtaining a solution in the form of equation (3.11) can be divided into four steps:

1. Expand the unknown vector in a series of basis functions, J_n, spanning $\vec{J}$ in the domain of L_{op}.
2. Determine a suitable inner product and define a set of weighting functions.
3. Take the inner products and thereby form the matrix equation.
4. Solve the matrix equation for the unknowns $\vec{J}$.

3-2. GALERKIN'S METHOD

For electromagnetic input impedance and radiation problems a specialization of the general method of moments is particularly convenient. In the first of the four steps above the current distribution function $\vec{J}$ is expanded in a finite series of basis functions $\vec{J}_j$ ($j = 1, \ldots, N$) defined in the domain of L_{op}.

$$\vec{J} = \sum_j I_j \vec{J}_j \tag{3.12}$$

with $I_j \in C$

Substitution of equation (3.12) into (3.1) yields

$$L_{op}\left(\sum_j I_j \vec{J}_j\right) = (E_x \vec{x}) \tag{3.13}$$

and, because of the linearity of L_{op},

$$\sum_j I_j L_{op} (\vec{J}_j) = (E_x \vec{x}) \tag{3.14}$$

results.

In the second step a set of weighting functions $\vec{W}_k$ $(k = 1, \ldots N)$ is defined which is chosen to be identical with the basis functions i.e.

$$\left\{ \vec{W}_m \right\} = \left\{ \vec{J}_m \right\}$$

and then the following inner product is formulated:

$$\sum_j I_j < \vec{W}_k, L_{op} (\vec{J}_j) > = < \vec{W}_k, (E_x \vec{x}) > \tag{3.15}$$

This leads to the matrix equation

$$\begin{bmatrix} < \vec{J}_1, L_{op} (\vec{J}_1) > & < \vec{J}_1, L_{op} (\vec{J}_2) > & \cdots \\ < \vec{J}_2, L_{op} (\vec{J}_1) > & \cdot & \\ \cdot & & \ddots \\ \cdot & & \\ \cdot & & \\ \cdot & & \\ \cdot & & \\ \cdot & & \cdot \end{bmatrix} \begin{bmatrix} I_1 \\ I_2 \\ \cdot \\ \cdot \\ \cdot \\ \cdot \\ \cdot \\ \cdot \\ I_N \end{bmatrix} = \begin{bmatrix} < \vec{J}_1, (E_x \vec{x}) > \\ < \vec{J}_2, (E_x \vec{x}) > \\ \cdot \\ \cdot \\ \cdot \\ \cdot \\ \cdot \\ \cdot \\ < \vec{J}_N, (E_x \vec{x}) > \end{bmatrix} \tag{3.16}$$

Equation (3.16) may be solved by standard matrix inversion techniques for the unknown current vector [J], i.e.,

$$[J] = [Z]^{-1} [V] \tag{3.17}$$

where $[Z]$ = generalized impedance matrix

$[V]$ = generalized voltage vector

3-3. CHOICE OF BASIS FUNCTIONS

For the numerical solution of a given input impedance problem, one of the fundamental decisions to be made is the choice of basis functions $\vec{J}_j$. Theoretically these are infinitely many sets of basis functions but practically there are only a few which provide an optimum solution to the trade-off between accuracy and computer time for the specific problem. However, it is true that the closer the basis functions J_n resemble the actual current distribution on the radiator, the better the convergence and stability of the generalized impedance matrix.

There are two classes of basis functions:

1. The entire-domain basis functions. These are defined and are non-zero over the entire domain of L_{op} except possibly for a countable union of sets with measure zero. They also satisfy the boundary conditions for the specific problem.
2. The sub-domain basis functions which are non-zero functions over parts of the domain. In the case of wire radiators this consists of dividing the antenna into overlapping or non-overlapping sections.

The implementation of one or the other kind of basis functions depends on the specific problem. In the case of arbitrarily shaped radiators the problem can be simplified if sub-domain basis functions

are used to approximate parts of the radiator by N wire segments. Also in the case of certain geometries (linear dipole, open or closed circular loop) if the segments representing the radiator are identical then there is an appreciable reduction in computer time. This is due to the fact that the formed integrals extend on the sub-domains and not on the entire domain.

For the problem of the printed/embedded dipole the most appropriate set of basis functions is found to be of the following form (see Figure 3.1)

$$\vec{J}_j = \vec{x}\left\{P_{j-1}\,\frac{\sin[k(x'-x_{j-1})]}{\sin k\ell_x} + P_j\,\frac{\sin[k(x_{j+1}-x')]}{\sin k\ell_x}\right\}\delta(z+h) \qquad (3.18)$$

with

$$P_{j-1} = \begin{cases} 1 & x_{j-1} \le x' \le x_j \\ 0 & \text{elsewhere} \end{cases} \qquad (3.19)$$

and

$$P_j = \begin{cases} 1 & x_j \le x' \le x_{j+1} \\ 0 & \text{elsewhere} \end{cases} \qquad (3.20)$$

These basis functions, together with the inner product defined earlier, will be used for the formation of the matrix equation in the next section.

3-4. FORMULATION OF THE MATRIX EQUATION

As mentioned previously, the choice of basis functions is determined by many factors dictated by the problem under consideration. For the case of many parallel dipoles printed on or embedded in the dielectric, (see Figure 3.2) the basis functions can be modified slightly to be of the form

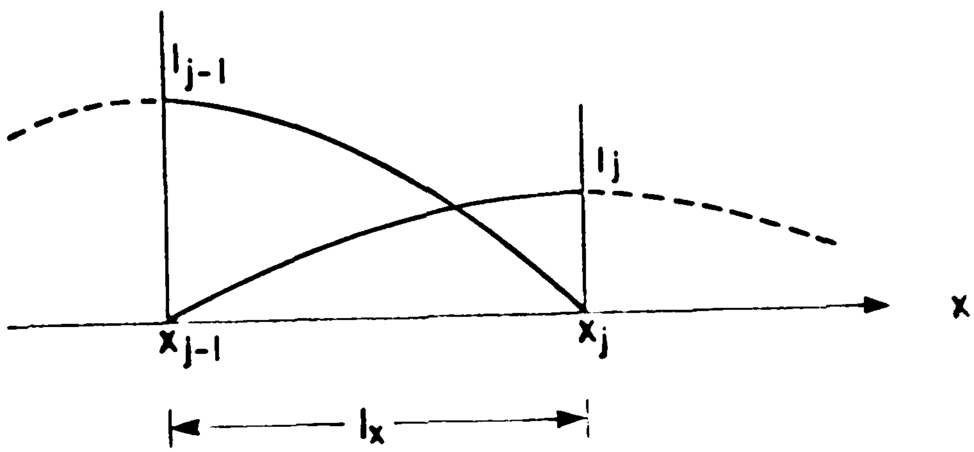

Figure 3.1: Piecewise-Sinusoidal Currents on aWire Segment

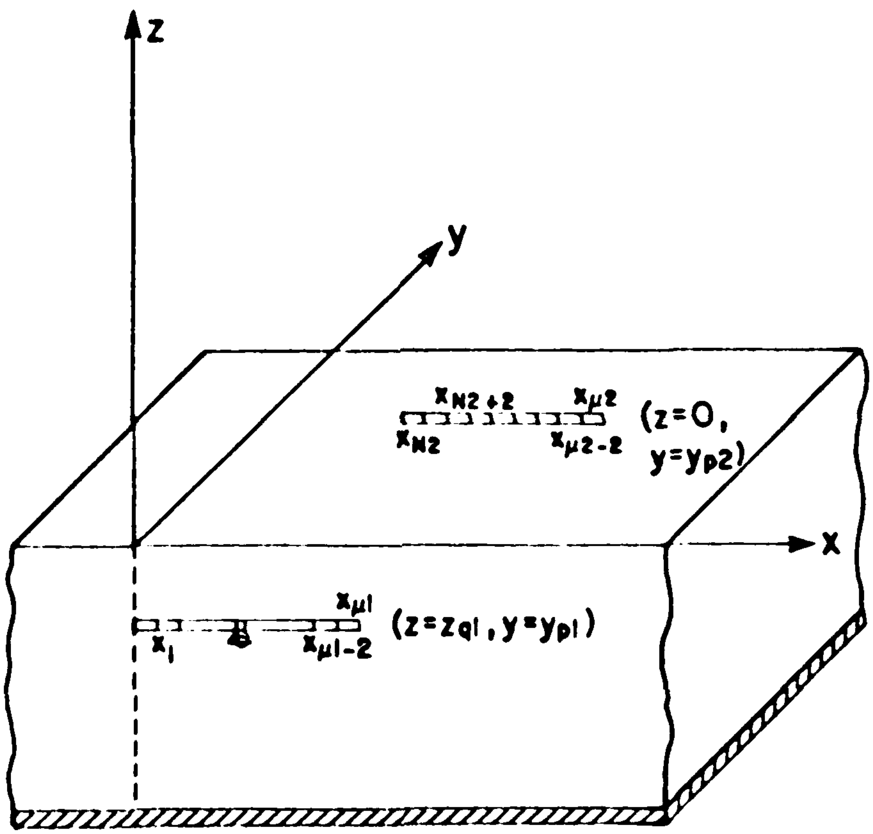

Figure 3.2: Array of Two Dipoles in the Dielectric Substrate.

$$\vec{J}_j^{pq} = f(x,x';j) \quad \delta(y'-y_p) \quad \delta(z'-z_q) \tag{3.21}$$

In this case, the current distribution inside a surface surrounding all the dipoles will be

$$\vec{J} = \sum_p \sum_q \sum_{j=N(p,q)+1}^{M(p,q)-1} I_j^{pq} \; \vec{J}_j^{pq} \tag{3.22}$$

By substituting (3.22)into (3.1), and by using (3.2) and (3.3) it can be found that the electric field in air and in the dielectric is as follows:

$$\begin{aligned} E_x = \sum_p \sum_q \sum_{j=N(p,q)+1}^{M(p,q)-1} I_j^{pq} \frac{1}{\sin k_o \ell_x} \cdot & \\ \Bigg\{ k_o^2 \int_{x_{j-1}}^{x_j} G \sin [k_o(x'-x_{j-1})] \, dx' \; + & \\ + \, k_o^2 \int_{x_j}^{x_{j+1}} G \sin[k_o(x_{j+1}- x')] \, dx' \; - & \\ - \, 2k_o \cos k_o \ell_x \, (G_x - G) \Big|_{x'= x_j} + & \\ + \, k_o(G_x-G) \Big|_{x'=x_{j-1}} + k_o(G_x-G) \Big|_{x'=x_{j+1}} \Bigg\} \; \delta(y'-y_p) \quad \delta(z-z_q) & \end{aligned} \tag{3.23}$$

and

$$
\begin{aligned}
E_x^d = \sum_p \sum_q \sum_{j=N(p,q)+1}^{M(p,q)-1} \quad & I_j^{pq} \, \frac{1}{\sin k\ell_x} \cdot \\
& \Bigg\{ k^2 \int_{x_{j-1}}^{x_j} G^d \sin[k\,(x'-x_{j-1})]\,dx' + \\
& + k^2 \int_{x_j}^{x_{j+1}} G^d \sin[k\,(x_{j+1}-x')]\,dx' - \\
& - 2k \cos k\ell_x \,(G_x^d - G^d)\big|_{x'=x_j} + \\
& + k(G_x^d - G^d)\big|_{x'=x_{j-1}} + k(G_x^d - G^d)\big|_{x'=x_{j+1}} \Bigg\} \;\; \delta(y'-y_p) \;\; \delta(z'-z_q)
\end{aligned}
\tag{3.24}
$$

The location of the voltage generator determines which of these two expressions should be used for the formation of the matrix equation. For the case of Figure 2, where the excitation is on an embedded dipole, equation (3.24) is substituted into (3.7). By using equations (3.3), (3.15) and (3.22) one can determine in a straightforward manner that the elements of the generalized impedance matrix are given by

$$
\begin{aligned}
Z_{kj}^{uv/pq} = \; & \left[\frac{1}{\sin k\ell_x}\right]^2 \; \delta(y-y_u) \;\; \delta(z-z_v) \;\; \delta(z'-z_q) \;\; \delta(y'-y_p) \\
& \Bigg\{ \sum_{a=-1,0} \; \sum_{a'=-1,0} k^2 \int_{x_{k+a}}^{x_{k+a+1}} dx \int_{x_{j+a'}}^{x_{j+a'+1}} dx' \cdot
\end{aligned}
$$

$$\sin\{k|\ell_x a + (x_{k+a+1} - x)|\}\cdot$$

$$\sin\{k|\ell_x a' + (x_{j+a+1} - x')|\}\cdot$$

$$G^d\left(\sqrt{(x-x')^2 + (y-y')^2}\ ;\ z;\ z'\right) +$$

$$+\sum_{a=-1,0}\ \sum_{a'=-1,0,1} k\ [1-(2\cos k\ell_x + 1)\cdot\delta(a')]\cdot\int_{x_{k+a}}^{x_{k+a+1}} dx$$

$$\sin\{k|\ell_x a + (x_{k+a+1} - x)|\}\cdot$$

$$\left[G_x^d\left(\sqrt{(x-x')^2 + (y-y')^2}\ ;\ z;\ z'\right) -\right.$$

$$\left.-G^d\left(\sqrt{(x-x_{j+a'})^2 + (y-y')^2}\ ;\ z;\ z'\right)\right]\ \Bigg\} \qquad (3.25)$$

The matrix equation then takes the final form

$$\left[Z_{kj}^{\mu\nu/pq}\right]\cdot\left[I_{kj}^{pq}\right] = \left[V_{kj}^{\mu\nu}\right] \qquad (3.26)$$

where $V_{kj}^{\mu\nu}$ are the elements of the excitation vector.

For the excitation of the driven dipole shown in Figure 3.2 one can use a voltage gap generator or a frill of magnetic current [36] located at the feed point. From these two ways the second one although it has an exact (or nearly so) model of the physical gap at the feed point, it complicates the problem especially in the case of a printed dipole since half of the dipole's cross section is in the air and half embedded in the dielectric. For this reason a voltage gap generator is considered at the feed point and all the elements of the

excitation vector become zero except for the one which corresponds to the infinitesimally thin gap.

CHAPTER 4

EVALUATION OF THE SOMMERFELD TYPE INTEGRALS

4-1. SINGULAR POINTS AND RELATED SURFACE WAVES

As shown in Chapter 3, the elements of the generalized impedance matrix consist of a summation of double and triple integrals. One of these integrals is a semi-infinite integration resulting from the Green's function. The integrand of this integral is an expression of transcendental functions multiplied by Bessel function of the first-kind and zero-order. Furthermore this is a Sommerfeld-type integral and the existence of essential singularities in its integrand necessitates very careful treatment. In this chapter, the computation of these integrals will be shown explicitly. In addition, the approximations employed will be justified and an estimation of the error intoduced by these approximations will be made.

From equation (3.25) it is obvious that all the singularities of the integrals considered here result from the Green's function. Furthermore as was shown in Chapter 2, the integrand in the semi-infinite integrals is a function of the parameter λ through the radicals

$$u = [\lambda^2 - k^2]^{\frac{1}{2}} \tag{4.1}$$

$$u_c = [\lambda^2 - k_c^2]^{\frac{1}{2}} \tag{4.2}$$

which are double-valued functions of the complex variable λ. However, the sign of the radical u does not affect the single-valuedness of the integrals, as the terms involving the radical u are even functions of λ. Therefore, only the branch cut contributed by the radical u_c is considered. The choice of the branch cut is not arbitrary. Its

position is determined by single-valuedness and convergence of the integrals, as well as the outgoing wave character of propagation.

At first, by considering the requirement of an outgoing wave it can be shown (see Appendix D) that the real and imaginary parts of the integration parameter λ must satisfy the following relations

$$\mathrm{Re}[\lambda] > 0 \tag{4.3}$$

$$\mathrm{Im}[\lambda] > 0 \tag{4.4}$$

A possible position of the branch cuts governed by these two relations is shown in Figure 4.1. For a given complex λ, u_o can be written as follows:

$$u_o = \sqrt{\lambda - k_o} \cdot \sqrt{\lambda + k_o} \tag{4.5}$$

with

$$\sqrt{\lambda - k_o} = \sqrt{r_1}\, e^{j\phi_1/2} \tag{4.6}$$

$$\sqrt{\lambda + k_o} = \sqrt{r_2}\, e^{j\phi_2/2} \tag{4.7}$$

From (4.6), (4.7) and (4.5) one obtains

$$u_o = \sqrt{r_1 r_2}\, e^{j(\phi_1 + \phi_2)/2} \tag{4.8}$$

From Figure 4.1 it can be observed that, for all λ in the first quadrant, the angles ϕ_1 and ϕ_2 are both positive, with

$$0 \le \phi_1 < 90^\circ + \delta \tag{(4.9)}$$

and

$$0 \le \phi_2 < 90^\circ - \delta \tag{4.10}$$

By considering (4.9) and (4.10) the inequality

$$0 \le \frac{\phi_1 + \phi_2}{2} < 90 \qquad \text{results.}$$

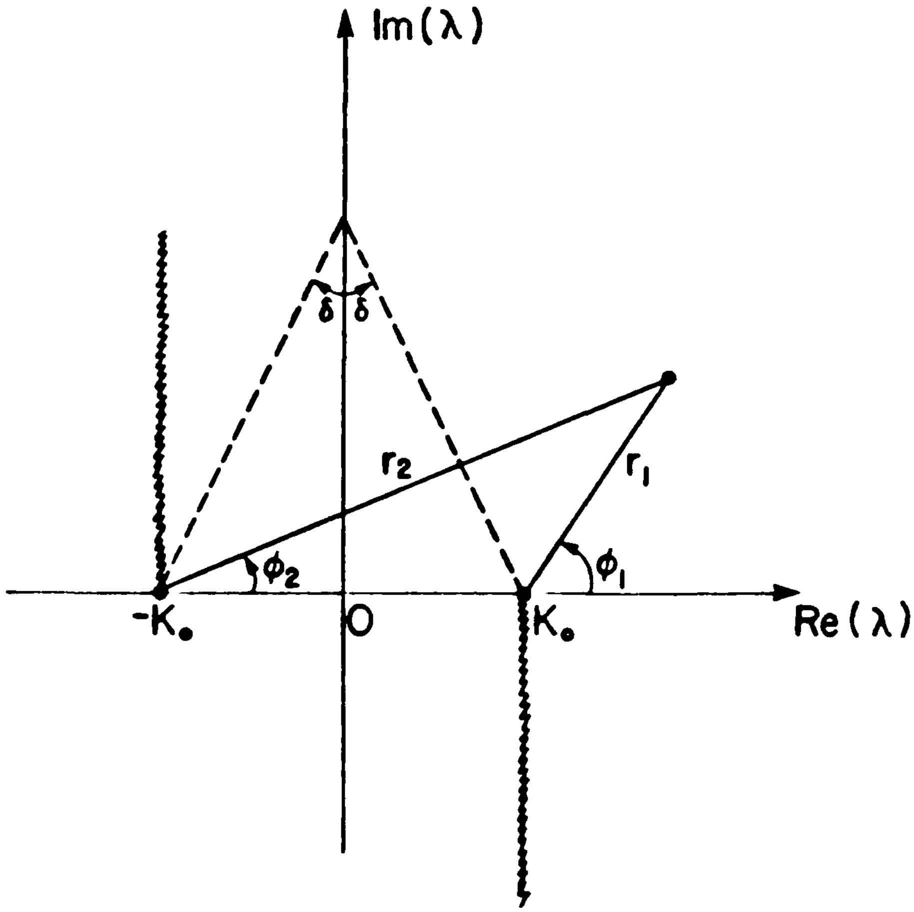

Figure 4.1: Complex Plane Geometry

This means that both the imaginary part and the real part of the radical u_o are positive. Thus the choice of branch cuts as shown in Figure 4.2 satisfies conditions (4.3) and (4.4). This choice also imposes the following relations:

$$\mathrm{Re}(u_o) > 0 \qquad \mathrm{Im}(u_o) > 0 \tag{4.11}$$

$$\mathrm{Re}(u) > 0 \qquad \mathrm{Im}(u) > 0 \tag{4.12}$$

In Chapter 2 it was shown that all the components of the dyadic Green's function were of the form

$$\underset{(i=x,z)}{G_i} = \int_o^\infty J_o(\lambda\rho) \frac{N(\lambda,b,h,\varepsilon_r)}{D(\lambda,b,h,\varepsilon_r)} d\lambda \tag{4.13}$$

$N(\lambda,b,h,\varepsilon_r)$ is a complex function with singularities of order less than one (at most), while the function $D(\lambda,b,h,\varepsilon_r)$ is of the form

$$D(\lambda,b,h,\varepsilon_r) = f_1(\lambda,b) \cdot f_2(\lambda,b) \tag{4.14}$$

or

$$D(\lambda,b,h,\varepsilon_r) = f_1(\lambda,b) \tag{4.15}$$

with $f_1(\lambda,b)$, $f_2(\lambda,b)$ given by

$$f_1(\lambda,b) = u_o \sinh(ub) + u \cosh(ub) \tag{4.16}$$

$$f_2(\lambda,b) = \varepsilon_r u_o \cosh(ub) + u \sinh(ub) \tag{4.17}$$

The integrand in equation (4.13) has poles whenever the function $D(\lambda,b,h,\varepsilon_r)$ becomes zero or when either one of the functions $f_1(\lambda,b)$, $f_2(\lambda,b)$ become zero. The zeros of these two functions lead to surface-wave modes. Particularly, the zeros of $f_1(\lambda,b)$ give rise to TE surface waves while the zeros of $f_2(\lambda,b)$ correspond to TM surface

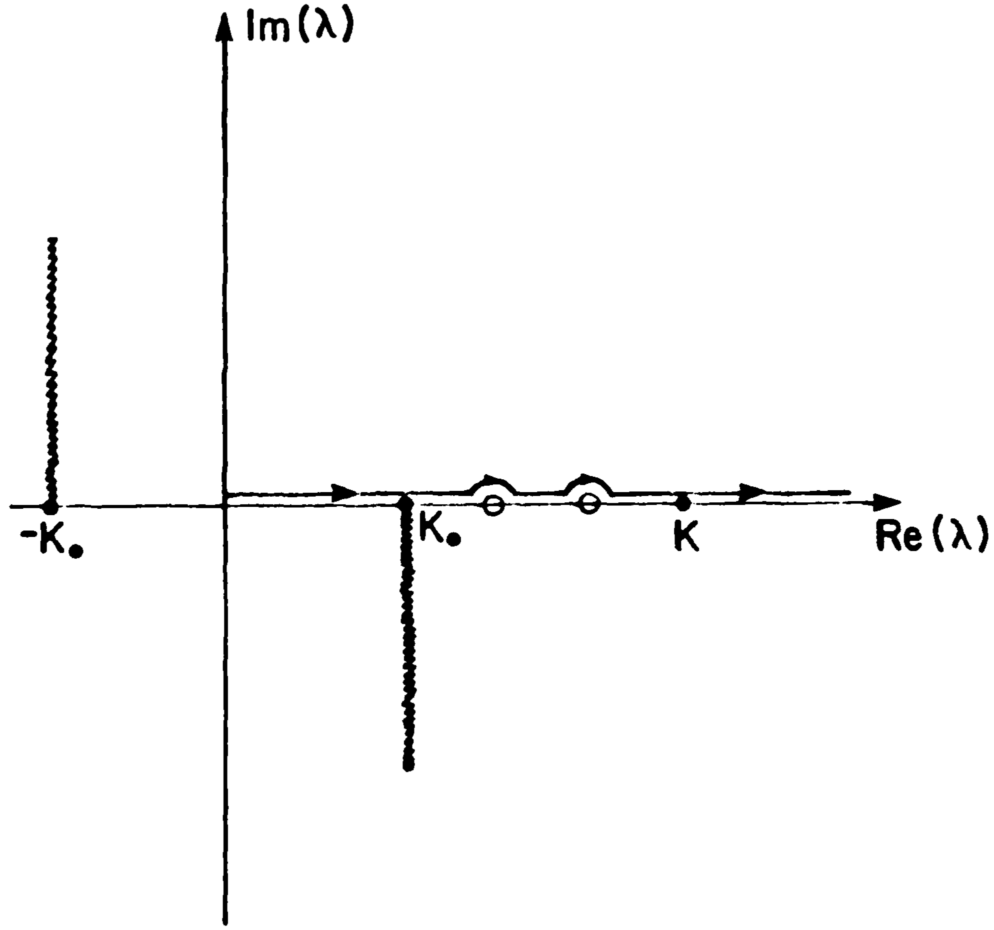

Figure 4.2: Path of Integration

waves. Assuming that k, k_o are real numbers (lossless dielectric) the roots of equations

$$u_o = -u \coth(ub) \tag{4.18}$$

and

$$\epsilon_r u_o = -u \tanh(ub) \tag{4.19}$$

lie in the strip $k_o \leq \mathrm{Re}(\lambda) \leq k$ and are all real. Graphical solutions for the roots of these two equations are shown in Figures 4.3 and 4.4 with the circles having radii a given by

$$a^2 = (\sqrt{\epsilon_r}-1) \quad (k_o b)^2 \tag{4.20}$$

From these figures it is obvious that a surface-wave mode exists only if a is greater than $\frac{\pi}{2}$. As $k_o b$ increases, the number of proper and improper roots increase continually. The proper roots characterized by positive real values for u_o and positive imaginary values for u lie on the proper Riemman sheet while the improper roots, characterized by negative real values for u_o and positive imaginary values for u, lie on the improper Riemman sheet. Because of their location, only the proper roots yield surface wave modes and these have a significant effect on the input impedance and radiation characteristics of printed antennas.

4-2. NUMERICAL INTEGRATION OF THE INTEGRALS

The integrals in the expression for the elements of the generalized impedance matrix can be put in the following two forms:

$$I_1 = \int_{x_k}^{x_{k+1}} dx\, \phi(x) \int_{x_j}^{x_{j+1}} dx' \sigma(x') \int_0^\infty J_o(\lambda r_1)\, f(\lambda, b, \epsilon_r)\, \lambda d\lambda \tag{4.21}$$

and

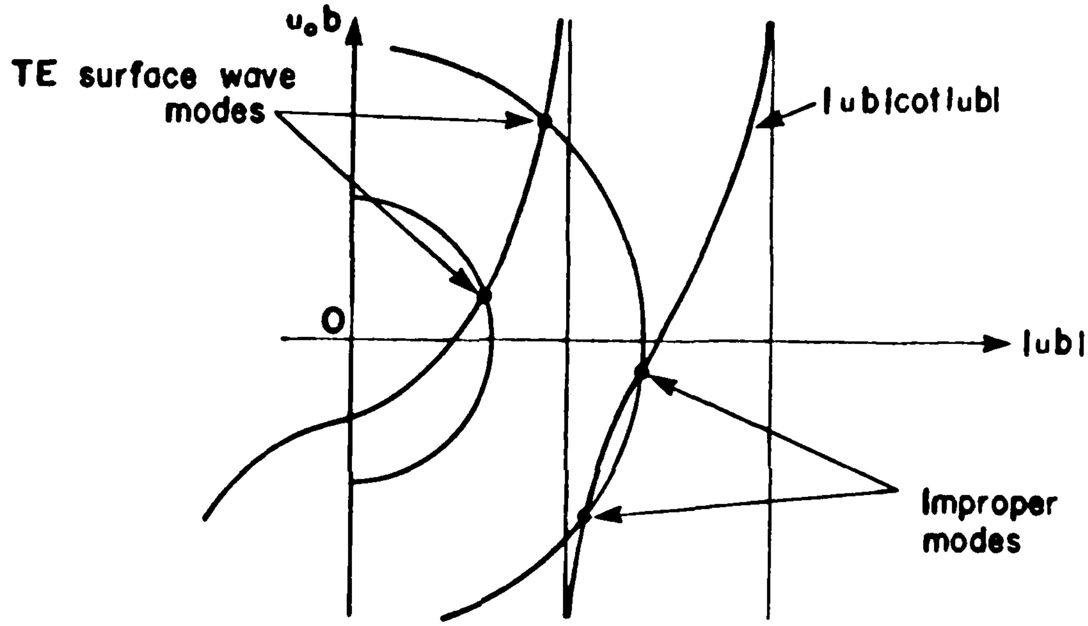

Figure 4.3: Graphical Solution of the Equation $u_o b = |ub| \cot |ub|$

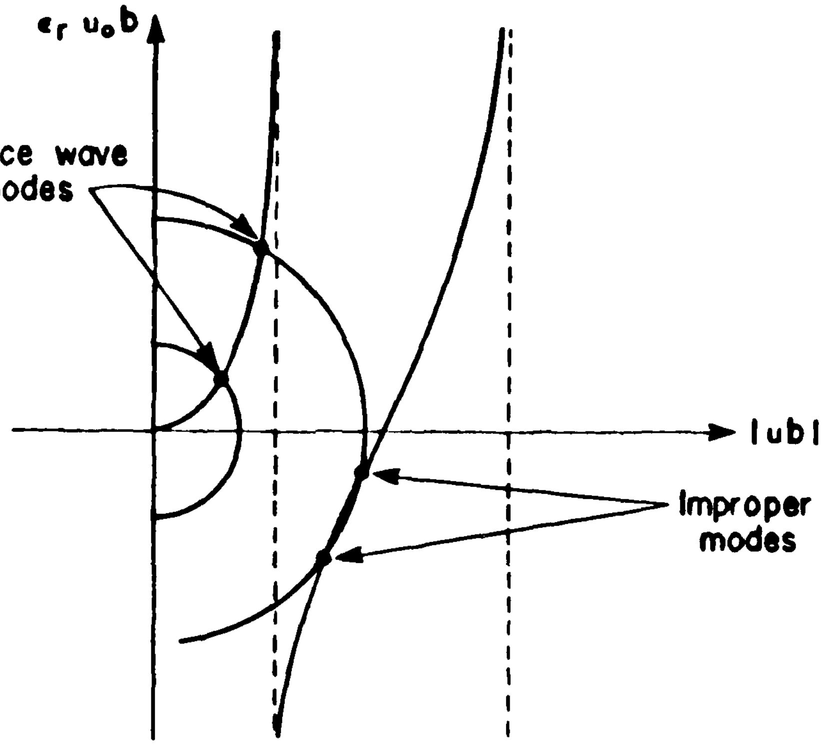

Figure 4.4: Graphical Solution of the Equation $\epsilon_r u_o b = |ub| \tan |ub|$

$$I_2 = \int_{x_k}^{x_{k+1}} dx\ \phi(x) \int_0^{\infty} J_o(\lambda \rho_2)\ f(\lambda, b, \varepsilon_r)\ \lambda d\lambda \tag{4.22}$$

with

$$\rho_1 = [(x-x')^2 + (y-y')^2]^{\frac{1}{2}} \tag{4.23}$$

$$\rho_2 = [(x-x_j)^2 + (y-y')^2]^{\frac{1}{2}} \tag{4.24}$$

The infinite integration is performed along the real axis and is completed in two steps:

1) Numerical integration over the interval $[0,A]$ where A satisfies the relationship $\coth(\sqrt{A^2 - k^2}\ b) \doteq 1$

2) Analytical evaluation of the tail contribution which is actually the integration over the path $[A,\infty)$.

These two integrations will be analyzed separately because they have to be treated in very different ways.

4-3. <u>INTEGRATION OVER THE INTERVAL</u> [0,A]

The integrals given by equ. (4.21)and (4.22) are now in the form

$$I_1 = \int_{x_k}^{x_{k+1}} dx\ \phi(x) \int_{x_j}^{x_{j+1}} dx'\ \sigma(x') \int_0^A J_o(\lambda\rho_1)\ f(\lambda, b, \varepsilon_r)\ \lambda d\lambda \tag{4.25}$$

$$I_2 = \int_{x_k}^{x_{k+1}} dx\ \phi(x) \int_0^A J_o(\lambda\rho_2)\ f(\lambda, b, \varepsilon_r)\ \lambda d\lambda \tag{4.26}$$

Consider that the function $F(\rho, b, \varepsilon_r)$ is given by

$$F(\rho, B, \varepsilon_r) = \int_0^A J_o(\lambda\rho)\ f(\lambda, b, \varepsilon_r)\ \lambda d\lambda \tag{4.27}$$

In order to find the first-order derivative of the function $F(\rho, b, \varepsilon_r)$ with respect to x, both sides of equation (4.27) are differentiated and the order of integration and differentiation is interchanged, yielding

$$\frac{d\ F(\rho,b,\varepsilon_r)}{dx} = \int_0^A \frac{d\ J_o(\lambda\rho)}{dx}\ f\ (\lambda,b,\varepsilon_r)\ \lambda d\lambda \tag{4.28}$$

Since ρ is the distance between the source and the observation point, given by

$$\rho = [(x-x')^2 + (y-y')^2]^{1/2} \tag{4.29}$$

the derivative of this zero-order Bessel function (equation 4.28) can be written as follows:

$$\frac{d\ J_o(\lambda\rho)}{dx} = -\lambda\ \frac{J_1(\lambda\rho)}{\rho}\ (x-x') \tag{4.30}$$

Equations (4.30) and (4.28) result in the following relation:

$$\frac{d\ F(\rho,b,\varepsilon_r)}{dx} = -\ \frac{x-x'}{\rho} \int_0^A J_1(\lambda\rho)\ f(\lambda,b,\varepsilon_r)\lambda^2 d\lambda \tag{4.31}$$

From (4.31) it is obvious that the derivative of $F(\rho,b,\varepsilon_r)$ with respect to x can take large values for specific b and ε_r which in turn increases considerably the error of integration in (4.25) and (4.26).

In order to avoid this undesirable integration error it has been found necessary to interchange the order of integration so that the space domain integration can be performed first. Thus, equations (4.25) and (4.26) take the form

$$I_1 = \int_0^A d\lambda\ \lambda\ f(\lambda,b,\varepsilon_r) \int_{x_k}^{x_{k+1}} dx\ \phi(x) \int_{x_j}^{x_{j+1}} dx'\ \sigma(x')\ J_o(\lambda\rho_1) \tag{4.32}$$

$$I_2 = \int_0^A d\lambda\ \lambda\ f(\lambda,b,\varepsilon_r) \int_{x_k}^{x_{k+1}} dx\ \phi(x)\ J_o(\lambda\rho_2) \tag{4.33}$$

Because of the way A has been defined, A is much larger than k. Therefore as λ moves from 0 to A, it passes through the values k_o and

k, causing the radicals u_o and u to alternate between pure real and pure imaginary values. This fact, as well as the existence of poles between k_o and k, make it necessary to divide the integration interval into the following subintervals:

1) $0 < \lambda < k_o$: The integration over this interval is performed numerically, using a modified Romberg-quadrature method [39], [40] for the integration with respect to λ and Gaussian-quadrature with fixed points [41] for the double and single x and x'-integrations. The integrals contribute to the radiation resistance and to the reactive part of the input impedance.
2) $k_o < \lambda < k$: For the integration over this interval a singularity extraction technique is used (see Appendix E) which transforms the integral into a finite series plus an integral of a slowly varying function. This finite series gives the contribution of the surface wave modes and the number of its terms depends on the thickness of the dielectric as well as the dielectric constant ε_r.
3) $k < \lambda < A$: Numerical integration is again invoked here in exactly the same way as it is performed in the first sub-interval.

4-4. <u>TAIL CONTRIBUTION</u>

In this case the integration with respect to λ is extended along the interval $[A, \infty)$. The use of the equality

$$\coth\left(\sqrt{\lambda^2 - k^2}\, b\right) = 1 \quad \text{for } \lambda \geq A \tag{4.34}$$

simplifies the integrand to a form which involves radicals of u_o, u. The order of integration is not changed in the integrals (4.21) - (4.22) but the infinite integration is evaluated analytically by making some approximations which are found to introduce a negligible error. From these results the integrations obtained by the method of moments are computed numerically. A technique of extraction of the fast varying terms is adopted to obtain better accuracy and to reduce computer time.

Using the relation (4.34) the Green's function as it appears in Pocklington's Integral Equations (2.52) and (2.53) is given by

$$G_x(\text{tail}) = \int_A^\infty J_o(\lambda\rho)\, e^{-u_o z} \frac{e^{uz'}}{u_o+u}\, \lambda d\lambda \qquad \begin{matrix} z \geq 0 \\ z' \leq 0 \end{matrix} \quad (4.35)$$

$$G(\text{tail}) = \int_A^\infty J_o(\lambda\rho)\, e^{-u_o z}\, e^{uz'} \left[\frac{1}{u_o+u} - \frac{1}{\varepsilon_r u_o + u}\right] \lambda d\lambda \qquad \begin{matrix} z \geq 0 \\ z' \leq 0 \end{matrix} \quad (4.36)$$

$$G_x^d(\text{tail}) = \frac{1}{2}\int_A^\infty J_o(\lambda\rho) \left[\frac{e^{-u|z+z'|}}{u}\, \frac{u-u_o}{u+u_o} + \frac{e^{-u|z+z'|}}{u}\right] \lambda d\lambda \quad z,z' \leq 0 \quad (4.37)$$

$$G^d(\text{tail}) = \frac{1}{2}\int_A^\infty J_o(\lambda\rho)\, e^{-u|z+z'|} \left[\frac{1}{u_o+u} - \frac{\varepsilon_r}{\varepsilon_r u_o + u}\right] \lambda d\lambda \qquad z,z' \leq 0 \quad (4.38)$$

where the factors $-\dfrac{j\omega\mu_o}{2\pi k_o^2}$ and $-\dfrac{j\omega\mu_o}{2\pi k^2}$ have been suppressed.

Since $\lambda > A$, with A sufficiently larger than k_o and k, after application of the binomial series expansion to these radicals the tail part of the integrals can be written as

$$G_x(\text{tail}) = \frac{1}{2}\, \frac{1}{[1-\varepsilon_1(A)]\,[1-\varepsilon_2(A)]} \left\{\frac{1}{\rho} - F_o\right\} \qquad (4.39)$$

$$G(\text{tail}) = \frac{1}{2}\left\{\frac{1}{[1-\varepsilon_1(A)]\ [1-\varepsilon_2(A)]} - \frac{2}{(\varepsilon_r+1)[1-\varepsilon_2(A)][1-\varepsilon_3(A)]}\right\}\cdot\left\{\frac{1}{\rho} - F_o\right\} \tag{4.40}$$

$$G_x^d(\text{tail}) = -\frac{\varepsilon_1(A)}{2[1+\varepsilon_1(A)]}\left\{\frac{1}{R_1} - F_1\right\} + \frac{1}{2}\left\{\frac{1}{R_2} - F_2\right\} \tag{4.41}$$

$$G^d(\text{tail}) = \left\{\frac{1}{4}\ \frac{1}{1+\varepsilon_1(A)} - \frac{1}{2}\ \frac{1}{(1+\varepsilon_r)[1+\varepsilon_3(A)]}\right\}\cdot\left\{\frac{1}{R_1} - F_1\right\} \tag{4.42}$$

where

$$\rho = [(x-x')^2 + (y-y')^2]^{1/2} \tag{4.43}$$

$$F_o = A\ J_o(A\rho) - \frac{\pi A}{2}\ [J_1(A\rho)\ H_o(A\rho) - J_o(A\rho)\ H_1(A\rho)] \tag{4.44}$$

$$R_1 = [(z+z')^2 + \rho^2\ [1+\varepsilon_4(A)]^2]^{1/2} \tag{4.45}$$

$$R_2 = [(z-z')^2 + \rho^2\ [1+\varepsilon_4(A)]^2]^{1/2} \tag{4.46}$$

$$F_1 = \int_o^{\sqrt{A^2-k^2}} J_o\ (t\rho[1+\varepsilon_4(A)])\ e^{-t|z+z'|}\ dt \tag{4.47}$$

$$F_2 = \int_o^{\sqrt{A^2-k^2}} J_o\ (t\rho[1+\varepsilon_4(A)])\ e^{-t|z-z'|}\ dt \tag{4.48}$$

The integrals (4.47) and (4.48) are evaluated numerically while the functions $\varepsilon_1(A)$, $\varepsilon_2(A)$, $\varepsilon_3(A)$ and $\varepsilon_4(A)$ are correction functions because of the error introduced from the neglected higher order terms in the binomial expansion. For a value of A approximately equal to $\frac{120}{2\pi}$ the error is no larger than 10^{-4} of the value of the tail contri-

bution and it can be neglected.

By substituting these expressions for the tail part of the Green's function into equations (4.21) and (4.22) and by using a technique for extraction of the fast varying terms one can show that the integrals are reduced to a summation of integrals. The integrads are summations of slowly varying functions and a finite series of logarithmic functions resulting from the integration of the terms $\frac{1}{\rho}$, $\frac{1}{R_1}$ and $\frac{1}{R_2}$ in equations (4.39) to (4.42).

CHAPTER 5

NUMERICAL RESULTS

5-1. DESIGN PROCEDURE FOR MICROSTRIP DIPOLES

This chapter presents design procedures for microstrip dipoles printed on or embedded in the dielectric substrate. Numerical computations have been performed for very thin wire dipoles with a radius $a = 0.0001\ \lambda_o$. The dipoles are center-fed by an in phase unit voltage delta gap generator except for one particular case where the dipole is fed asymmetrically. All the dimensions presented are normalized with respect to the free space wavelength λ_o. Due to an assumed time dependency of $e^{j\omega t}$, inductive reactance is positive in all plots. The material given here relates the antenna geometry (dipole length, substrate thickness, dielectric constant, dipole-ground plane distance and feed point location) to antenna characteristics (resonant length, resonant resistance, current distribution and bandwidth). The presentation of the numerical results is completed in three steps; at first a dipole printed on the dielectric interface is considered and its characteristics are discussed in terms of the dielectric constant and substrate thickness. After that, this dipole is considered as being embedded in the dielectric and the change in its performance is studied. At the position $b' = \frac{b}{2}$ the dipole characteristics are considered in terms of the dielectric constant and the substrate thickness and are compared to the corresponding values for the printed dipole.

5-2. DIPOLE PRINTED ON THE DIELECTRIC INTERFACE

a. RELATIVE DIELECTRIC CONSTANT VARIATION

One of the most important characteristics of a given dipole is its input impedance. Figures 5.1, 5.2 and 5.3 show the real and imaginary parts of the input impedance when the thickness of the dielectric substrate is equal to $0.1016\lambda_o$. The relative dielectric constant with values of 2, 10 and 35 permits the excitation of one, two and three surface waves respectively. From these figures as well as additional data, it has been concluded that, as the relative permitivity increases, the reactance becomes increasingly capacitive. The indicated trend is that fewer resonances occur with larger ε_r. In addition the input resistance curves show an increasing number of oscillations and a decreasing maximum value. The latter observation implies less and less energy radiated into space, i.e. a decrease in the radiation efficiency of the antenna, since energy is trapped in the dielectric substrate in the form of surface modes. Figure 5.4 shows how the resonant length L_r varies as a function of ε_r. The effect on the resonant length of each new excited surface wave is expressed as a discontinuity in the derivative $\frac{\partial L_r(\varepsilon_r)}{\partial \varepsilon_r}$ which happens exactly at the transition points. Figure 5.4 is also another interpretation of the decreasing radiation efficiency of the antenna since L_r decreases with increasing ε_r. Figure 5.5 shows the current distribution on a dipole of length L = $0.65\ \lambda_o$ with substrate thickness b = $0.1016\ \lambda_o$ and for ε_r equal to 2, 10 and 35. The increasing ε_r (from 2 to 35) results in a larger number of zeros of the current distribution and more electromagnetic

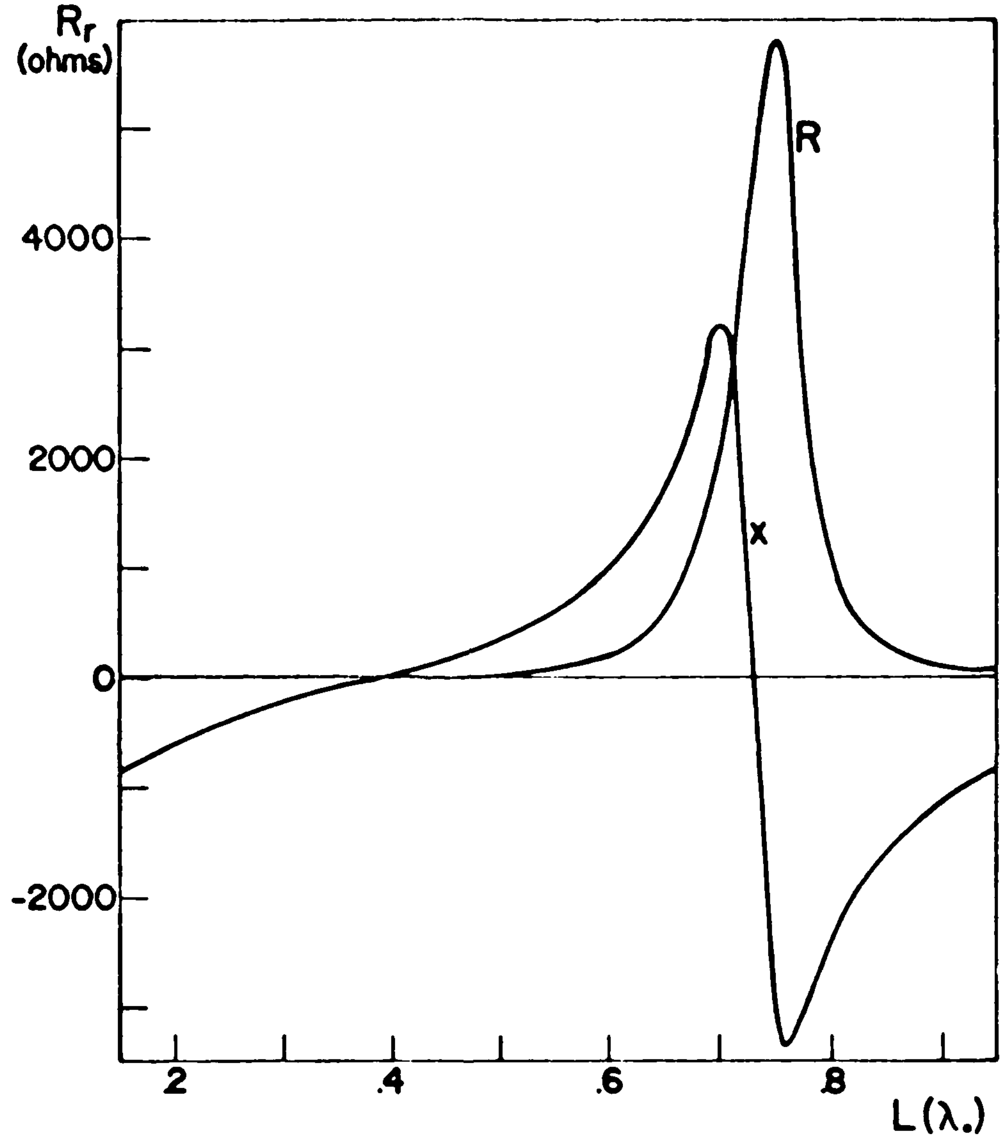

Figure 5.1: Input Impedance for a Printed Dipole with $\epsilon_r=2$ and $b=0.1016\lambda_o$ Resonant Length $L_r=0.38\lambda_o$

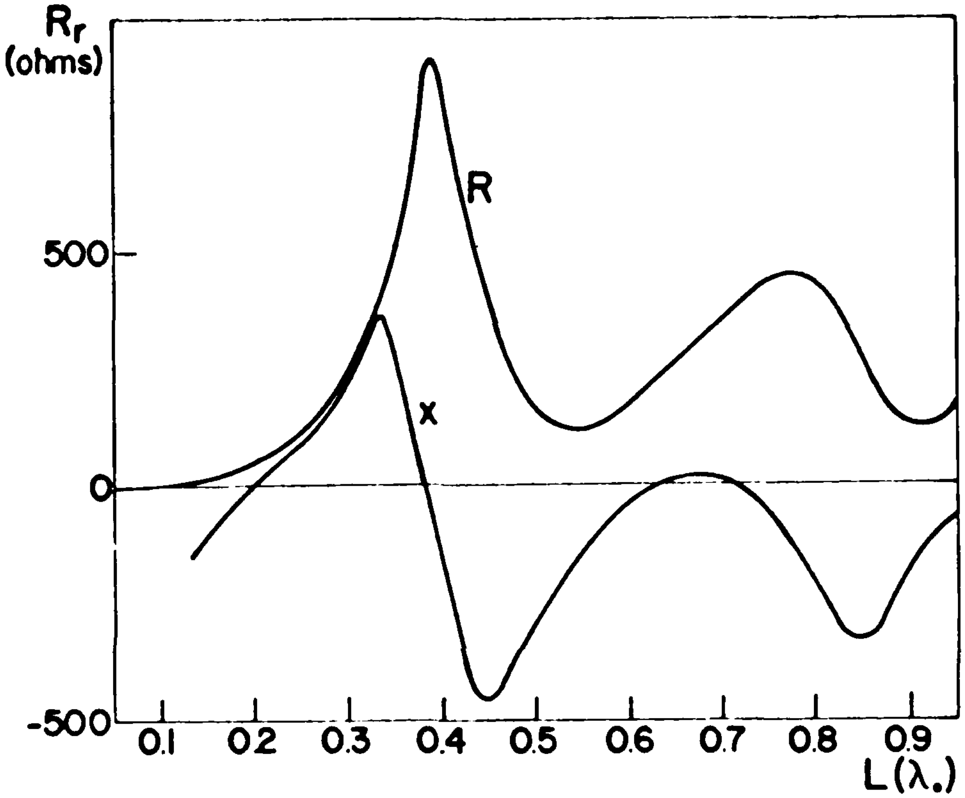

Figure 5.2: Input Impedance for a Printed Dipole with $\epsilon_r=10$ and $b=0.1016\lambda_0$ Resonant Length $L_r=0.205\lambda_0$

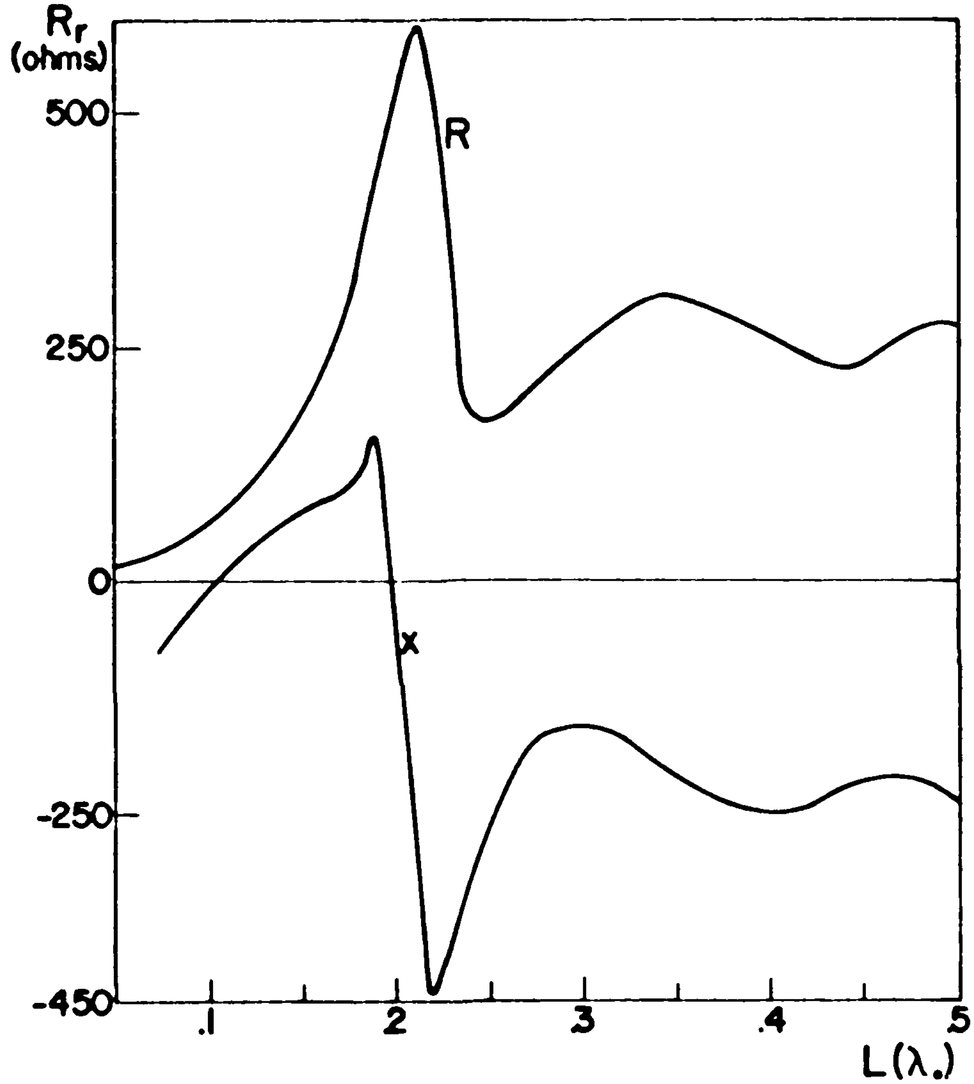

Figure 5.3: Input Impedance for a Printed Dipole with ϵ_r=35 and b=0.1016λ_o Resonant Length L_r=0.1025λ_o

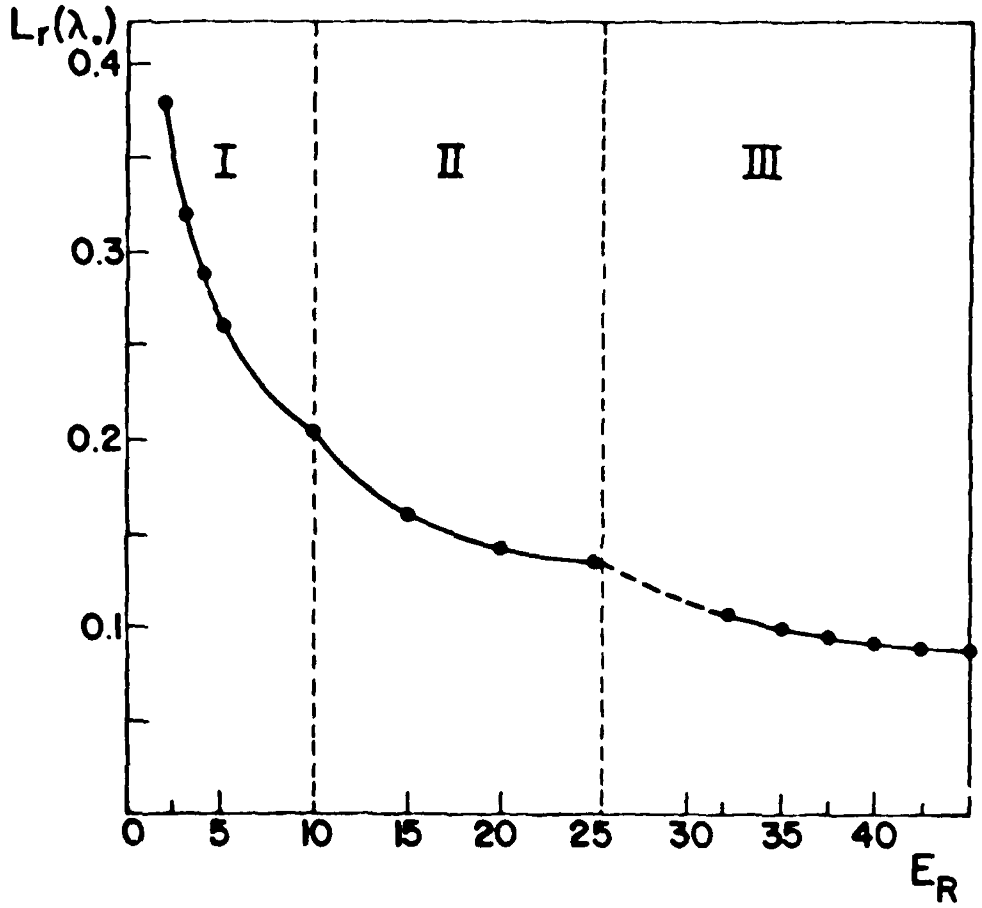

Figure 5.4: Resonant Length vs. Relative Dielectric Constant ϵ_r for the Printed Dipole with $b=0.1016\lambda_0$
I: One Surface Wave
II: Two Surface Waves
III: Three Surface Waves

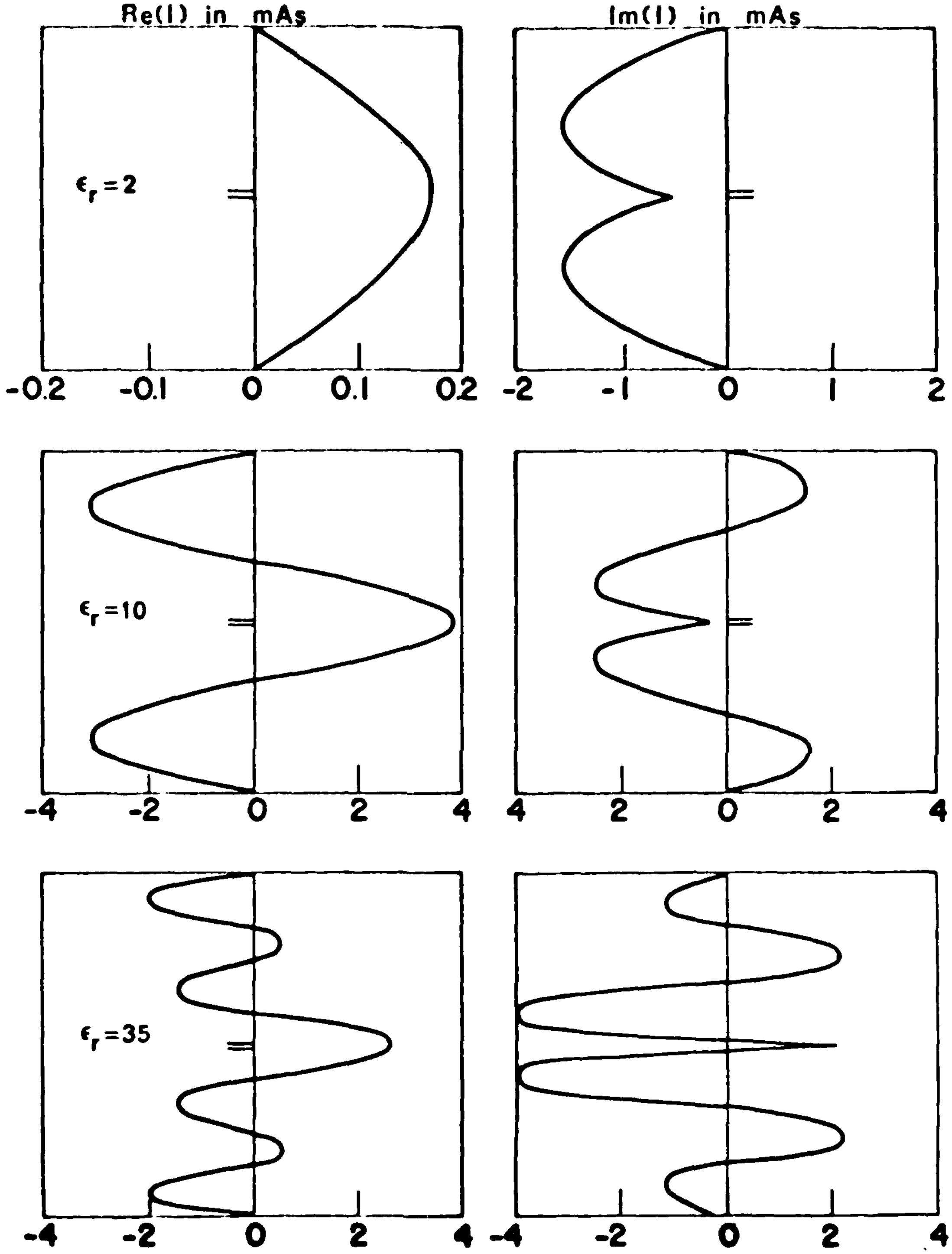

Figure 5.5: Current Distribution on a Printed Dipole with $b=0.1016\lambda_o$ and Length $L=0.65\lambda_o$

energy trapped in the dielectric which again means less radiated power.

b. SUBSTRATE THICKNESS VARIATION

As in section 5.2a, Figures 5.6, 5.7 and 5.8 show the real and imaginary parts of the input impedance when the relative dielectric constant is equal to 2.35 while the substrate thickness b takes the values 0.1016 λ_o, 0.25 λ_o and 0.46 λ_o causing one, two and three surface waves respectively to be excited. As the substrate thickness increases, despite the fact that more surface waves are excited, the possibility of many resonances is not affected. However, the increasing substrate thickness makes the resonant length varying as shown in Figure 5.9. In the region of one surface wave (I) the resonant length increases, reaches a maximum for b approximately equal to 0.32 λ_o (region II) and continues decreasing as b becomes larger. As in the case where the dielectric constant changes, here again the effect of each new excited surface wave on the resonant length L_r is expressed as a step discontinuity in the derivative $\frac{\partial L_r(\varepsilon_r)}{\partial \varepsilon_r}$. The definition of the bandwidth BW is assumed to be given by

$$BW = \frac{\omega_2 - \omega_1}{\omega_o} \tag{5.1}$$

where ω_2, ω_1 are the 3dB points of the response of the dipole considered by its equivalent circuit (see Appendix F). The bandwidth of the dipole and its resonant resistance as functions of the dielectric constant are shown in Figures 5.11 and 5.12. In these two figures, the fact that the bandwidth curve follows in shape the resonant-length curve is quite interesting. Both the resonant resistance and the bandwidth have their minimum value at $b = 0.38\lambda_o$ and their maximum value at $b = 0.22\lambda_o$ while

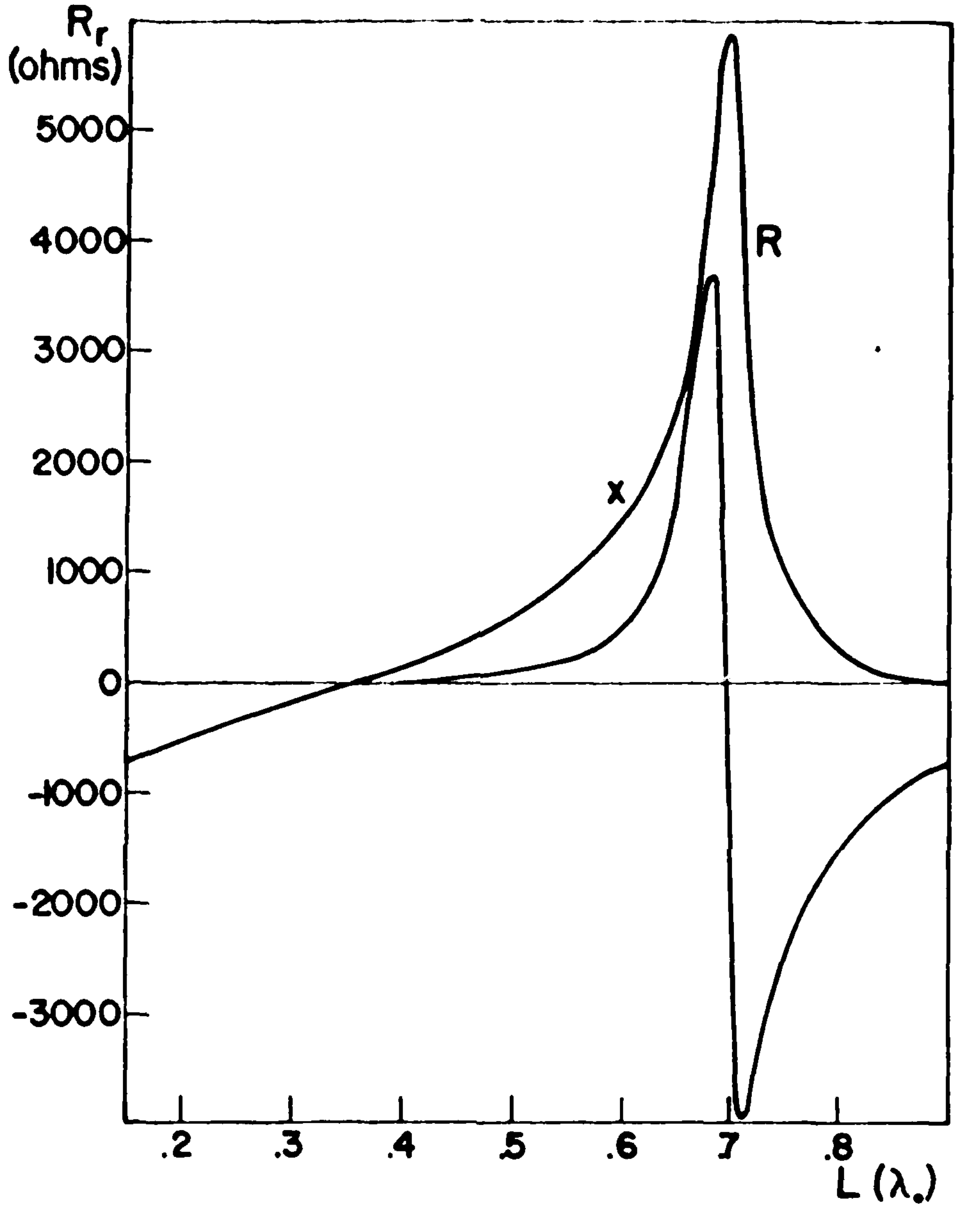

Figure 5.6: Input Impedance for a Printed Dipole with $\epsilon_r = 2.35$ and $b = 0.1016\lambda_o$ Resonant Length $L_r = 0.3575\lambda_o$

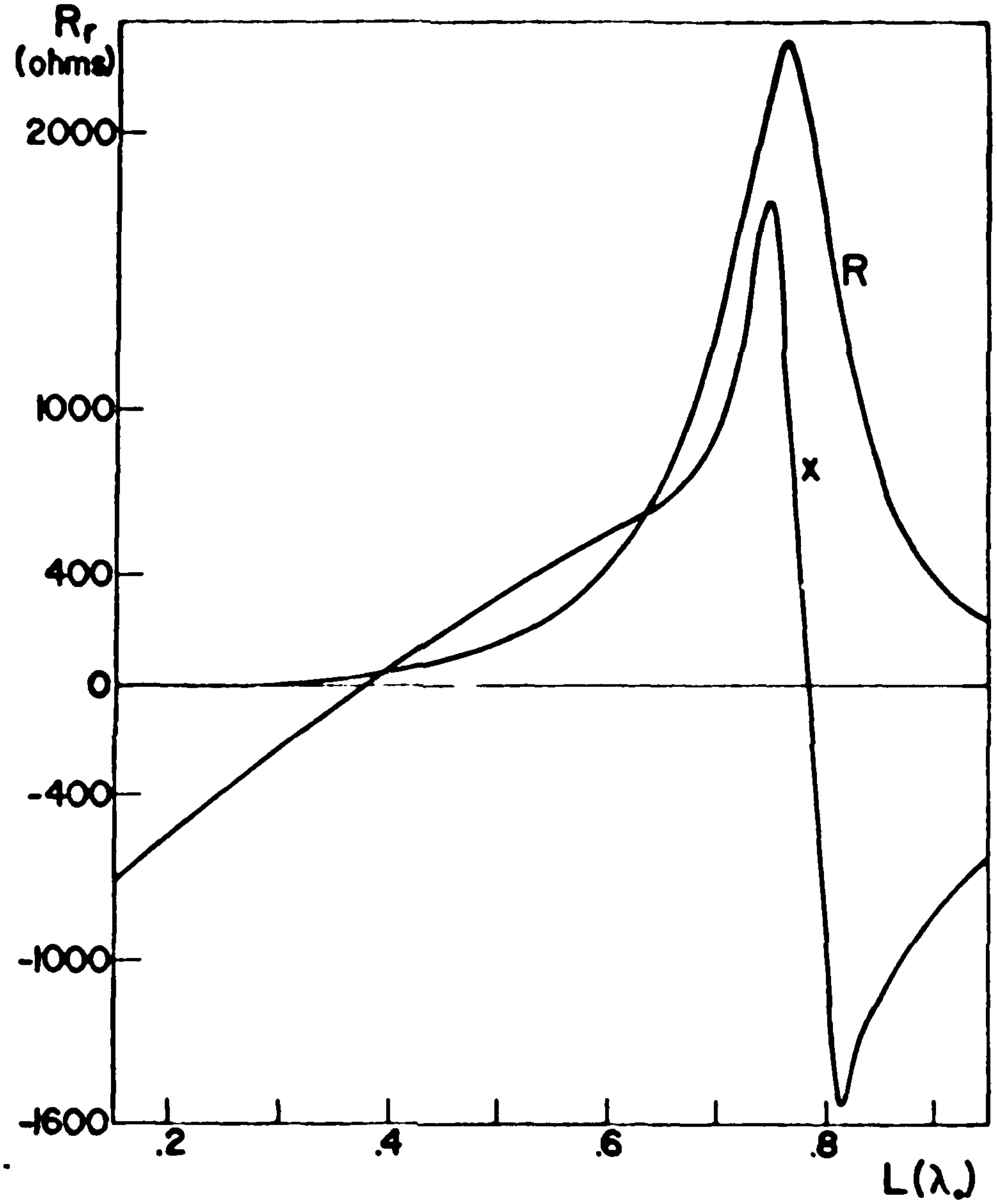

Figure 5.7: Input Impedance for a Printed Dipole with $\epsilon_r = 2.35$ and $b = 0.25\lambda_o$ Resonant Length $L_r = 0.381\lambda_o$

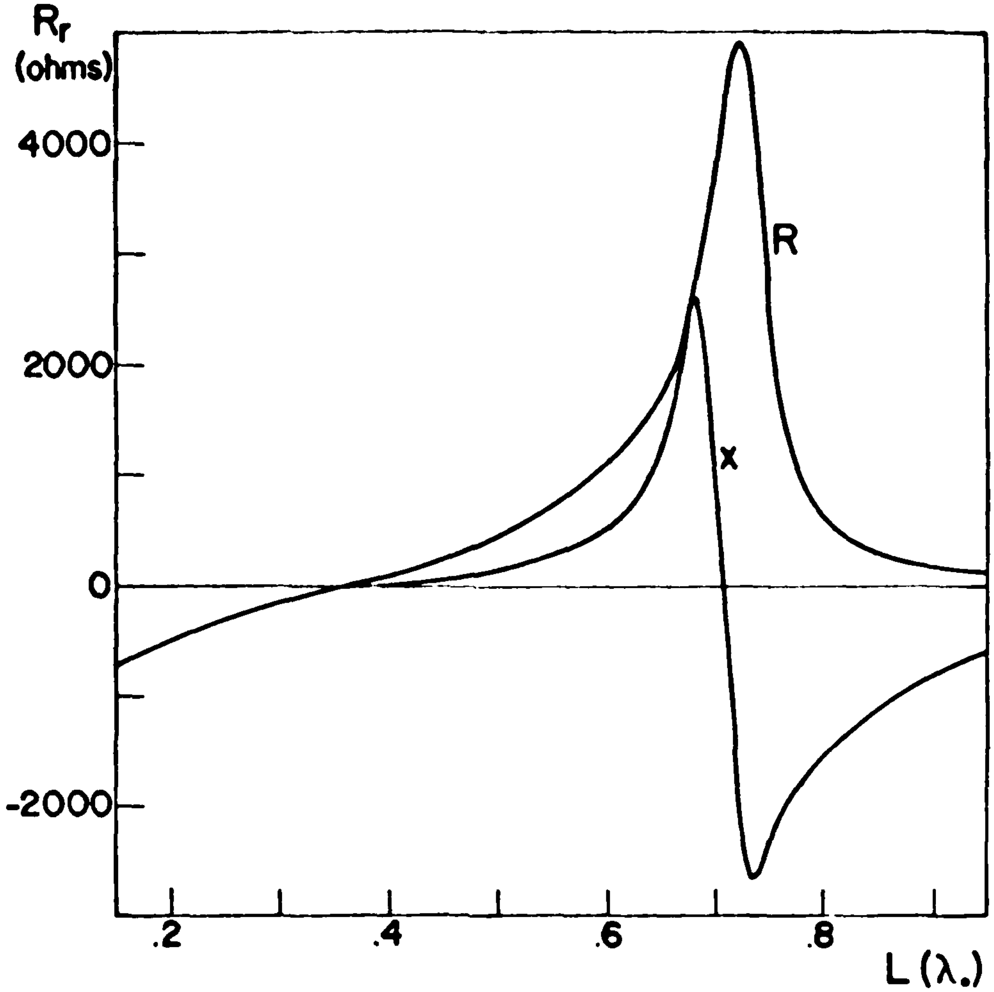

Figure 5.8: Input Impedance for a Printed Dipole with $\epsilon_r = 2.35$ and $b = 0.46\lambda_o$ Resonant Length $L_r = 0.3675\lambda_o$

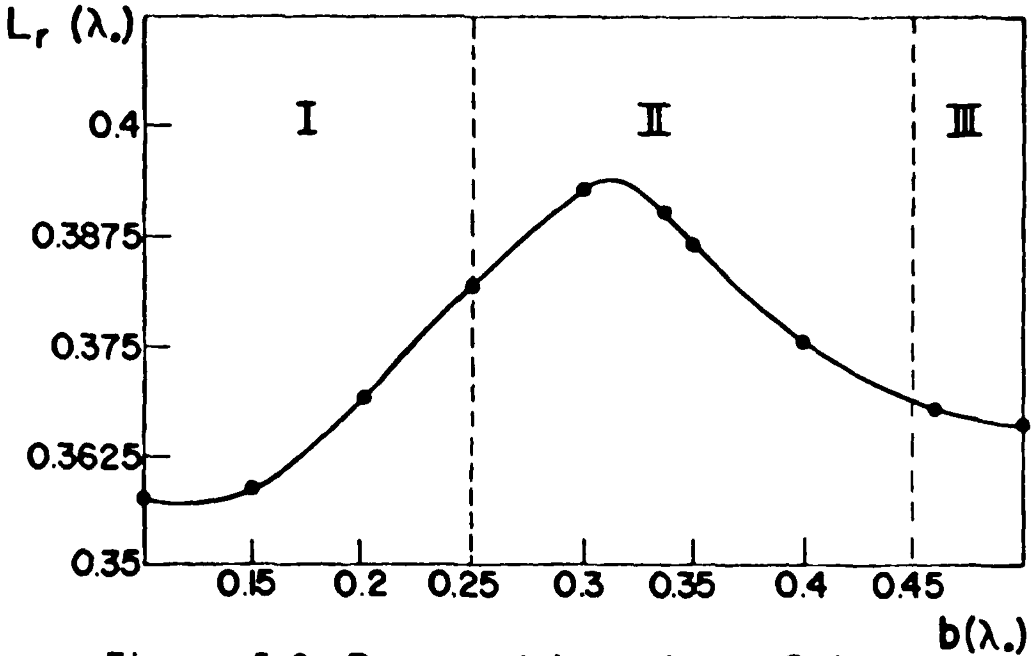

Figure 5.9: Resonant Length vs. Substrate Thickness b for a Printed Dipole with $\epsilon_r = 2.35$
I: One Surface Wave
II: Two Surface Waves
III: Three Surface Waves

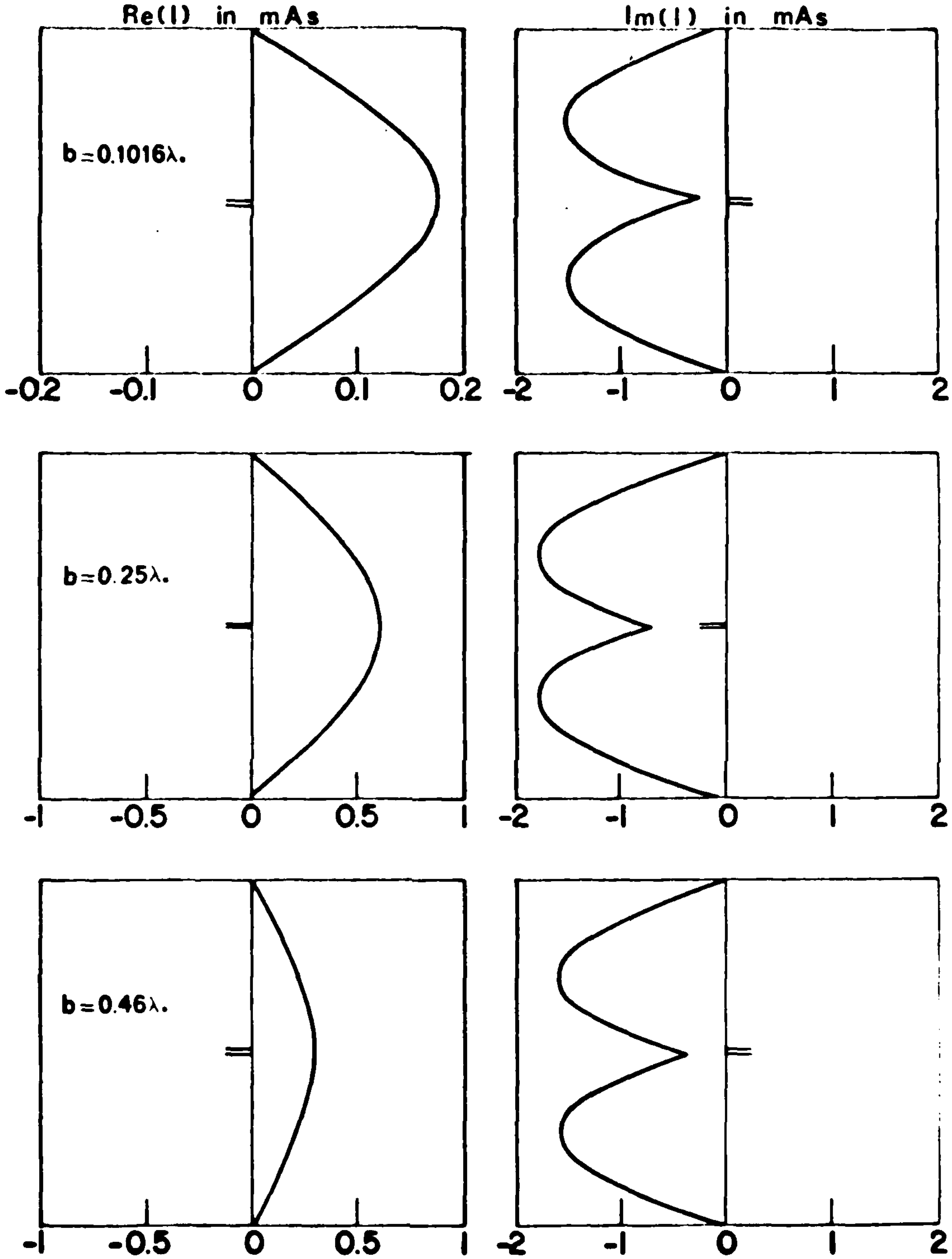

Figure 5.10: Current Distribution on a Printed Dipole with $\epsilon_r = 2.35$ and Length $L=0.65\lambda_o$

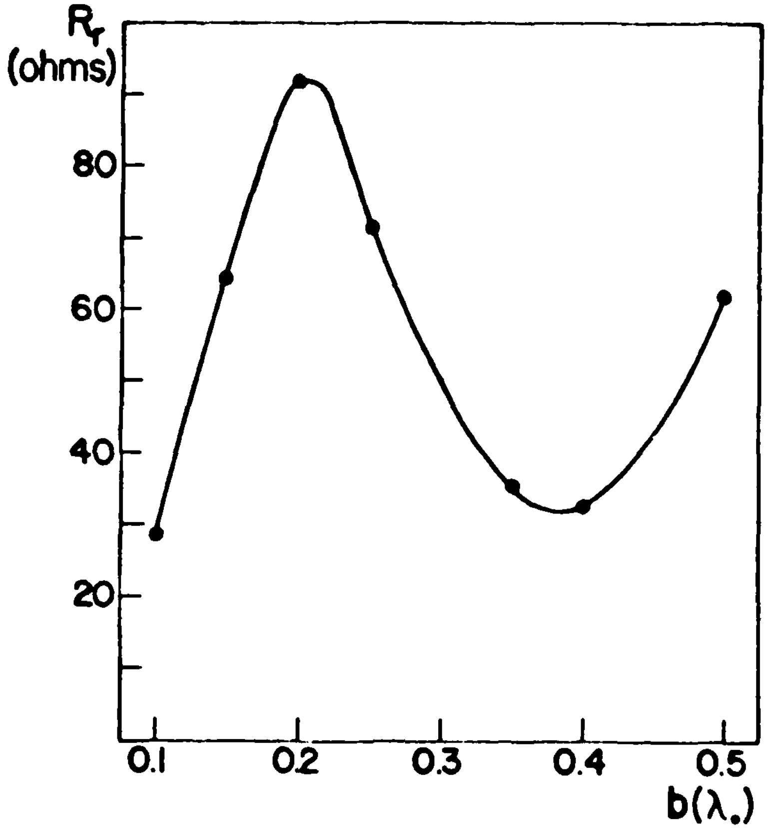

Figure 5.11: Resonant Resistance vs. Substrate Thickness b for a Printed Dipole with ϵ_r=2.35

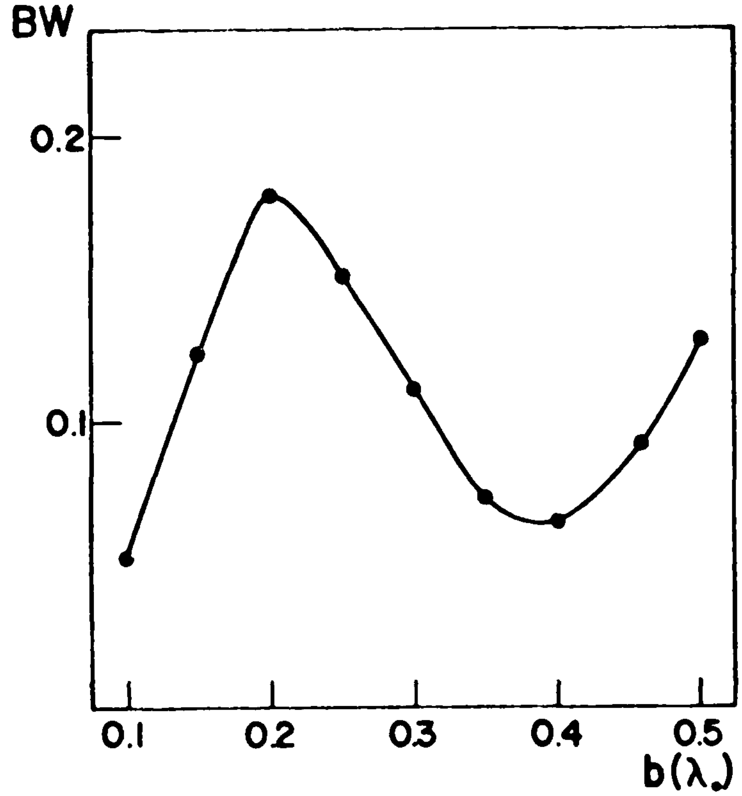

Figure 5.12: Bandwidth vs.Substrate Thickness b for a Printed Dipole with $\epsilon_r = 2.35$

the maximum resonant length occurs between these two values. The current distributions on a dipole of length $L = 0.65\ \lambda_o$ with $\epsilon_r = 2.35$ and for b equal to $0.1016\ \lambda_o$, $0.25\ \lambda_o$ and $0.46\ \lambda_o$ are given in Figure 5.10. From these figures it can be observed that the increasing number of surface waves coming from changes in the value of b does not affect the current distribution so much as it does when ϵ_r changes. Here again larger substrate thickness means more electromagnetic energy trapped in the dielectric and less radiated.

5-3. DIPOLE EMBEDDED IN THE SUBSTRATE

a. VARIATION OF DIPOLE EMBEDDING POSITION

Figure 5.13 shows the real and imaginary parts of the input impedance of a dipole printed on the dielectric interface with relative dielectric constant $\epsilon_r = 3.25$ and substrate thickness $b = 0.1016\ \lambda_o$. If the dipole is embedded in the dielectric substrate, the input impedance will change as shown in Figures 5.14, 5.15 and 5.16. From these figures it can be observed easily that the shape of the curves remains the same while the maxima and minima are shifted to smaller values of the dipole length. Figure 5.17 shows the resonant length L_r as a function of the dipole-ground plane distance. The change in the current distribution as a dipole of length $L = 0.65\ \lambda_o$ is placed closer to the perfect conductor plane is shown in Figures 5.20 and 5.21 for four different cases: $b' = b$, $b' = \frac{99}{100}\ b$, $b' = \frac{9}{10}\ b$ and $b' = \frac{2}{3}\ b$ where b' is the dipole-ground plane distance. Also Figures 5.18 and 5.19 show the resonant resistance R_r and the bandwidth BW as functions of b-b', the distance of the dipole from the air-dielectric interface.

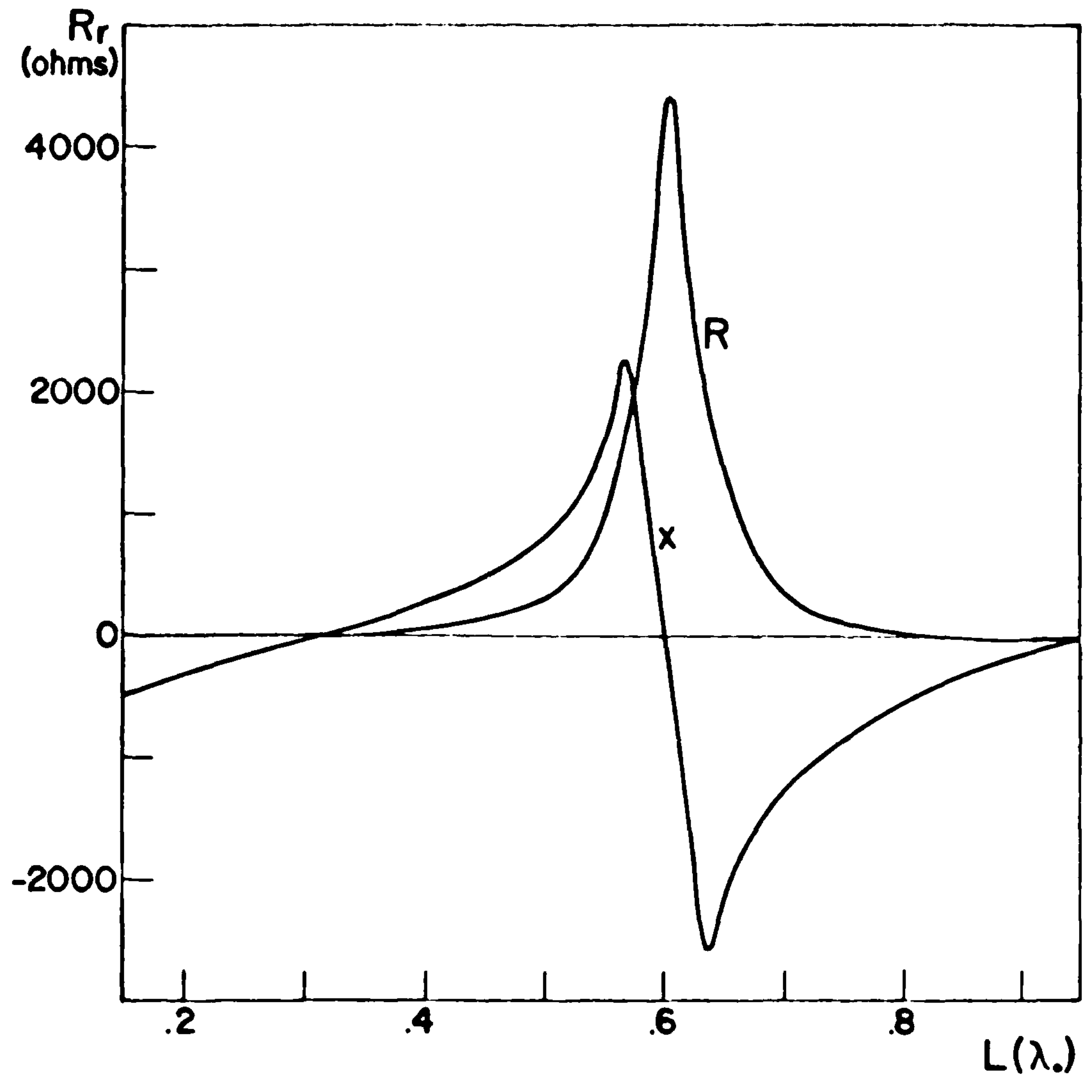

Figure 5.13 : Input Impedance for a Dipole with Embedding Distance b−b′=0, ϵ_r =3.25 and b=0.1016λ_o Resonant Length L_r=0.32λ_o

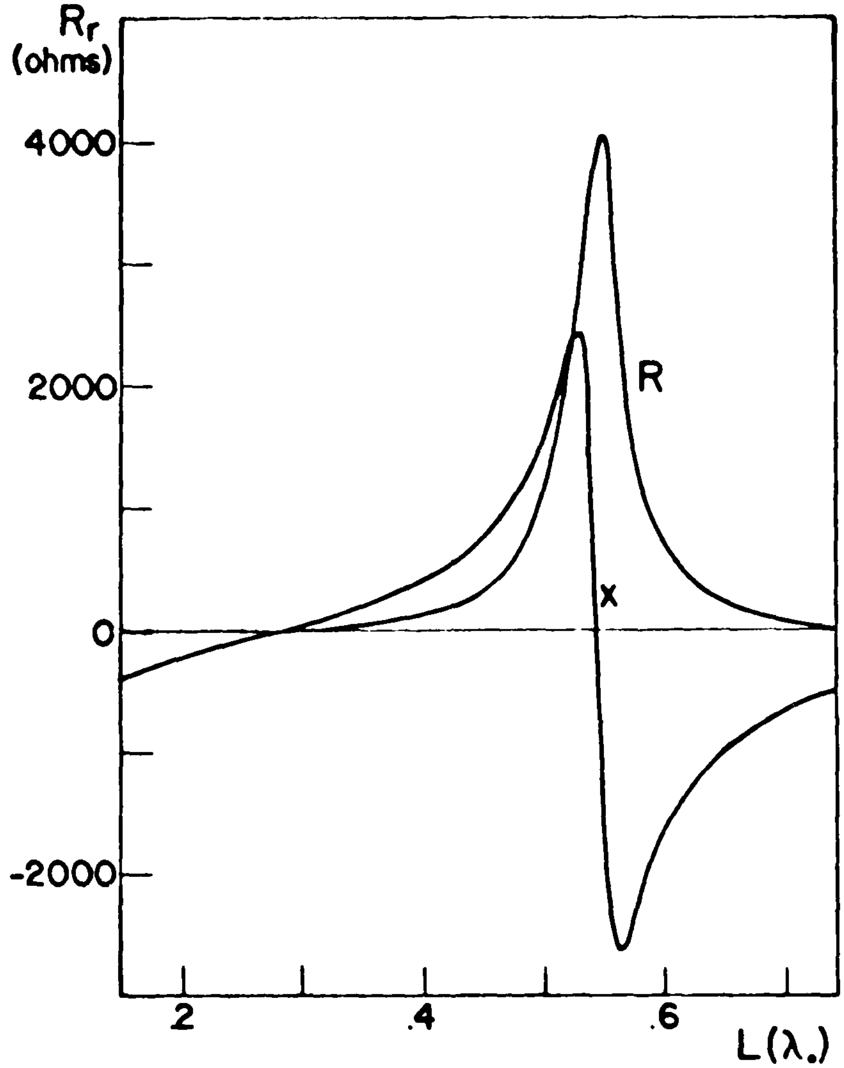

Figure 5.14: Input Impedance for a Dipole with Embedding Distance b−b′=b/100 ϵ_r=3.25 and b=0.1016λ_o Resonant Length L_r=0.2840λ_o

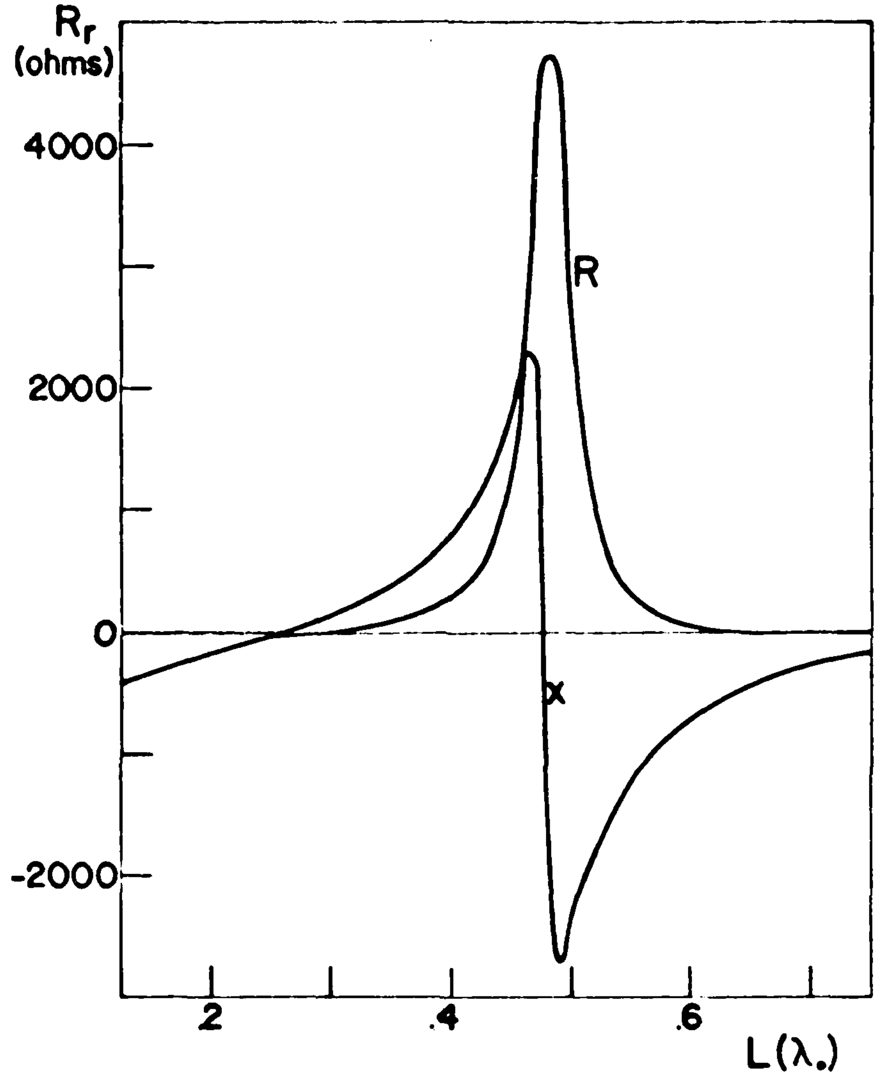

Figure 5.15: Input Impedance for a Dipole with Embedding Distance b-b'=b/10 $\epsilon_r = 3.25$ and $b = 0.1016\lambda_o$ Resonant Length $L_r = 0.2534\lambda_o$

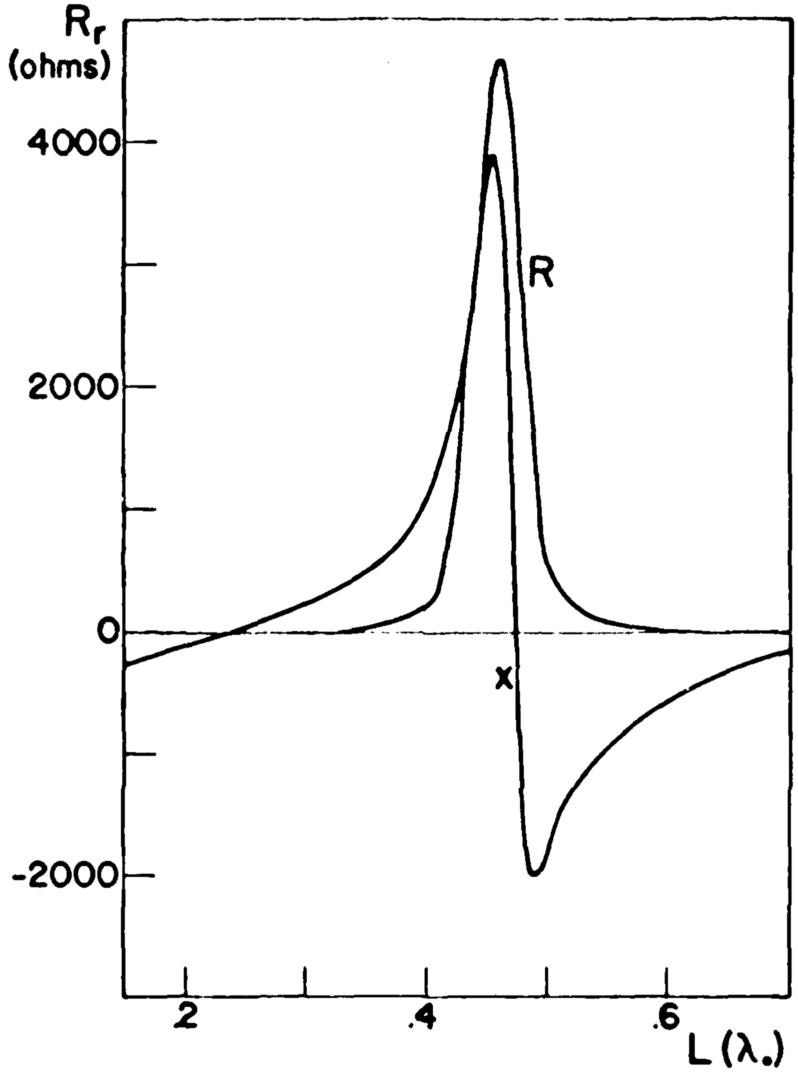

Figure 5.16: Input Impedance for a Dipole with Embedding Distance $b-b'=b/3$ $\epsilon_r=3.25$ and $b=0.1016\lambda_o$ Resonant Length $L_r=0.24\lambda_o$

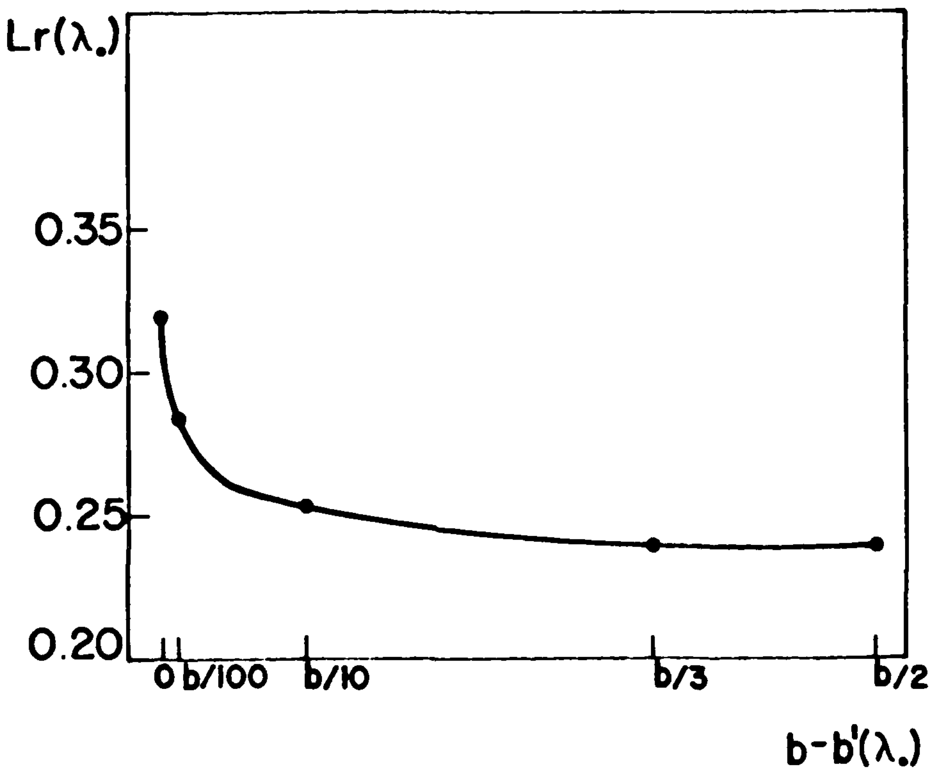

Figure 5.17: Resonant Length vs. Embedding Distance b-b' for a Dipole with ϵ_r=3.25 and b=0.1016λ_o

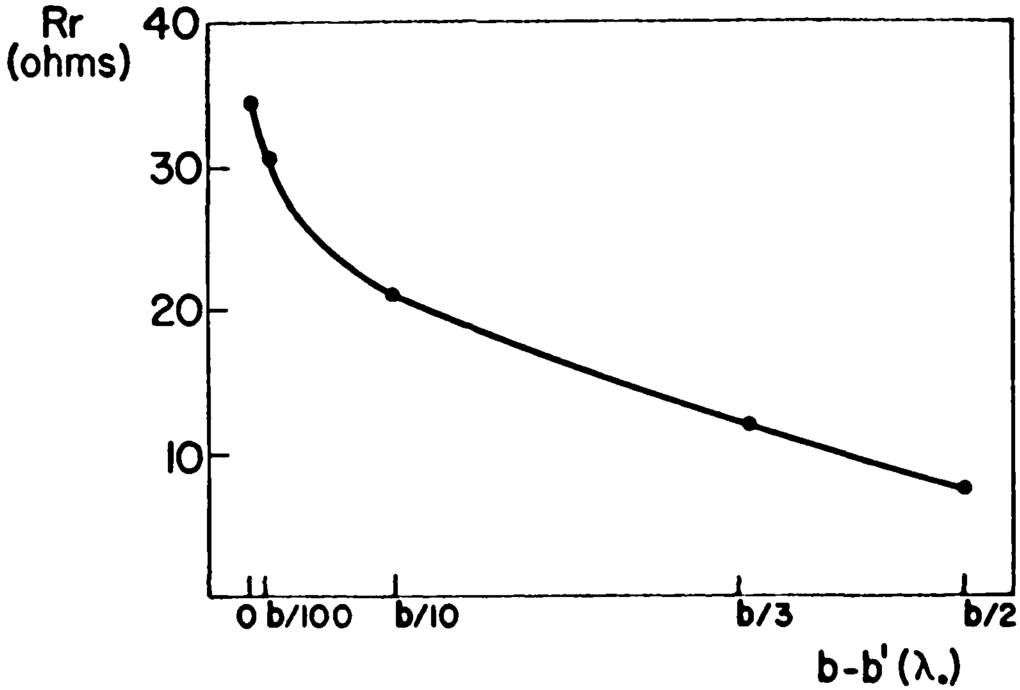

Figure 5.18: Resonant Resistance vs. Embedding Distance b-b' for a Dipole with ϵ_r=3.25 and b=0.1016λ_0

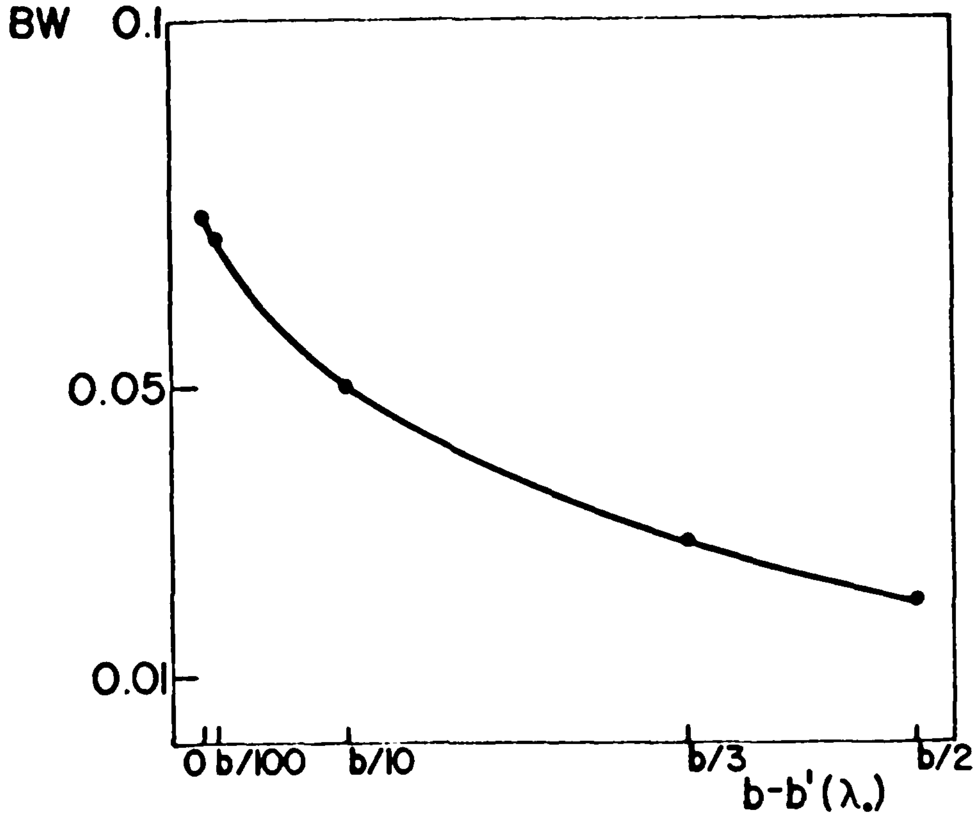

Figure 5.19: Bandwidth vs. Embedding Distance b−b′ for a Dipole with $\epsilon_r = 3.25$ and $b = 0.1016\lambda_0$

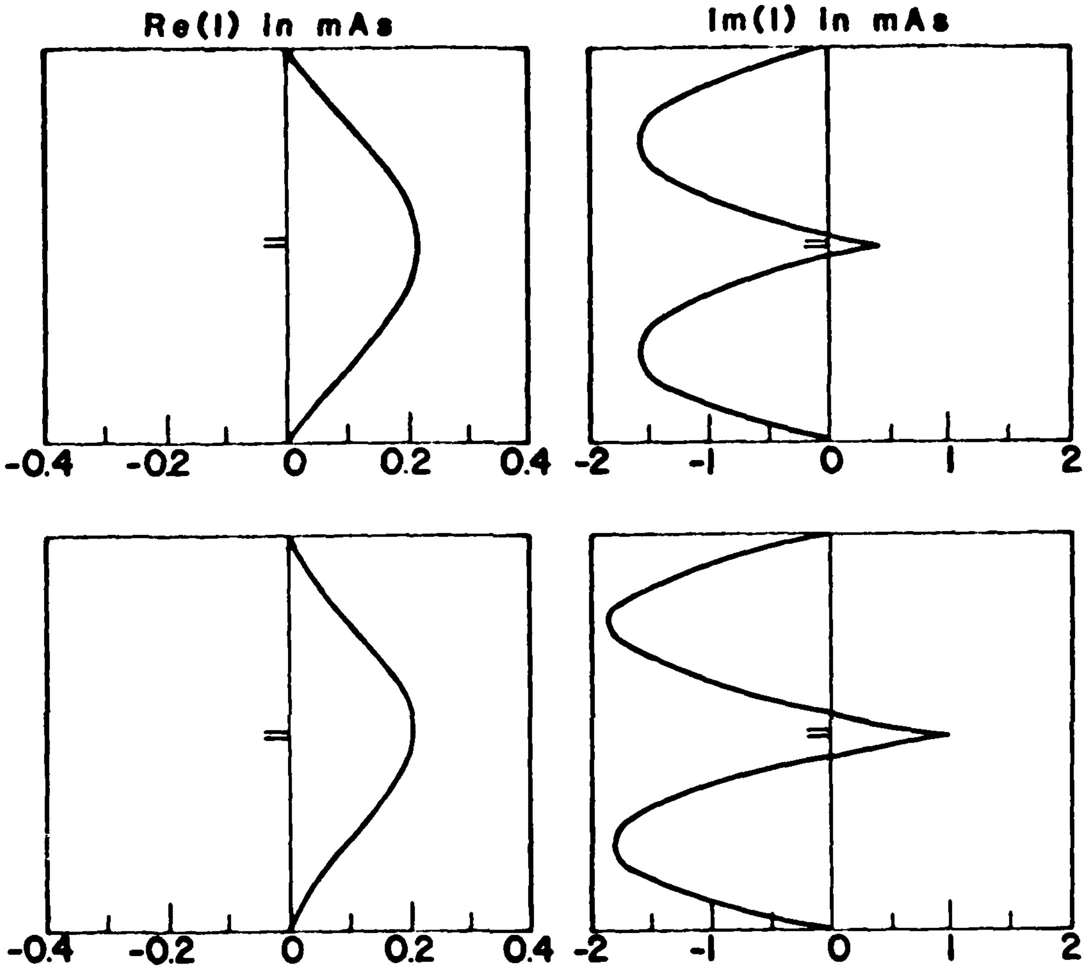

Figure 5.20: Current Distribution for a Dipole Embedded in the Substrate with ϵ_r=3.25,b=0.1016 and Length L =0.65λ
(a): Embedding Distance b−b′=0
(b): Embedding Distance b−b′=b/100

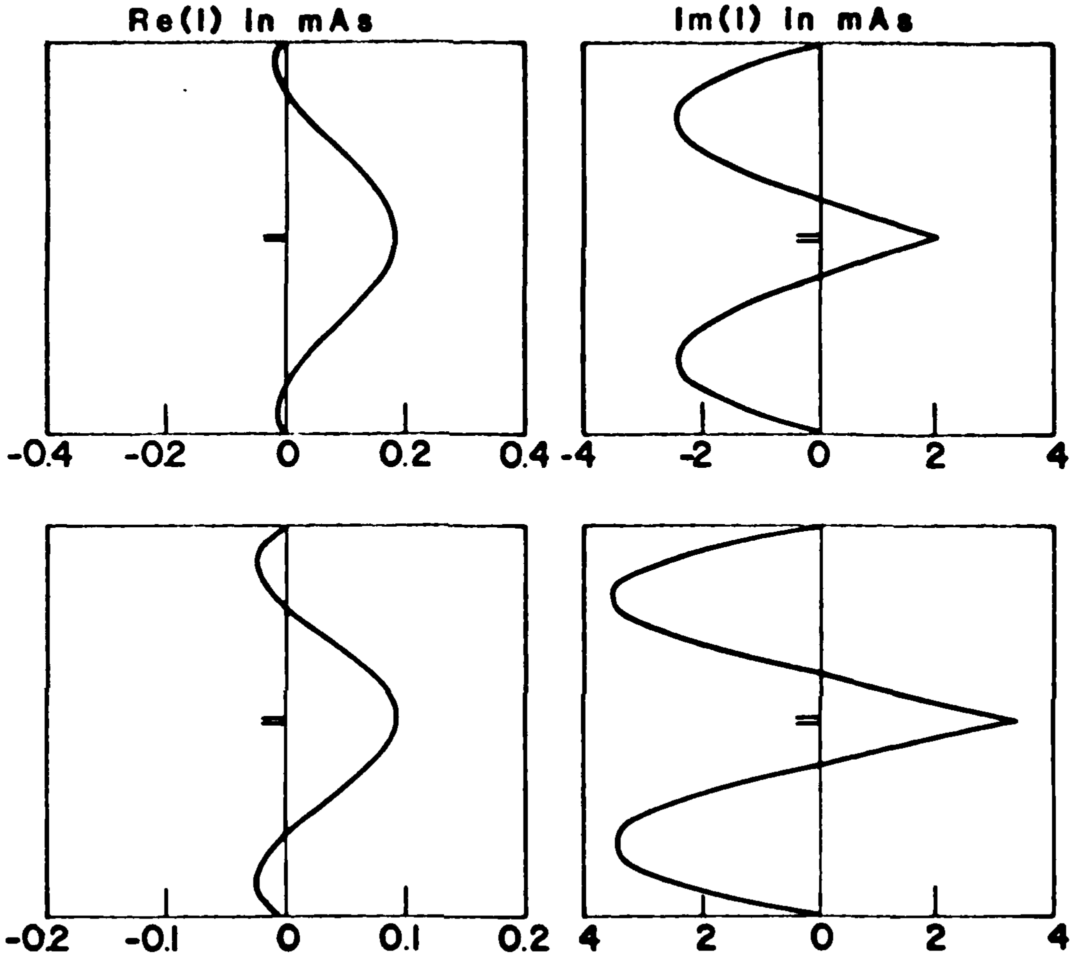

Figure 5.21: Current Distribution for a Dipole Embedded in the Substrate with ϵ_r =3.25,b=0.1016 and Length L=0.65λ_0
(c): Embedding Distance b−b′=b/10
(d): Embedding Distance b−b′=b/3

The high slope of these two curves as well as of the resonant length curve (Figure 5.17) for small values of b-b' is characteristic of the air-dielectric substrate electrical discontinuity.

b. RELATIVE DIELECTRIC CONSTANT VARIATION

We consider now the dipole shown in Figure 5.22. The thickness of the dielectric substrate is equal to 0.1016 λ_o and when it is combined with $\epsilon_r = 2$ and $\epsilon_r = 10$ it permits the excitation of one and two surface waves respectively. The real and imaginary parts of the input impedance for these two cases are shown in Figures 5.23 and 5.24. From these figures it can be observed that for the case of two surface waves, as well as for the case of one surface wave, many resonances are possible as the length of the dipole increases.

This does not happen when the same dipole is printed on the dielectric interface. Figure 5.25 shows how the resonant length L_r varies as a function of ϵ_r for three different positions of the dipole: a) printed on the interface(1), b) embedded in the substrate at a distance $\frac{2}{3}$ B (2), and c) $\frac{B}{2}$ (3) from the ground plane. It is quite interesting to note that as the dipole enters the dielectric substrate, its resonant Length-Dielectric Constant curve does not change shape but moves to smaller values for the resonant length. This means that curve 5.17 maintains its shape as the dielectric constant ϵ_r changes. For this reason it is expected again that the effect of each new excited surface wave on the resonant length will be expressed as a discontinuity in the derivative $\frac{\partial L_r(\epsilon_r)}{\partial \epsilon_r}$ and the curve $L_r = f(\epsilon_r)$ for ϵ_r larger than 10 will exhibit a similar variation as the one for the printed dipole (Figure 5.5). Figure 5.26 shows the current distribution

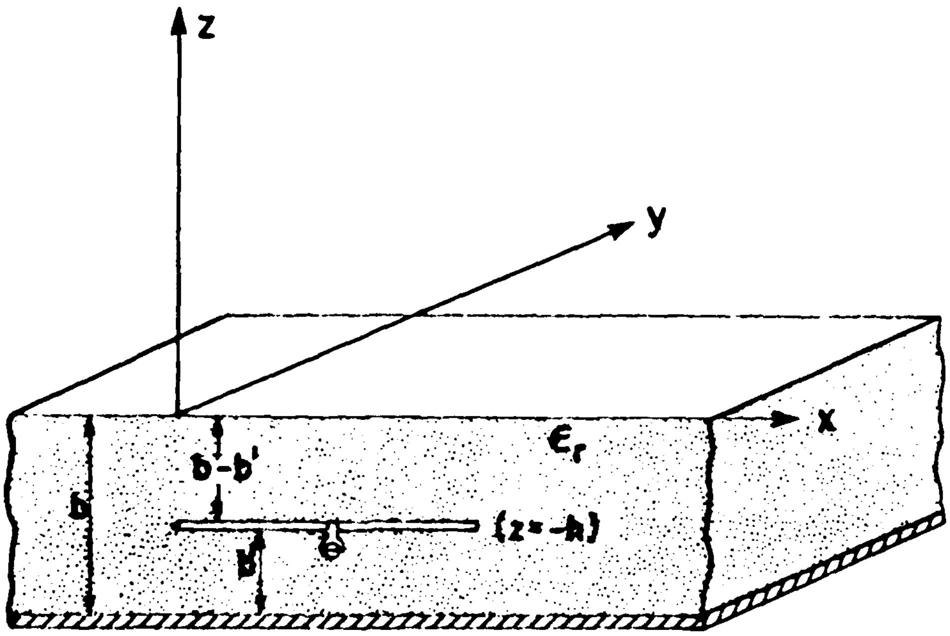

Figure 5.22: Dipole Embedded in the Dielectric Substrate

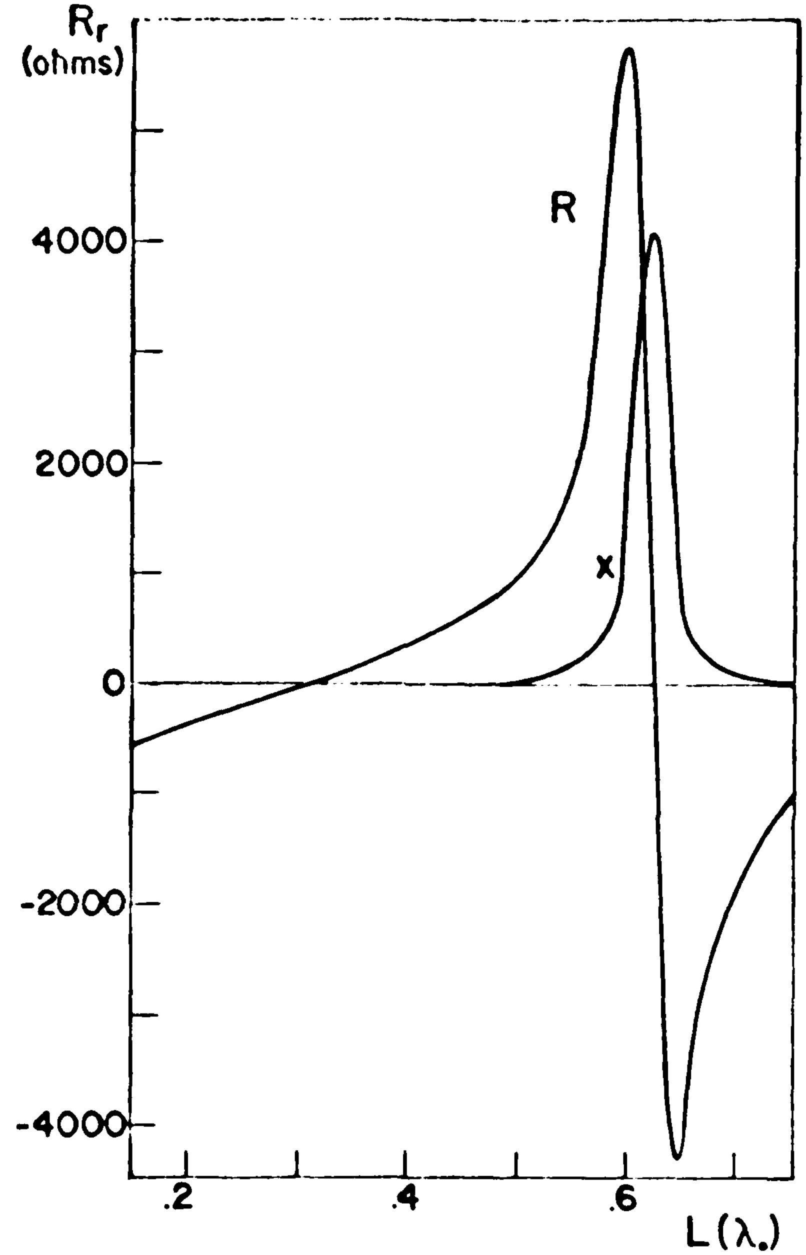

Figure 5.23: Input Impedance for a Dipole Embedded in the Substrate with $b'=b/2, \epsilon_r=2$ and $b=0.1016\lambda_\circ$ Resonant Length $L_r=0.319\lambda_\circ$

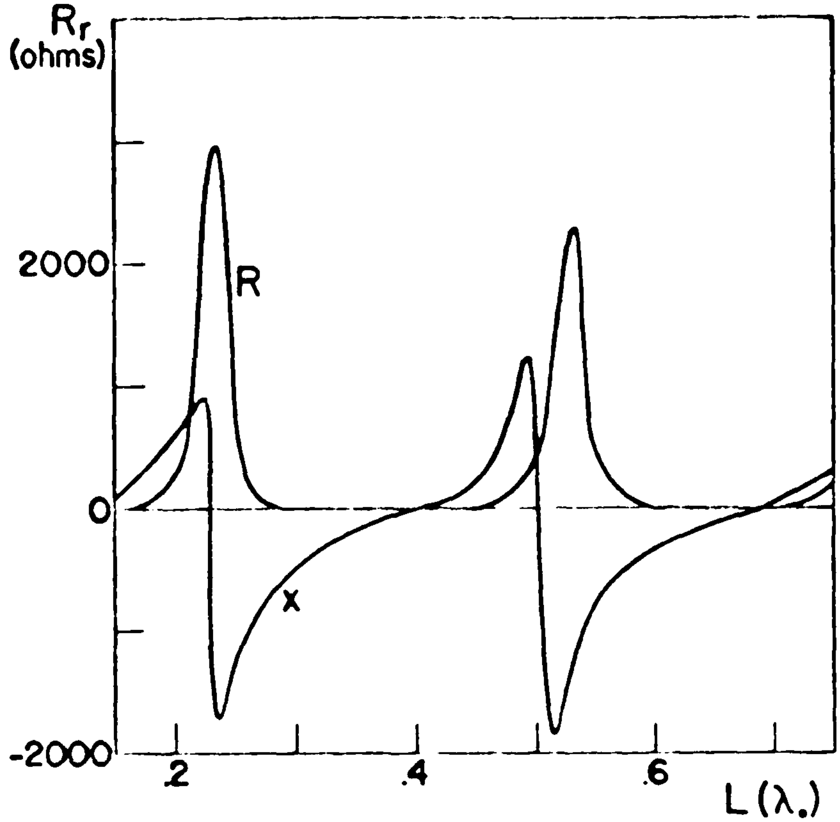

Figure 5.24: Input Impedance for a Dipole Embedded in the Substrate with $b' = b/2$, $\epsilon_r = 10$ and $b = 0.1016\lambda_o$ Resonant Length $L_r = 0.137\lambda_o$

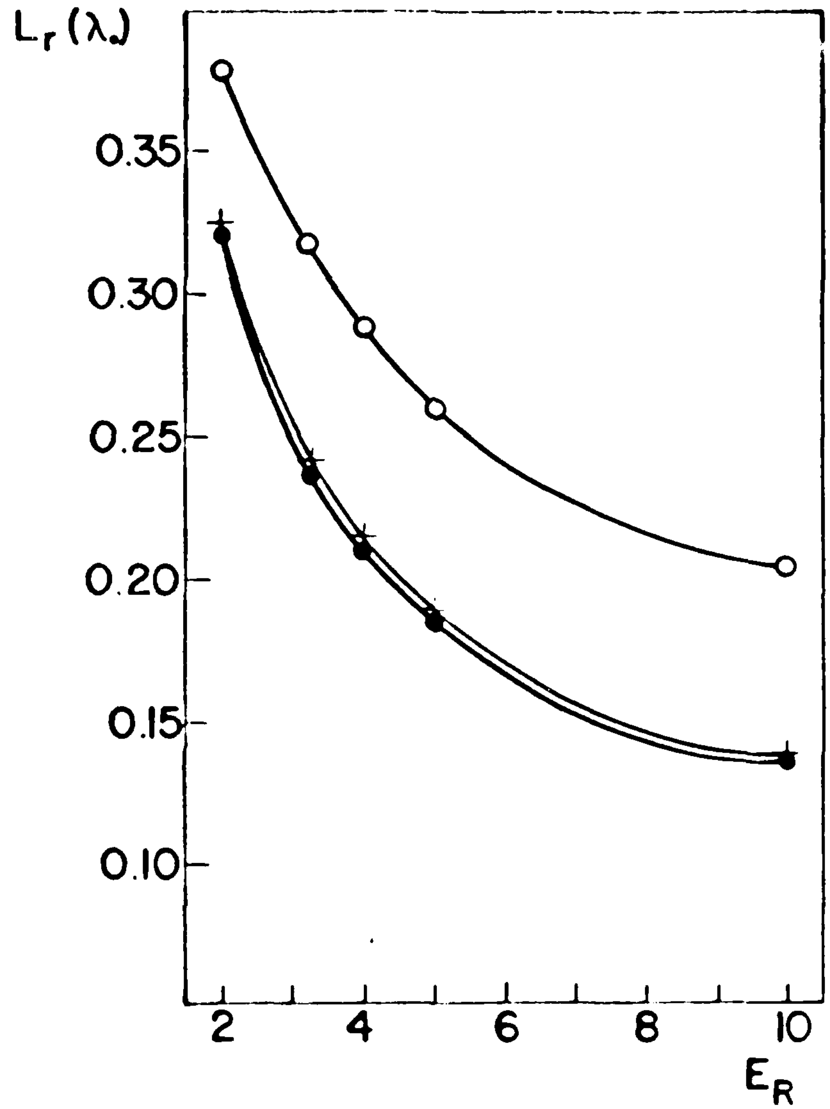

Figure 5.25: Resonant Length vs. Relative Dielectric Constant ϵ_r for a Dipole with b=0.1016λ.

o—o Dipole on the Interface

●—● Dipole in the Substrate b'=b/2

+—+ Dipole in the Substrate b'=2b/3

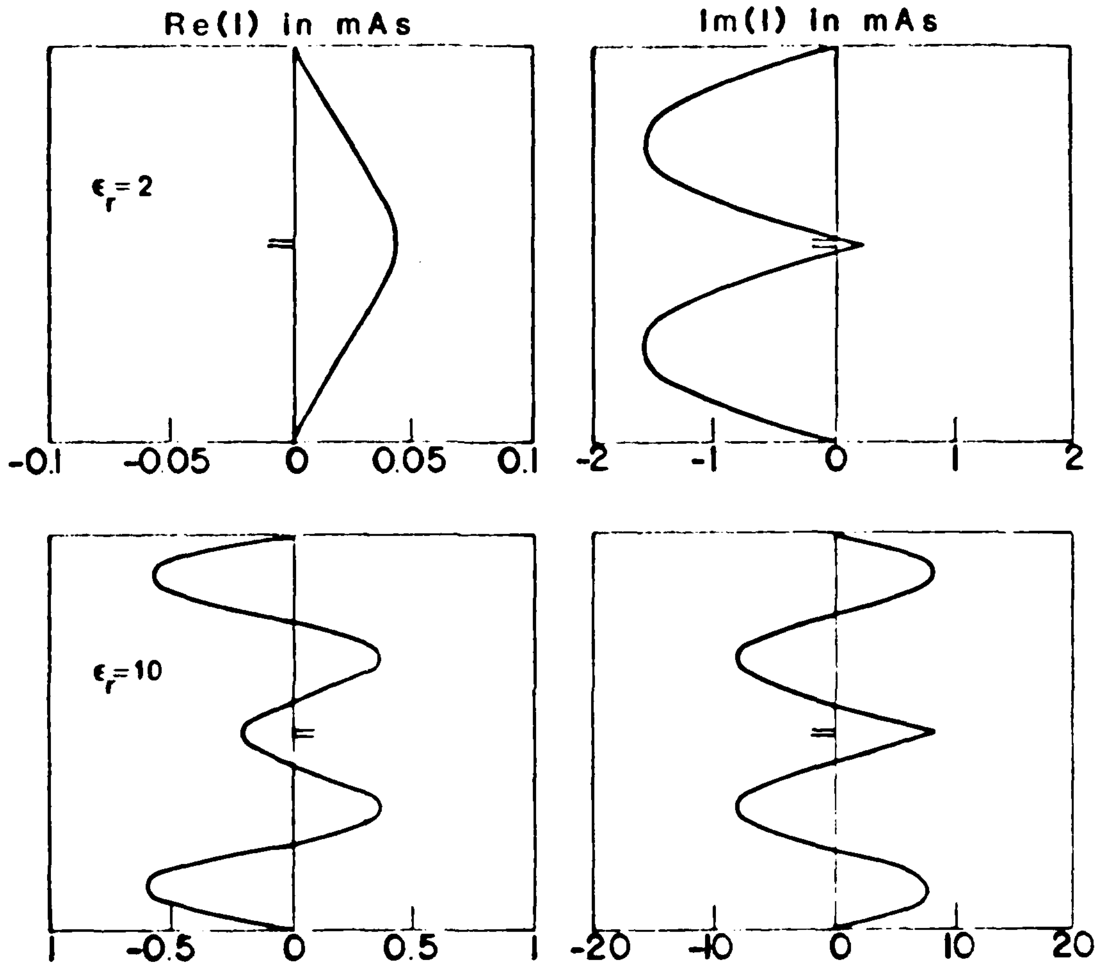

Figure 5.26: Current Distribution on a Dipole Embedded in the Substrate with $b' = b/2, b = 0.1016\lambda_c$ and $L = 0.65\lambda_c$

on the dipole of Figure 5.22 with its length equal to 0.65 λ_o and for two values of ε_r (ε_r = 2, 10). The increase in the number of zeros resulting from the increasing relative dielectric constant is, as in the case of the printed dipole, characteristic of the substrate properties.

c. SUBSTRATE THICKNESS VARIATION

The dipole of Figure 5.22 will now be considered again. For this dipole with a relative dielectric constant for the substrate equal to 2.35, the real and imaginary parts of the input impedance for three different values of the substrate thickness are given in Figures 5.27, 5.28 and 5.29. These three values of b (0.1016 λ_o, 0.25 λ_o and 0.46 λ_o) cause one, two and three surface waves to be excited. As shown in Figure 5.30, the resonant length as a function of the substrate thickness goes through a minimum in region I (one surface wave) and continues increasing in regions II (two surface waves) and III (three surface waves) with a step discontinuity in its derivative $\frac{\partial L_r(b)}{\partial b}$ at the point where a third surface wave is excited. Assuming the same definition of bandwidth as in section 5.2, one can determine its variation with respect to substrate thickness b. In addition the resonant resistance as a function of the same parameter is shown in Figures 5.31 and 5.32. From these figures one can see that the resonant resistance R_r is monotonically increasing as b increases with step discontinuities in the derivative $\frac{\partial R_r(b)}{\partial b}$ at the points where a new surface wave is excited. The bandwidth BW follows in shape the variation of R_r but it exhibits much larger slope. Figure 5.33 shows the current distribution of the dipole of Figure 5.22 when l = 0.65 λ_o, ε_r = 2.35 and b =

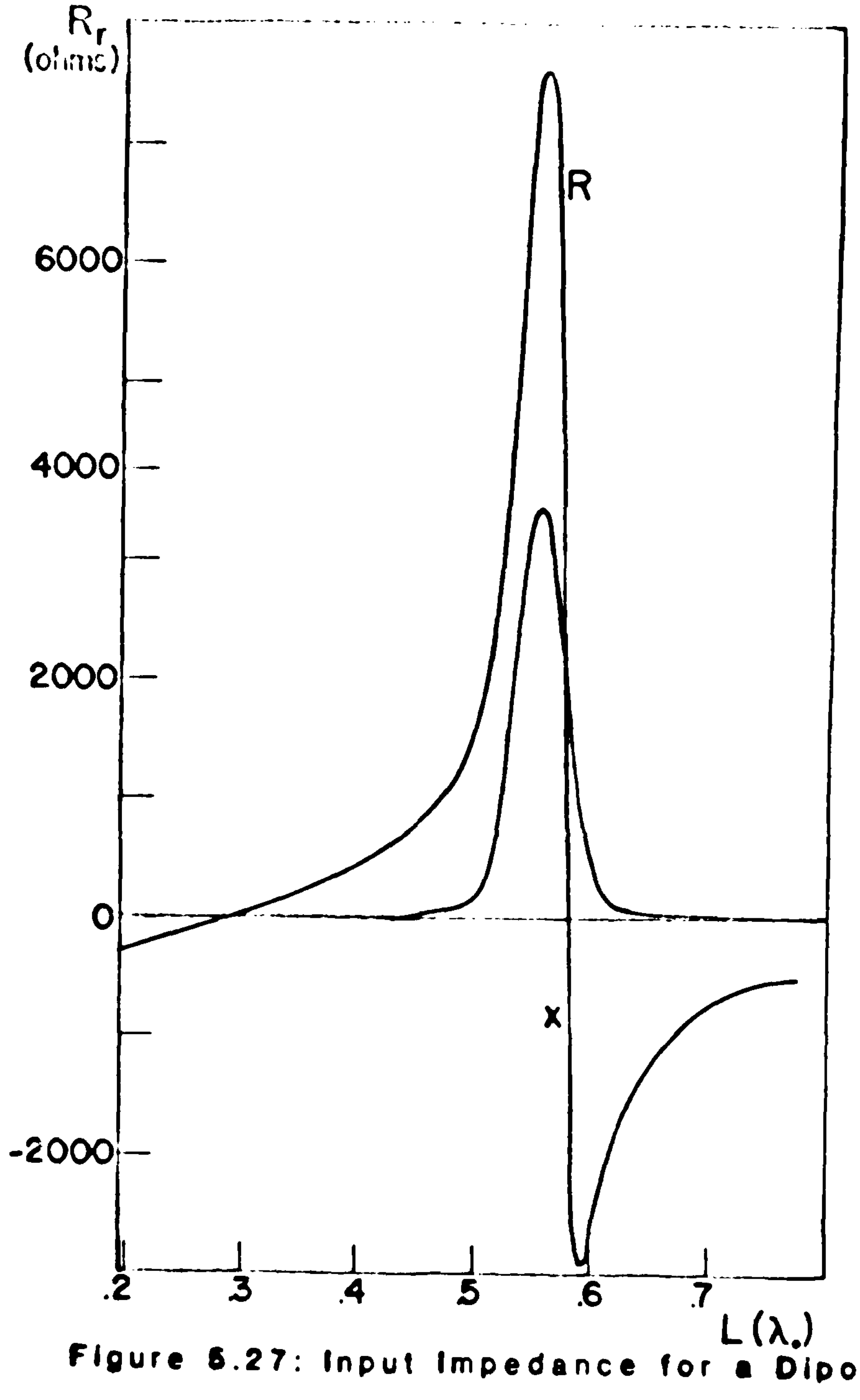

Figure 5.27: Input Impedance for a Dipole Embedded in the Substrate with $b' = b/2$, $\epsilon_r = 2.35$ and $b = 0.1016\lambda_0$ Resonant Length $L_r = 0.289\lambda_0$

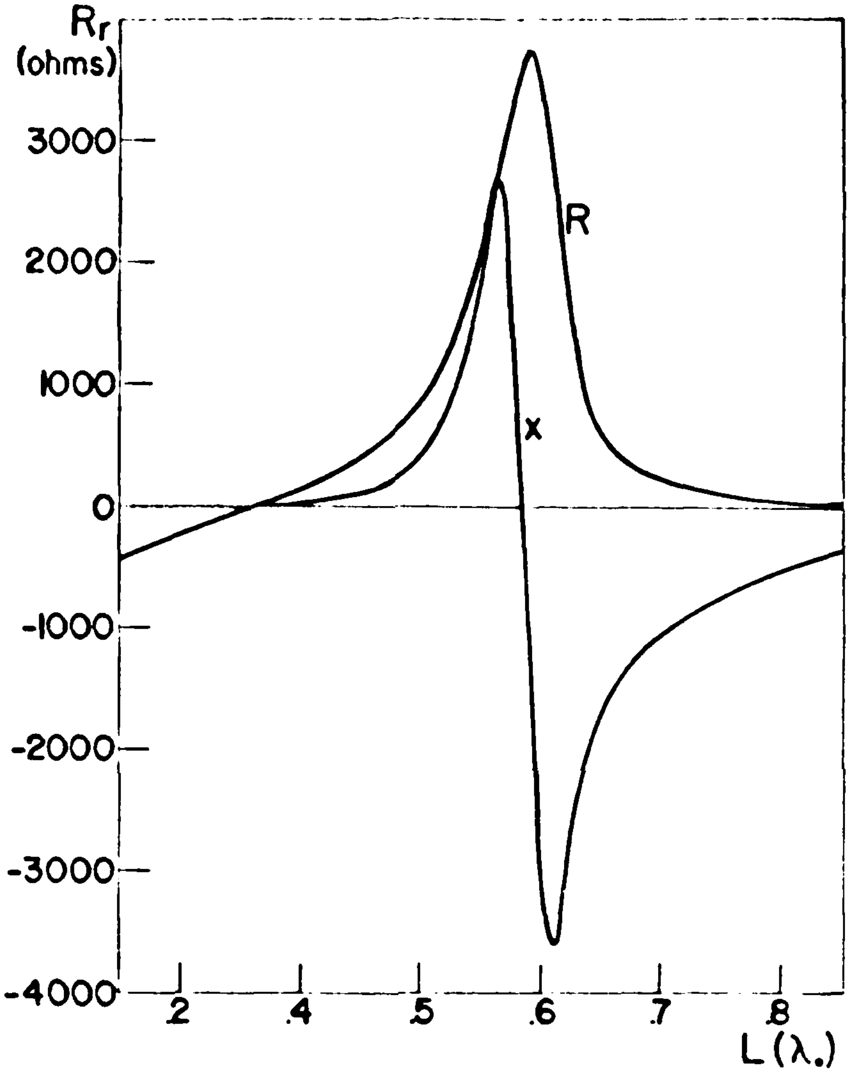

Figure 5.28: Input Impedance for a Dipole Embedded in the Substrate with $b'=b/2$, $\epsilon_r=2.35$ and $b=0.25\lambda_0$ Resonant Length $L_r=0.263\lambda_0$

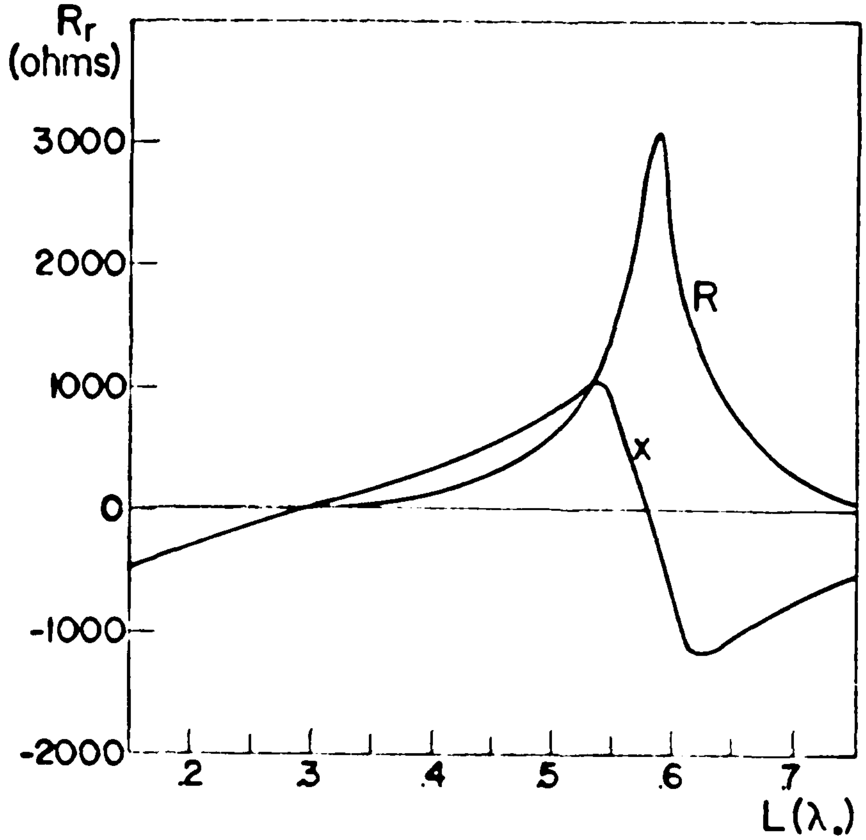

Figure 5.29: Input Impedance for a Dipole Embedded in the Substrate with $b'=b/2$, $\epsilon_r=2.35$ and $b=0.46\lambda_o$. Resonant Length $L_r=0.3\lambda_o$.

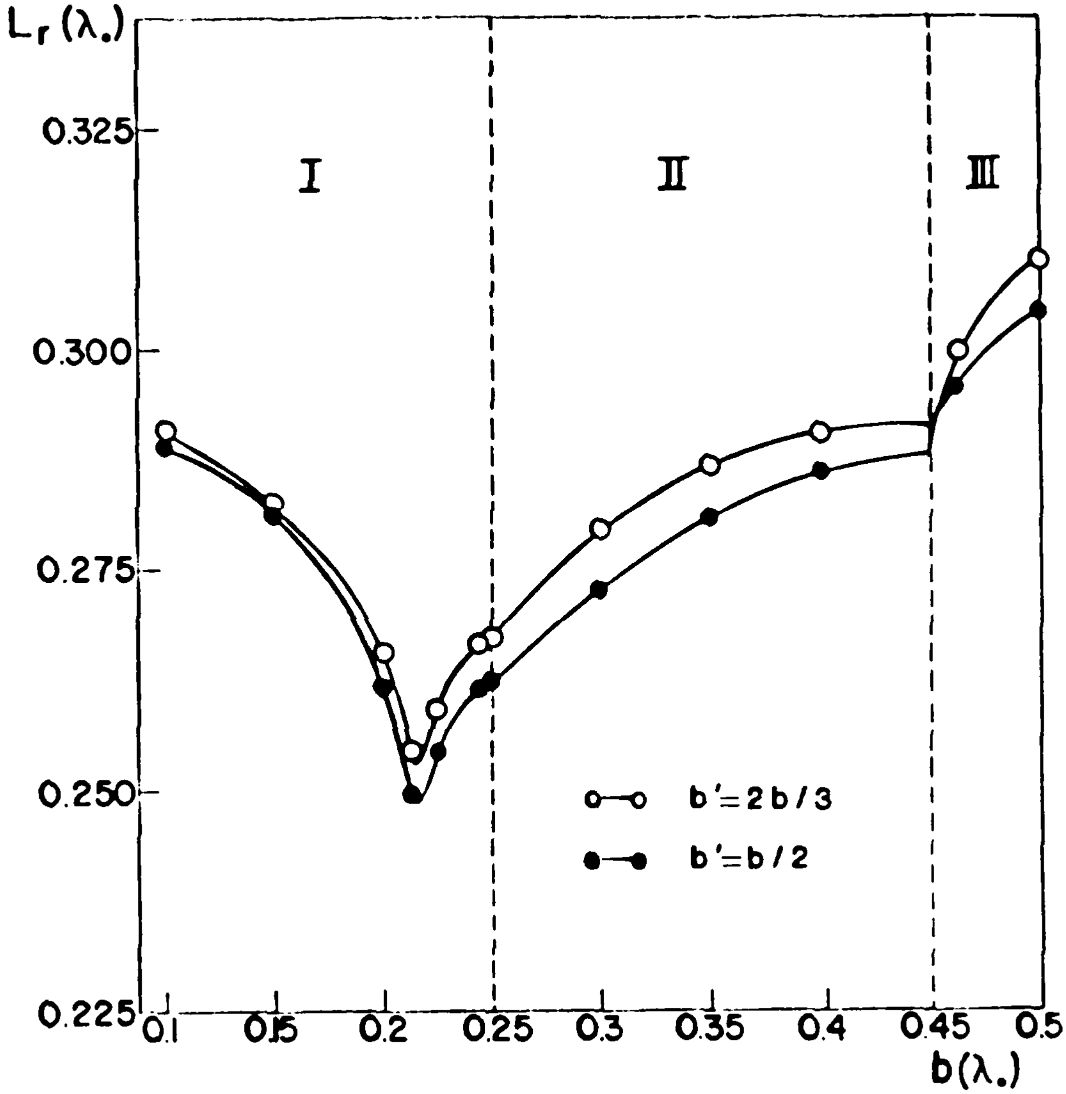

Figure 5.30: Resonant Length vs. Substrate Thickness b for a Dipole Embedde in the Substrate with $\epsilon_r=2.35$

I: One Surface Wave

II: Two Surface Waves

III: Three Surface Waves

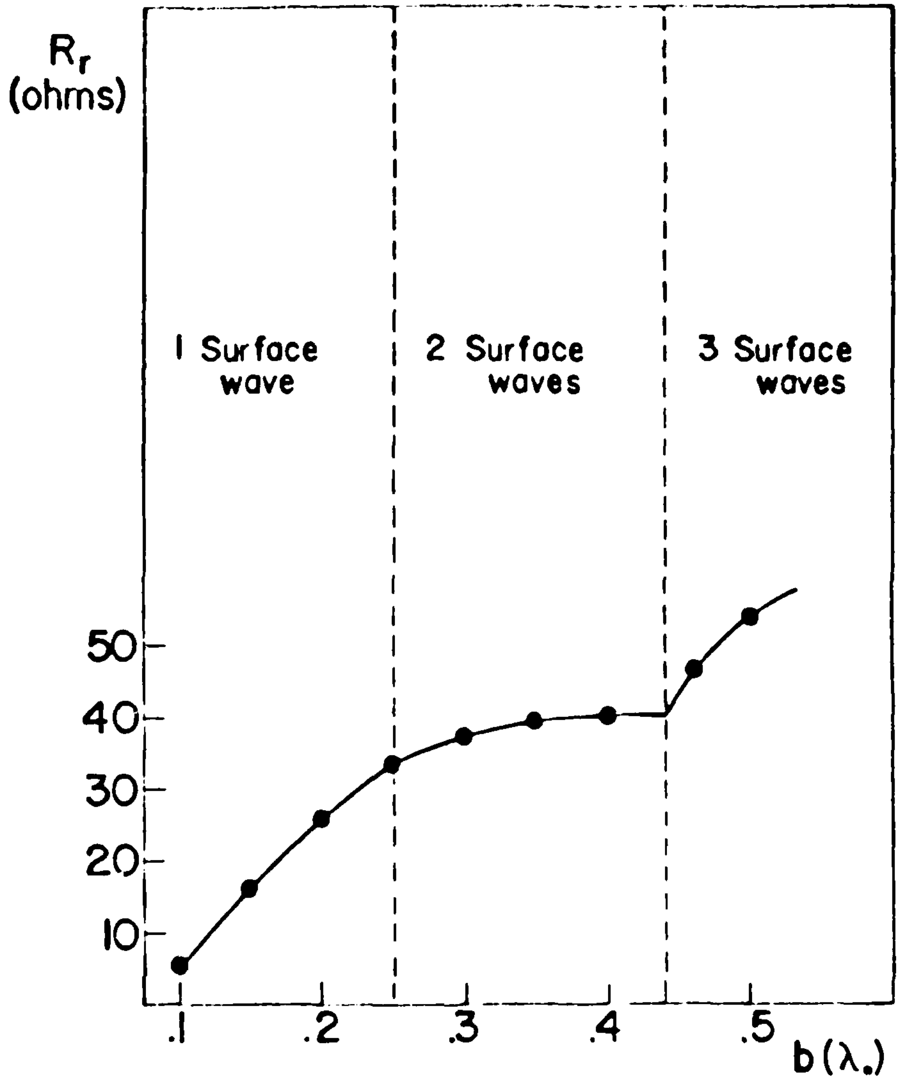

Figure 5.31: Resonant Resistance vs. Substrate Thickness b for a Dipole Embedded in the Substrate with $b'=b/2$ and $\epsilon_r=2.35$

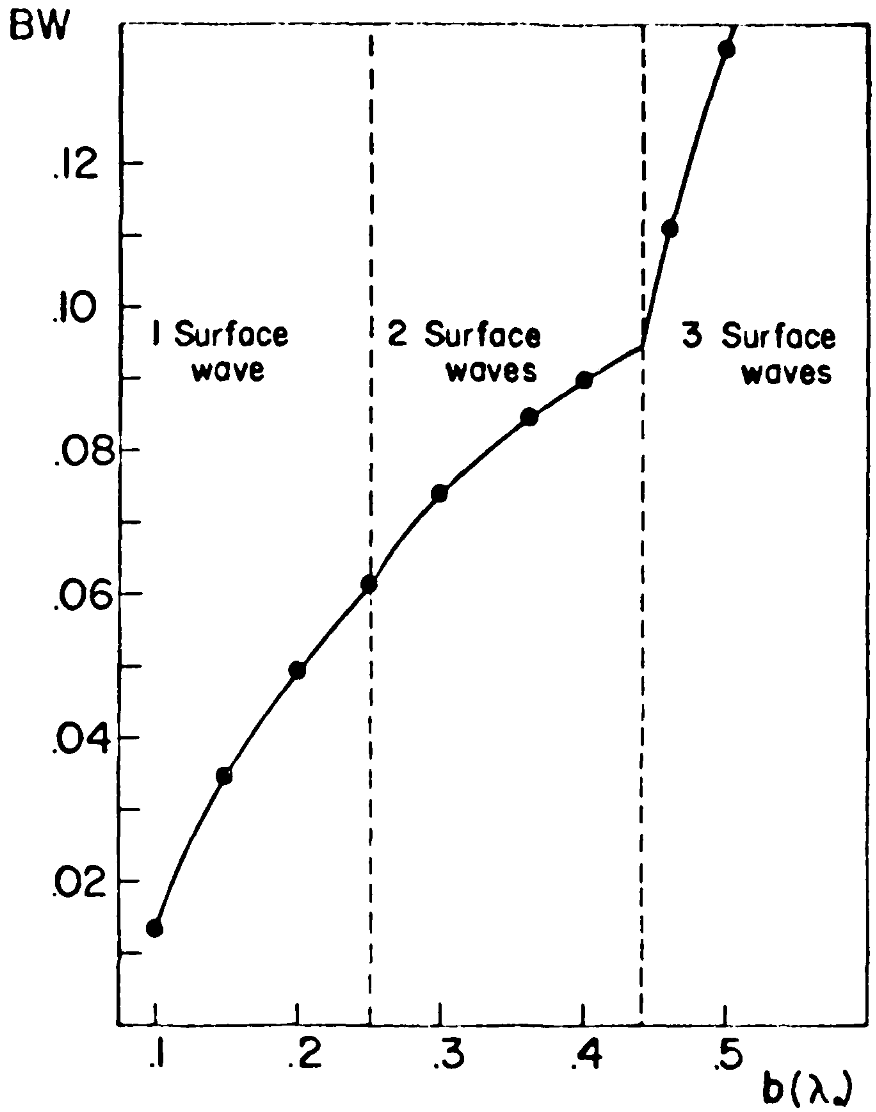

Figure 5.32: Bandwidth BW vs. Substrate Thickness b for a Dipole Embedded in the Substrate with $b'=b/2$ and $\epsilon_r=2.35$

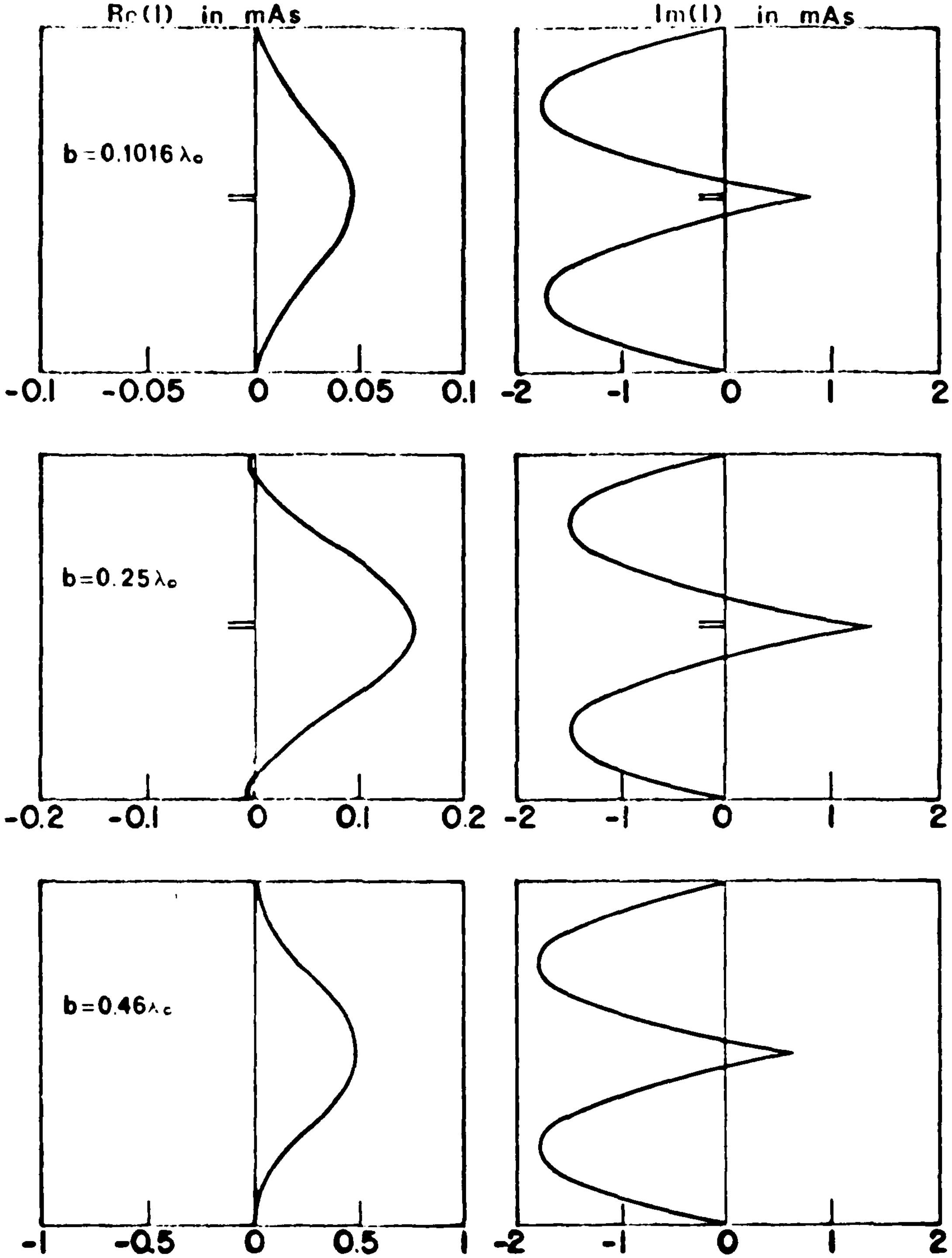

Figure 6.33: Current Distributionn on a Dipole Embedded in the Substrate with $\epsilon_r = 2.35$ $b' = b/2$ and $L = 0.65\lambda_o$

$0.1016\ \lambda_o$, $0.25\ \lambda_o$ and $0.46\ \lambda_o$.

Figures 5.34 and 5.35 show the current distribution as a function of the length of the dipole (Figure 5.22) when $b' = 2b/3$, $b = 0.1016\ \lambda_o$ and $\varepsilon_r = 2.35$. The feed point is not located at the middle of the dipole contrary to all the cases which were studied until now. The distance of the feed point from the nearest end of the dipole is 1/4 of the dipole length.

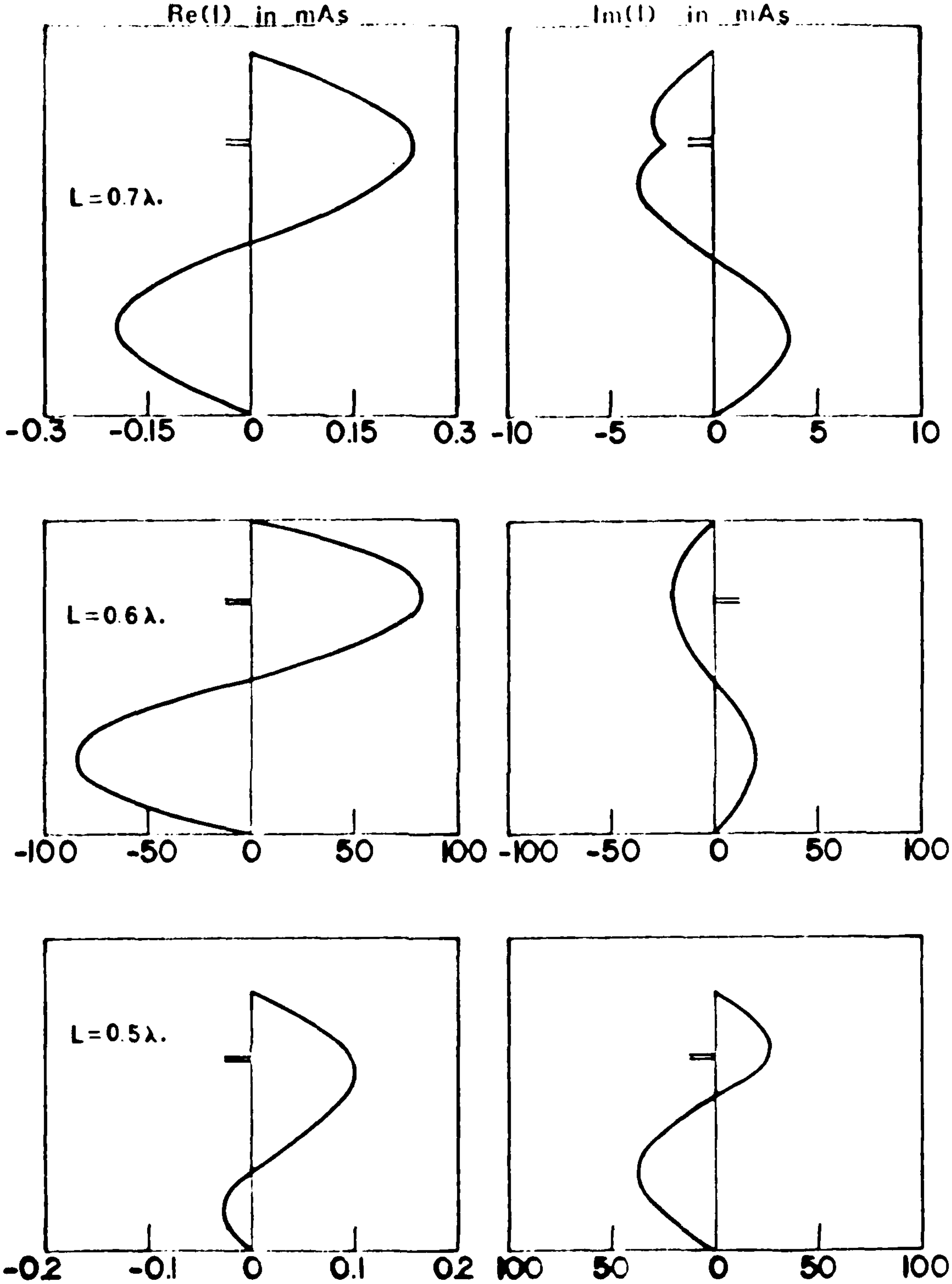

Figure 5.34: Current Distribution on a Dipole Embedded in the Substrate with $b' = b/2, \epsilon_r = 2.35$ and Different Lengths

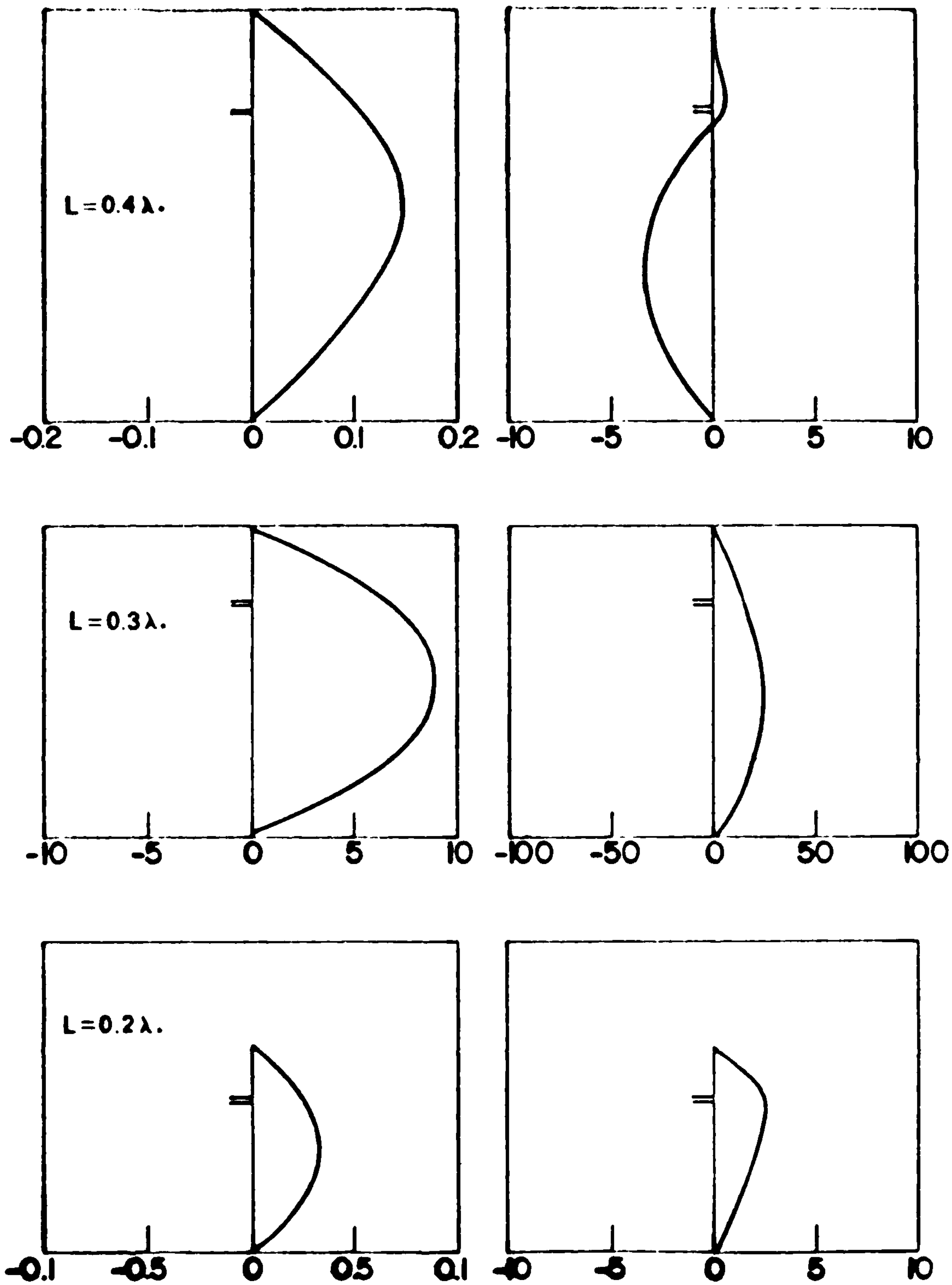

Figure 5.35: Current Distribution on a Dipole Embedded in the Substrate with $b' = b/2$, $\epsilon_r = 2.35$ and Different Lengths

BIBLIOGRAPHY

1. G. A. Deschamps, "Microstrip Microwave Antennas," 3rd USAF Symp. on Antennas, 1953.

2. H. Gutton and G. Baissinot, "Flat Aerial for Ultra High Frequencies," French Patent No. 703113, 1955.

3. E. V. Byron, "A New Flush-Mounted Antenna Element for Phased Array Application," Proc. Phased-Array Antenna Symp., 1970, 187.

4. R. E. Munson, "Single Slot Cavity Antennas Assembly," U.S. Patent No. 3713162, Jan. 23, 1973.

5. J. Q. Howell, "Microstrip Antennas," Dig. Int. Symp. Antennas Propagat. Soc., Williamsburg, VA, Dec. 1972, 177.

6. H. D. Weinschel, "Progress Report on Development of Microstrip Cylindrical Arrays for Sounding Rockets," Physic. and Sci. Lab., New Mexico State Univ., Las Cruces, 1973.

7. G. G. Sanford, "Conformal Microstrip Phased Array for Aircraft Tests with ATS-6," Proc. Nat. Electronics Conf., vol. 29, Oct. 1974, 252.

8. G. W. Garvin, R. E. Munson, L. T. Ostwald and K. G. Schroeder, "Low Profile Electrically Small Missile Base Mounted Microstrip Antennas," Dig. Int. Symp. Antennas Propagat. Soc., Urbana, IL, June 1975, 244.

9. J. Q. Howell, "Microstrip Antennas," IEEE Trans. Antennas Propagat., vol. AP-23, no. 1, Jan. 1975, 90.

10. H. D. Weinschel, "A Cylindrical Array of Circularly Polarized Microstrip Antennas," Dig. Int. Symp. Antennas Propagat. Soc., Urbana, IL, June 1975, 177.

11. J. R. James and G. J. Wilson, "New Design Techniques for Microstrip Antenna Arrays," Proc. 5th European Micro. Conf., Hamburg, Sept. 1975, 102.

12. R. E. Munson, "Conformal Microstrip Antennas and Microstrip Phased Arrays," IEEE Trans. Antennas Propagat., vol. AP-22, No. 1, Jan. 1974, 74.

13. A. G. Derneryd, "Linear Microstrip Array Antennas," Chalmer Univ. Technol. Goteborge, Sweden, Tech. Rep. TR 75[illegible], Oct. 1975.

14. N. K. Uzunoglu and P. Katehi, "Coupled Microstrip Disc Resonators," IEEE Trans. Microwave Theory and Technique, Vol. MTT-28, No. 2, Feb. 1980, 94.

15. Y. T. Lo, D. D. Harrison, D. Solomon, G. A. Deschamps, and F. R. Ore, "Study of Microstrip Antennas, Microstrip Phased Arrays, and Microstrip Feed Networks," Rome Air Development Center, Tech. Rep. TR-77-406, Oct. 21, 1977.

16. A. G. Derneryd, "A Theoretical Investigation of the Rectangular Microstrip Antenna Element," Rome Air Development Center, Tech. Rep. TR-77-206, June, 1977.

17. L. C. Shen and S. A. Long, "Low Profile Printed Circuit Antennas," Dept. Elec. Engr., Univ. Houston, Houston, TX, Contract DAAG-29-75-0187, Final Rep., Oct. 1977.

18. K. R. Carver and E. L. Coffey, "Theoretical Investigation of the Microstrip Antenna," Physic. and Sci. Lab., New Mexico State Univ., Las Cruces, Tech. Rep. PT-00929, Jan. 23, 1979.

19. A. Waterman and D. G. Henry, "Stripline Strap-on Antenna Array," Abstracts 21st USAF Antenna Symp., Allerton Park, IL, Oct. 12-14, 1971.

20. K. R. Carver, "A Modal Exp. ion Theory for the Microstrip Antenna," Dig. Int. Symp. Antennas Propagat. Soc., Seattle, WA, June 1979 101.

21. T. E. Nowicki, "Microwave Substrates, Present and Future," Proc. Workshop Printed Circuit Antenna Tech., New Mexico State Univ., Las Cruces, Oct. 1979, 26/1.

22. G. R. Traut, "Glad Laminates of PTFE Composites for Microwave Antennas," Proc. Workshop Printed Circuit Antenna Tech., New Mexico State Univ., Las Cruces, Oct. 1979, 27/1.

23. M. Olyphant, Jr. and T. E. Nowicki, "Microwave Substrates Support MIC Technology," Microwaves, Part 1, Vol. 19, No. 12, Nov. 1980, 74.

24. I. E. Rana and N. G. Alexopoulos, "Current Distribution and Input Impedance of Printed Dipoles," IEEE Trans. Antennas Propagat., Vol. AP-29, No. 1, Jan. 1981, 99.

25. N. G. Alexopoulos and I. E. Rana, "Mutual Impedance Computation Between Printed Dipoles," IEEE Trans. Antennas Prop Vol. AP-29, No. 1, Jan. 1981, 106.

26. E. H. Newman and P. Tulyathan, "Analysis of Microstrip Antennas Using Moments Method," IEEE Trans. Antennas Propagat., Vol. AP-29, No. 1, Jan. 1981, 47.

27. K. K. Mei, "Unimoment Method of Solving Antenna and Scattering Problems," IEEE Trans. Antennas Propagat., to be published.

28. D. B. Rutledge, S. E. Schwarz and A. T. Adams, "Infrared and Submillimeter Antennas," Infrared Phys., Vol. 18, Dec. 1978, 713.

29. F. Mizuno, Y. Daiku, and S. Ono, "Design of Painted Resonant Antennas for Monolithic-Diode Detectors," IEEE Trans. Microwave Theory Tech., Vol. MTT-25, June 1977, 470.

30. D. B. Rutledge, S. E. Schwarz, T. L. Hwang, D. J. Angelakos, K. K. Mei, and S. Yokota, "Antennas and Waveguides for Far-Infrared Integrated Circuits," IEEE J-QE, May 1980, 508.

31. N. K. Uzunoglu, N. G. Alexopoulos and J. G. Fikioris, "Radiation Properties of Microstrip Dipoles," IEEE Trans. Antennas Propagat., Vol. AP-27, Nov. 1979, 853.

32. R. S. Elliott, "The Green's Function for Electric Dipoles Parallel to and Above or Within a Grounded Dielectric Slab," Hughes Aircraft, Los Angeles, CA, Tech. Rep. 5752.00/072, Feb., 1978.

33. I. E. Rana, Ph.D., Dept. Elec. Engr., Univ. of California, Los Angeles, 1979, 101.

34. A. Sommerfeld, "Partial Differential Equations in Physics," Academic Press, New York, 1949.

35. G. A. Thiele, "Computer Techniques for Electromagnetics," R. Mittra, Pergamon Press, New York, 1973, 7.

36. G. A. Thiele, "Analysis of Yagi-Uda Type Antennas," IEEE Trans. Antennas Propagat., Vol. AP-17, Jan. 1969, 24.

37. R. F. Harrington, "Field Computation by Moment Methods," Macmillan Company, New York.

38. R. E. Collin, "Field Theory of Guided Waves," McGraw-Hill, New York, 1960, 485-506.

39. A. M. Krasun and W. Prager, "Remark on Romberg Quandrature," Commun. of the ACM, Vol. 8, No. 4, April 1965, 236.

40. G. Fairweather, "Algorithm 351, Modified Romberg Quadrature," Commun. of the ACM, Vol. 12, No. 6, June 1969, 324.

41. A. H. Stroud, "Approximate Calculation of Multiple Integrals," Prentice-Hall, Englewood Cliffs, New York, 1971.

42. C. M. Butler, "An Outline of Linear Space Theory for Applications," A Short Course in Electromagnetic Theory, Dept. Elec. Engr., Univ. of Mississippi, MS, May 1973, 3 1.

Appendix A

INTEGRAL REPRESENTATION OF THE PRIMARY SOLUTION

As mentioned in Chapter 2, the primary solution is the particular solution to the wave equation given by:

$$G^{d}_{px} = -\frac{j\omega\mu_o}{4\pi k^2}\,\frac{e^{-jkr}}{r} \tag{A.1}$$

It is desired to bring the representation (A.1) of G^{d}_{px} into the form of superposition of eigenfunctions ψ_n. Since the cylindrical polar coordinates r, ϕ, z are involved, these eigenfunctions will be in the form [31]

$$\psi_n = J_n(\lambda\rho)\; e^{in\phi}\; e^{\pm i\sqrt{k^2-\lambda^2}\,z} \tag{A.2}$$

where $\rho = [(x-x')^2 + (y-y')^2]^{\frac{1}{2}}$ and λ are eigenvalues which for the case of an infinite cylinder with finite radius are restricted to a discrete spectrum. However, if $\rho \to \infty$ (as is the case here), λ has a continuous spectrum $0 \le \lambda < \infty$ corresponding to the unlimited medium. Also, from the eigenfunctions ψ_n only those are used which are independent of ϕ; therefore n must be zero. From this discussion it is concluded that the particular solution (A.1) may be put in the form:

$$G^{d}_{px} = -\frac{j\omega\mu_o}{4\pi k^2}\int_0^\infty \lambda\, A(\lambda)\, J_o(\lambda\rho)\, e^{-u|z+h|}\, d\lambda \tag{A.3}$$

with

$$u = [\lambda^2-k^2]^{\frac{1}{2}}$$
$$r = [\rho^2+(z+h)^2]^{\frac{1}{2}} \tag{A.4}$$

AD-A112 409 CALIFORNIA UNIV LOS ANGELES INTEGRATED ELECTROMAGNET--ETC F/G 9/5
PRINTED CIRCUIT DIPOLE CHARACTERISTICS FOR MICROWAVE, MILLIMETE--ETC(U)
DEC 81 P L KATEHI, N G ALEXOPOULOS DAAG29-79-C-0050
UNCLASSIFIED UCLA-ENG-81-28 ARO-15965.9-EL NL

2 of 2

END
DATE
FILMED
4-82
DTIC

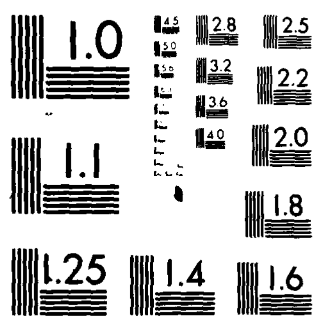

MICROCOPY RESOLUTION TEST CHART
NATIONAL BUREAU OF STANDARDS-1963-A

In equation (A.3) $A(\lambda)e^{-u|z+h|}$ is the Fourier-Bessel Transform of the function $\frac{e^{-jkr}}{r}$ and therefore is given by

$$A(\lambda)e^{-u|z+h|} = \int_0^\infty r\,\frac{e^{-jkr}}{r}\,J_o(\lambda\rho)\,d\rho \tag{A.5}$$

Equation (A.5) is easily simplified by considering $z = -h$ which gives

$$A(\lambda) = \int_0^\infty e^{-jk\rho}\,J_o(\lambda\rho)\,d\rho \tag{A.6}$$

In (A.6) $J_o(\lambda\rho)$ is replaced by its integral representation

$$J_o(\lambda\rho) = \frac{1}{2\pi}\int_{-\pi}^{\pi} e^{j\lambda\rho\cos w}\,dw \tag{A.7}$$

and the relation

$$\begin{aligned} A(\lambda) &= \frac{1}{2\pi}\int_{-\pi}^{\pi} dw \int_0^\infty e^{j\rho(-k+\lambda\cos w)}\,d\rho = \\ &= -\frac{1}{2\pi j}\int_{-\pi}^{\pi}\frac{dw}{-k+\lambda\cos w} \end{aligned} \tag{A.8}$$

results. The remaining integration in (A.8) gives

$$A(\lambda) = \frac{1}{u}$$

If equation (A.9) is substituted into (A.3) the following relation for G^d_{px} is obtained

$$G^d_{px} = -\frac{j\omega\mu_o}{4\pi k^2}\int_0^\infty J_o(\lambda\rho)\,e^{-u|z+h|}\,\frac{\lambda}{u}\,d\lambda \tag{A.10}$$

Appendix B

DERIVATION OF THE COMPONENTS G^d and G

During the formulation of Pocklington's integral equation the following two relations

$$\frac{\partial G_z}{\partial z} = - \frac{\partial G}{\partial x} \tag{B.1}$$

$$\frac{\partial G_z^d}{\partial z} = - \frac{\partial G^d}{\partial x} \tag{B.2}$$

were obtained. By observing that $\frac{\partial}{\partial x} = - \frac{\partial}{\partial x'}$, one can write these two equations as follows:

$$dG = \frac{\partial G_z}{\partial z} dx' \tag{B.3}$$

$$dG^d = \frac{\partial G_z^d}{\partial z} dx' \tag{B.4}$$

or

$$G = \int \frac{\partial G_z}{\partial z} dx' \tag{B.5}$$

$$G^d = \int \frac{\partial G_z^d}{\partial z} dx' \tag{B.6}$$

Equation (2.34) in Chapter 2 yields, for $h = 0$

$$G_z = - \frac{j\omega\mu_o}{2\pi k_o^2} (1-\epsilon_r) \cos\phi \int_o^\infty J_1(\lambda\rho)\, e^{-u_o z}$$

$$\left[\frac{\sinh(ub)}{f_1(\lambda,b)} - \frac{\cosh(ub)}{f_2(\lambda,b)}\right] \lambda^2 d\lambda \tag{B.7}$$

By differentiating (B.7) with respect to ρ and by changing the order of integration and differentiation one finds the following relation:

$$\frac{\partial G_z}{\partial z} = - \frac{j\omega\mu_o}{2\pi k_o^2} (1-\epsilon_r) \cos\phi \int_o^\infty (-u_o)\, J_1(\lambda\rho)\, e^{-u_o z} \cdot$$

$$\frac{\sinh(ub)\cosh(ub)}{f_1(\lambda,b)\cdot f_2(\lambda,b)} \lambda^2 d\lambda$$

$$= - \frac{j\omega\mu_o}{2\pi k_o^2} (1-\epsilon_r) \cos\phi \int_o^\infty u_o \frac{d\, J_o(\lambda\rho)}{d(\lambda\rho)}\, e^{-u_o z} \cdot$$

$$\frac{\sinh(ub)\cosh(ub)}{f_1(\lambda,b)\cdot f_2(\lambda,b)} \lambda^2 d\lambda \tag{B.8}$$

From the relations

$$\rho = [(x-x')^2 + (y-y')^2]^{\frac{1}{2}} \tag{B.9}$$

and

$$\cos\phi = \frac{x-x'}{\rho} \tag{B.10}$$

it is determined that

$$\frac{d\rho}{dx'} = - \cos\phi \tag{B.11}$$

and

$$\frac{d\, J_o(\lambda\rho)}{d(\lambda\rho)} = \frac{1}{\lambda} \frac{d\, J_o(\lambda\rho)}{dx'} \frac{dx'}{d\rho} =$$

$$= - \frac{1}{\lambda} \frac{d\, J_o(\lambda\rho)}{dx'} \frac{1}{\cos\phi} \tag{B.12}$$

A substitution of (B.12) into (B.8) yields the following relation

$$\frac{\partial G_z}{\partial z} = - \frac{j\omega\mu_o}{2\pi k_o^2} (\epsilon_r - 1) \int_o^\infty \frac{d\, J_o(\lambda\rho)}{dx'}\, e^{-u_o z} \cdot u_o$$

$$\frac{\sinh(ub)\cosh(ub)}{f_1(\lambda,b)\cdot f_2(\lambda,b)} \lambda\, d\lambda \tag{B.13}$$

while from (B.5) and (B.13) we have

$$G = -\frac{j\omega\mu_o}{2\pi k_o^2}(\epsilon_r - 1)\int_o^\infty J_o(\lambda\rho)\, e^{-u_o z} \cdot u_o\lambda$$

$$\frac{\sinh(ub)}{f_1(\lambda,b)}\frac{\cosh(ub)}{\cdot f_2(\lambda,b)}d\lambda \qquad (B.14)$$

In a similar manner

$$G^d = -\frac{j\omega\mu_o}{2\pi k^2}(1-\epsilon_r)\int_o^\infty J_o(\lambda\rho)\ \frac{u\sinh[u(b-h)]}{f_1(\lambda,b)} \cdot u$$

$$\frac{\sinh[u(z+b)]}{f_2(\lambda,b)}d\lambda \qquad (B.15)$$

results.

Appendix C

UNIQUENESS AND EXISTENCE OF THE SOLUTION OF THE FUNCTIONAL EQUATION $L_{op}(\vec{J})=(E_x\vec{x})$

A. Uniqueness

Let it be assumed that, for the equation $L_{op}(\vec{J})=(E_x\vec{x})$, two vectors $\vec{J}_1$ and $\vec{J}_2$ exist such that [42]

$$L_{op}(\vec{J}_1) = (E_x\vec{x}) \text{ and } L_{op}(\vec{J}_2) = (E_x\vec{x}) \tag{C.1}$$

A subtraction of one from the other yields the conclusion that

$$L_{op}(\vec{J}_1-\vec{J}_2) = 0 \quad \text{or} \quad L_{op}(\vec{d}) = \vec{0} \tag{C.2}$$

where $\vec{d}$ is the solution to the homogenous equation $L_{op}(\vec{J}) = \vec{0}$. Because of the physics of the problem, with no excitation the induced current on the dipole is identically zero and therefore $\vec{d} = \vec{0}$ which gives $\vec{J}_1 = \vec{J}_2$. Therefore the solution is unique.

B. Existence

The homogeneous adjoint equation

$$L^a_{op}(\vec{J}^a) = 0 \tag{C.3}$$

is considered with $\vec{J}^a$ in the adjoint domain $D(L^a_{op})$. By the definition of the adjoint operator

$$< L_{op}(\vec{J}), \vec{J}^a > = < \vec{J}, L^a_{op}(\vec{J}^a) > \tag{C.4}$$

or

$$< (E_x\vec{x}), \vec{J}^a > = < \vec{J}, \vec{0} > \tag{C.5}$$

Equation (C.5) reduces to

$$< (E_x \vec{x}),\ \vec{J}^a > = 0 \tag{C.6}$$

Since it has been proved that the operator L_{op} is self adjoint,

$$L_{op} = L_{op}^a \tag{C.7}$$

results.

Because of (C.7), equation (C.3) reduces to

$$L_{op} (\vec{J}^a) = 0 \tag{C.8}$$

which was shown earlier to have a solution identically equal to zero. Therefore equation (C.6) is satisfied, and the existence of the solution of the original functional equation is concluded.

Appendix D

CONDITIONS IMPOSED BY THE OUTGOING-PROPAGATION-CHARACTER REQUIREMENT

As shown in Chapter 2, both of the components of the Green's Function in air include a factor $e^{-u_o z}$ in their integrands. This factor, together with the exponential time dependance factor takes the form

$$\sigma(z,t) = e^{-u_o z + j\omega t} \tag{D.1}$$

The transformation

$$u_o = j\, k_o \cos w \quad (w \in C) \tag{D.2}$$

leads to the following relationship for λ

$$\lambda = k_o \sin w \tag{D.3}$$

Assuming that $w = \tau + jv$ one can show that equations (D.2) and (D.3) become

$$u_o = k_o \sin\tau \sinh v + j\, k_o \cos\tau \cosh v \tag{D.4}$$

$$\lambda = k_o \sin\tau \cosh v + j\, k_o \cos\tau \sinh v \tag{D.5}$$

Because of (D.4), equation (D.1) can be put in the form

$$\sigma(z,t) = e^{j[\omega t - k_o z \cos\tau \cos\tau \cosh v]}\, e^{-k_o z \sin\tau \sinh v} \tag{D.6}$$

In order to satisfy the outgoing character of the propagating waves, the following relations must be satisfied:

$$\sin\tau \sinh v > 0 \tag{D.7}$$

$$\cos\tau \cosh v > 0 \tag{D.8}$$

From (D.7), (D.8), and from the fact that the contour of integration with respect to λ is extended along the positive real axis it is obvious that

$$\sin\tau > 0 \quad (D.9)$$

$$\sinh\nu > 0 \quad (D.10)$$

$$\cos\tau > 0 \quad (D.11)$$

A consideration of inequalities (D.9) - (D.11) into (D.5) indicates that the real and imaginary parts of the parameter λ satisfy the relations

$$\mathrm{Re}\,[\lambda] > 0 \quad (D.12)$$

$$\mathrm{Im}\,[\lambda] > 0 \quad (D.13)$$

Appendix E

TECHNIQUE FOR THE EXTRACTION OF THE SINGULARITIES

As mentioned in Chapter 4, the integration along the interval $[k_o,k]$ faces the existence of a finite set of discrete essential singularities which with a surface wave character, affect considerably the input impedance and radiation characteristics.

If it is assumed that S is the set of these singularities then S is given by

$$S = \{x_i / [x_i = \text{root of } f_1(\lambda,b) = 0] \cup [x_i = \text{root of } f_2(\lambda,b) = 0] \text{ and } i = 1, 2, \ldots N\} \tag{E.1}$$

A partition $P\,[t_{n+1}]$ of the interval $[k_o,k]$ is considered such that

$$P\,[t_{n+1}] = \{t_o = k_o,\ t_1 < x_1,\ \ldots\ t_n < x_n,\ t_{n+1} = k\} \tag{E.2}$$

The integrals (4.32) and (4.33), with the λ-integration extended from k_o to k, can be put in the form

$$I = \sum_{r=0}^{n} \int_{t_r}^{t_{r+1}} d\lambda\, \lambda\, f(\lambda,b,\epsilon_r)\, FJ_o(\lambda, k_j) \tag{E.3}$$

where

$$FJ_o(\lambda; k_j) = \int_{x_k}^{x_{k+1}} dx\, z(x) \int_{x_j}^{x_{j+1}} dx'\, z(x')\, J_o(\lambda\rho_1) \tag{E.4}$$

or

$$FJ_o(\lambda, k_j) = \int_{x_k}^{x_{k+1}} dx\, z(x)\, J_o(\lambda\rho_2) \tag{E.5}$$

Equation (E.3) can also be written as follows:

$$I = \sum_{r=0}^{n} \int_{t_r}^{t_{r+1}} d\lambda\, \frac{g_r^{kj}(\lambda,b,\epsilon_r)}{\lambda - \lambda_r} \tag{E.6}$$

with $\phi_r(\lambda, b, \varepsilon_r) = \lambda(\lambda - x_r)\, f(\lambda, b, \varepsilon_r)\, FJ_o(\lambda\rho_{kj})$ (E.7)

In (E.6) the quantity $\dfrac{\phi_r^{kj}(x_r, b, \varepsilon_r)}{\lambda - x_r}$ is added and substracted giving

$$I = \sum_{r=0}^{N} \int_{t_r}^{t_{r+1}} d\lambda \frac{\phi_r^{kj}(\lambda, b, \varepsilon_r) - \phi_r^{kj}(x_r, b, \varepsilon_r)}{\lambda - x_r} +$$

$$+ \sum_{r=0}^{N} \int_{t_r}^{t_{r+1}} d\lambda \frac{\phi_r^{kj}(x_r, b, \varepsilon_r)}{\lambda - x_r} \tag{E.8}$$

or

$$I = \sum_{r=0}^{N} \int_{t_r}^{t_{r+1}} d\lambda \frac{\phi_r^{kj}(\lambda, b, \varepsilon_r) - \phi_r^{kj}(x_r, b, \varepsilon_r)}{\lambda - x_r} +$$

$$+ \sum_{r=0}^{N} \phi_r^{kj}(x_r, b, \varepsilon_r) \int_{t_r}^{t_{r+1}} \frac{d\lambda}{\lambda - x_r} \tag{E.9}$$

From equation (E.9) the integral can be put in the final form

$$I = \sum_{r=0}^{N} \int_{t_r}^{t_{r+1}} d\lambda \frac{\phi_r^{kj}(\lambda, b, \varepsilon_r) - \phi_r^{kj}(x_r, b, \varepsilon_r)}{\lambda - x_r}$$

$$+ \sum_{r=0}^{N} \phi_r^{kj}(x_r, b, \varepsilon_r) \left[\operatorname{Ln} \left| \frac{t_{r+1} - x_r}{x_r - t_r} \right| - j\pi \right] \tag{E.10}$$

In the equation above, the integrands

$$\frac{\zeta_r^{kj}(\lambda,t,\varepsilon_r) - \zeta_r^{kj}(x_r,b,\varepsilon_r)}{\lambda - x_r}$$

are slowly varying functions in the intervals $[t_r, t_{r+1}]$ and the integrals can be evaluated using a Gaussian-quadrature integration method with four fixed points [36].

Appendix F

BANDWIDTH OF A DIPOLE PRINTED ON OR EMBEDDED IN THE DIELECTRIC SUBSTRATE

We consider the dipole by its equivalent circuit (Fig. F-1). The impedance seen by the voltage generator is given by:

$$Z_{in} = R + j\,(\omega L - \frac{1}{\omega C}) \qquad (F.1)$$

With X being the imaginary part of the input impedance, equation (F.1) can be written as follows:

$$Z_{in} = R + j\,X \qquad (F.2)$$

with

$$X = \omega L - \frac{1}{\omega C}$$

A differentiation of both sides of equation (F.3) with respect to frequency yields the relation

$$\frac{dX}{d\omega} = L\left[1 + (\frac{\omega_r}{\omega})^2\right] \qquad (F.4)$$

with ω_r the resonant frequency of the dipole, given by

$$\omega_r = \frac{1}{\sqrt{LC}} \qquad (F.5)$$

With $\omega = \omega_r$ in equation (F.4), the derivative of the reactance with respect to frequency at resonance is given by

$$\frac{dX}{d\omega}\Big|_{\omega = \omega_r} = 2L \qquad (F.6)$$

If ω_1 and ω_2 ($\omega_2 > \omega_r$) are the 3 dB points on the response of the

tuned circuit (Fig. F-1) the quality factor Q satisfies both the relations

$$Q = \frac{\omega_r}{\omega_2 - \omega_1} \tag{F.7}$$

and

$$Q = \frac{\omega_r L}{R} \tag{F.8}$$

From equations (F.7) and (F.8) the relation

$$\omega_2 - \omega_1 = \frac{R}{L} \tag{F.9}$$

results.

If one substitutes (F.6) into (F.9) and if the following bandwidth (BW) definition is assumed

$$BW = \frac{\omega_2 - \omega_1}{\omega_r} \tag{F.10}$$

then the relation

$$BW = \frac{2R}{\left.\frac{dX}{d\omega}\right|_{\omega = \omega_r}} \cdot \frac{1}{\omega_r} \tag{F.11}$$

is concluded with

$$\left.\frac{dX}{d\omega}\right|_{\omega = \omega_r} = \frac{L}{2\pi c} \left.\frac{dX}{d(\frac{L}{\lambda})}\right|_{\frac{L}{\lambda} = L_r} \tag{F.12}$$

where c is the velocity of light in the medium surrounding the dipole and L is the length of the dipole. From equations (F.11) and (F.12) it can be found that the bandwidth is given by

$$BW = \frac{1}{L_r} \frac{2R}{\left.\frac{dX}{d(\frac{L}{\lambda})}\right|_{\frac{L}{\lambda} = L_r}} \tag{F.13}$$

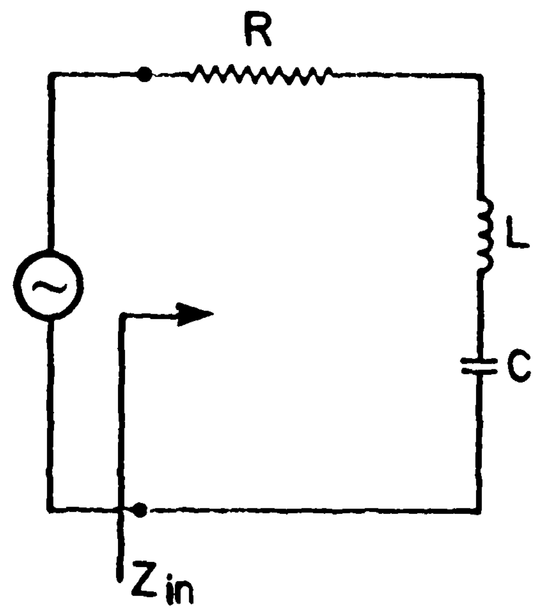

Figure F-1: Equivalent Circuit of a Dipole Printed on or Embedded in the Substrate

where L_r is the Resonant Length normalized with respect to free space wavelength.